

EUROPEAN JOURNAL OF BIOLOGY

Owner

Tansel Ak
Istanbul University, Turkey

Editor in Chief

Sehnaz Bolkent
Istanbul University, Turkey

Deputy Editor in Chief

Fusun Oztay
Istanbul University, Turkey

Editorial Board

Hafiz Ahmed
University of Maryland, USA

Ahmed Asan
Trakya University, Turkey

Ricardo Antunes de Azevedo
Universidade de Sao Paulo, Brazil

Levent Bat
Sinop University, Turkey

Mahmut Caliskan
Istanbul University, Turkey

Carmela Caroppo
Institute for Coastal Marine Environment, Italy

Cihan Demirci
Istanbul University, Turkey

Mustafa Djamgoz
Imperial College, United Kingdom

Editors

Amal Amer
The Ohio State University, USA

Gulriz Baycu Kahyaoglu
Istanbul University, Turkey

Aysegul Mulayim
Istanbul University, Turkey

Jan Zima
Charles University, Czech Republic

Aglıka Edrewa
Bulgarian Academy of Science, Bulgaria

Refet Gojak
University of Sarajevo, Bosnia

Ufuk Gunduz
Middle East Technical University, Turkey

Dietmar Keyser
University of Hamburg, Germany

Ayten Kimiran
Istanbul University, Turkey

Domenico Morabito
Université d'Orléans, France

Michael Moustakas
Aristotle University, Greece

Nurdan Ozkucur
Tufts University, USA

Statistical Editor

Ahmet Dirican
Istanbul University, Turkey

Language Editors

Elizabeth Mary Earl
Istanbul University, Turkey

Alan James Newson
Istanbul University, Turkey

Nesrin Ozoren
Bogazici University, Turkey

Majeti Narasimha Vara Prasad
University of Hyderabad, India

Thomas Sawidis
Aristotle University, Greece

Alex Sivan
The Hebrew University of Jerusalem, Israel

Nico M. Van Straalen
Vrije Universiteit, The Netherlands

Ismail Turkan
Ege University, Turkey

Argyro Zenetos
Hellenic Centre for Marine Research, Greece

Coert J. Zuurbier
*Academisch Medisch Centrum Universiteit,
The Netherlands*

Owner on behalf of the Istanbul University Faculty of Science: Yesim Oktem – Publication Type: Biannually – Printed at: İlbey Matbaa Kağıt Reklam Org. M.Üc. San. Tic. Ltd. Şti. 2.Matbaacılar Sitesi 3NB 3 Topkapı/Zeytinburnu, İstanbul, Turkey www.ilbeymatbaa.com.tr, Sertifika No: 17845 – Printing Date: June 2020

Publishing Company

Istanbul University Press
İstanbul Üniversitesi Merkez Kampüsü,
34452 Beyazıt, Fatih / İstanbul - Turkey
Phone: +90 (212) 440 00 00



İSTANBUL
UNIVERSITY
P R E S S

Aims and Scope

European Journal of Biology (Eur J Biol) is an international, scientific, open access periodical published in accordance with independent, unbiased, and double-blinded peer-review principles. The journal is the official publication of Istanbul University Faculty of Science and it is published biannually on June and December. The publication language of the journal is English. European Journal of Biology has been previously published as IUFS Journal of Biology. It has been published in continuous publication since 1940.

European Journal of Biology aims to contribute to the literature by publishing manuscripts at the highest scientific level on all fields of biology. The journal publishes original research and review articles, and short communications that are prepared in accordance with the ethical guidelines in all fields of biology and life sciences.

The scope of the journal includes but not limited to; botany, zoology, hydrobiology, animal and plant systematics, ecology, environmental biology, microbiology, radiobiology, molecular biology, biochemistry, genetics, biotechnology, physiology, toxicology, cell biology, cancer biology, neurobiology, developmental biology, stem cell biology, regenerative and reparative biology, nanobiotechnology, system biology, tissue engineering, biomaterials, and omic sciences.

The target audience of the journal includes specialists and professionals working and interested in all disciplines of biology.

The editorial and publication processes of the journal are shaped in accordance with the guidelines of the International Committee of Medical Journal Editors (ICMJE), World Association of Medical Editors (WAME), Council of Science Editors (CSE), Committee on Publication Ethics (COPE), European Association of Science Editors (EASE), and National Information Standards Organization (NISO). The journal is in conformity with the Principles of Transparency and Best Practice in Scholarly Publishing (doaj.org/bestpractice).

European Journal of Biology is currently indexed by Web of Science Zoological Record, CAB Abstracts (CABI), Chemical Abstracts Service (CAS) and TUBITAK-ULAKBIM TR Index.

Processing and publication are free of charge with the journal. No fees are requested from the authors at any point throughout the evaluation and publication process. All manuscripts must be submitted via the online submission system, which is available at dergipark.gov.tr/iufsjb. The journal guidelines, technical information, and the required forms are available on the journal's web page.

All expenses of the journal are covered by the Istanbul University.

Statements or opinions expressed in the manuscripts published in the journal reflect the views of the author(s) and not the opinions of the Istanbul University Faculty of Science, editors, editorial board, and/or publisher; the editors, editorial board, and publisher disclaim any responsibility or liability for such materials.

All published content is available online, free of charge at dergipark.gov.tr/iufsjb. Printed copies of the journal are distributed free of charge.



Editor in Chief: Prof. Sehnaz BOLKENT

Address: Istanbul University, Faculty of Science, Department of Biology, 34134 Vezneciler, Fatih, Istanbul, TURKEY

Phone: +90 212 4555700 (Ext. 15079)

Fax: +90 212 5280527

E-mail: sbolkent@istanbul.edu.tr

Instructions to Authors

European Journal of Biology (Eur J Biol) is an international, scientific, open access periodical published in accordance with independent, unbiased, and double-blinded peer-review principles. The journal is the official publication of Istanbul University Faculty of Science and it is published biannually on June and December. The publication language of the journal is English. European Journal of Biology has been previously published as IUFS Journal of Biology. It has been published in continuous publication since 1940.

European Journal of Biology aims to contribute to the literature by publishing manuscripts at the highest scientific level on all fields of biology. The journal publishes original research and review articles, and short communications that are prepared in accordance with the ethical guidelines in all fields of biology and life sciences.

The scope of the journal includes but not limited to; botany, zoology, hydrobiology, animal and plant systematics, ecology, environmental biology, microbiology, radiobiology, molecular biology, biochemistry, genetics, biotechnology, physiology, toxicology, cell biology, cancer biology, neurobiology, developmental biology, stem cell biology, regenerative and reparative biology, nanobiotechnology, system biology, tissue engineering, biomaterials, and omic sciences.

The editorial and publication processes of the journal are shaped in accordance with the guidelines of the International Council of Medical Journal Editors (ICMJE), the World Association of Medical Editors (WAME), the Council of Science Editors (CSE), the Committee on Publication Ethics (COPE), the European Association of Science Editors (EASE), and National Information Standards Organization (NISO). The journal conforms to the Principles of Transparency and Best Practice in Scholarly Publishing (doaj.org/bestpractice).

Originality, high scientific quality, and citation potential are the most important criteria for a manuscript to be accepted for publication. Manuscripts submitted for evaluation should not have been previously presented or already published in an electronic or printed medium. Manuscripts that have been presented in a meeting should be submitted with detailed information on the organization, including the name, date, and location of the organization.

Manuscripts submitted to European Journal of Biology will go through a double-blind peer-review process. Each submission will be reviewed by at least three external, independent peer reviewers who are experts in their fields in order to ensure an unbiased evaluation process. The editorial board will invite an external and independent editor to manage the evaluation processes of manuscripts submitted by editors or by the editorial board members of the journal. The Editor in Chief is the final authority in the decision-making process for all submissions.

An approval of research protocols by the Ethics Committee in accordance with international agreements (World Medical Association Declaration of Helsinki "Ethical Principles for Medi-

cal Research Involving Human Subjects," amended in October 2013, www.wma.net) is required for experimental, clinical, and drug studies. If required, ethics committee reports or an equivalent official document will be requested from the authors.

For manuscripts concerning experimental research on humans, a statement should be included that shows the written informed consent of patients and volunteers was obtained following a detailed explanation of the procedures that they may undergo. Information on patient consent, the name of the ethics committee, and the ethics committee approval number should also be stated in the Materials and Methods section of the manuscript. It is the authors' responsibility to carefully protect the patients' anonymity. For photographs that may reveal the identity of the patients, signed releases of the patient or of their legal representative should be enclosed.

European Journal of Biology requires experimental research studies on vertebrates or any regulated invertebrates to comply with relevant institutional, national and/or international guidelines. The journal supports the principles of Basel Declaration (basel-declaration.org) and the guidelines published by International Council for Laboratory Animal Science (ICLAS) (iclas.org). Authors are advised to clearly state their compliance with relevant guidelines.

European Journal of Biology advises authors to comply with IUCN Policy Statement on Research Involving Species at Risk of Extinction and the Convention on the Trade in Endangered Species of Wild IUCN Policy Statement on Research Involving Species at Risk of Extinction and the Convention on the Trade in Endangered Species of Wild Fauna and Flora.

All submissions are screened by a similarity detection software (iThenticate by CrossCheck).

In the event of alleged or suspected research misconduct, e.g., plagiarism, citation manipulation, and data falsification/fabrication, the Editorial Board will follow and act in accordance with COPE guidelines.

Each individual listed as an author should fulfil the authorship criteria recommended by the International Committee of Medical Journal Editors (ICMJE - www.icmje.org). The ICMJE recommends that authorship be based on the following 4 criteria:

- 1 Substantial contributions to the conception or design of the work; or the acquisition, analysis, or interpretation of data for the work; AND
- 2 Drafting the work or revising it critically for important intellectual content; AND
- 3 Final approval of the version to be published; AND
- 4 Agreement to be accountable for all aspects of the work in ensuring that questions related to the accuracy or integrity of any part of the work are appropriately investigated and resolved.

In addition to being accountable for the parts of the work he/she has done, an author should be able to identify which co-authors are responsible for specific other parts of the work. In addition, authors should have confidence in the integrity of the contributions of their co-authors.

All those designated as authors should meet all four criteria for authorship, and all who meet the four criteria should be identified as authors. Those who do not meet all four criteria should be acknowledged in the title page of the manuscript.

European Journal of Biology requires corresponding authors to submit a signed and scanned version of the authorship contribution form (available for download through the journal's web page) during the initial submission process in order to act appropriately on authorship rights and to prevent ghost or honorary authorship. If the editorial board suspects a case of "gift authorship," the submission will be rejected without further review. As part of the submission of the manuscript, the corresponding author should also send a short statement declaring that he/she accepts to undertake all the responsibility for authorship during the submission and review stages of the manuscript.

European Journal of Biology requires and encourages the authors and the individuals involved in the evaluation process of submitted manuscripts to disclose any existing or potential conflicts of interests, including financial, consultant, and institutional, that might lead to potential bias or a conflict of interest. Any financial grants or other supports received for a submitted study from individuals or institutions should be disclosed to the Editorial Board. To disclose a potential conflict of interest, the ICMJE Potential Conflict of Interest Disclosure Form should be filled and submitted by all contributing authors. Cases of a potential conflict of interest of the editors, authors, or reviewers are resolved by the journal's Editorial Board within the scope of COPE and ICMJE guidelines.

The Editorial Board of the journal handles all appeal and complaint cases within the scope of COPE guidelines. In such cases, authors should get in direct contact with the editorial office regarding their appeals and complaints. When needed, an ombudsperson may be assigned to resolve cases that cannot be resolved internally. The Editor in Chief is the final authority in the decision-making process for all appeals and complaints.

When submitting a manuscript to European Journal of Biology, authors accept to assign the copyright of their manuscript to Istanbul University Faculty of Science. If rejected for publication, the copyright of the manuscript will be assigned back to the authors. European Journal of Biology requires each submission to be accompanied by a Copyright Transfer Form (available for download at the journal's web page). When using previously published content, including figures, tables, or any other material in both print and electronic formats, authors must obtain permission from the copyright holder. Legal, financial and criminal liabilities in this regard belong to the author(s).

Statements or opinions expressed in the manuscripts published in European Journal of Biology reflect the views of the author(s) and not the opinions of the editors, the editorial board, or the publisher; the editors, the editorial board, and the publisher disclaim any responsibility or liability for such materials. The final responsibility in regard to the published content rests with the authors.

MANUSCRIPT SUBMISSION

European Journal of Biology endorses ICMJE-Recommendations for the Conduct, Reporting, Editing, and Publication of Scholarly Work in Medical Journals (updated in December 2015 - <http://www.icmje.org/icmje-recommendations.pdf>). Authors are required to prepare manuscripts in accordance with the CONSORT guidelines for randomized research studies, STROBE guidelines for observational original research studies, STARD guidelines for studies on diagnostic accuracy, PRISMA guidelines for systematic reviews and meta-analysis, ARRIVE guidelines for experimental animal studies, TREND guidelines for non-randomized public behaviour, and COREQ guidelines for qualitative research.

Manuscripts can only be submitted through the journal's online manuscript submission and evaluation system, available at the journal's web page. Manuscripts submitted via any other medium will not be evaluated.

Manuscripts submitted to the journal will first go through a technical evaluation process where the editorial office staff will ensure that the manuscript has been prepared and submitted in accordance with the journal's guidelines. Submissions that do not conform to the journal's guidelines will be returned to the submitting author with technical correction requests.

During the initial submission, authors are required to submit the following:

- Copyright Transfer Form,
- Author Contributions Form, and

ICMJE Potential Conflict of Interest Disclosure Form (should be filled in by all contributing authors). These forms are available for download at the journal's web page.

Preparation of the Manuscript

Title page: A separate title page should be submitted with all submissions and this page should include:

- The full title of the manuscript as well as a short title (running head) of no more than 50 characters,
- Name(s), affiliations, and highest academic degree(s) of the author(s),
- Grant information and detailed information on the other sources of support,
- Name, address, telephone (including the mobile phone number) and fax numbers, and email address of the corresponding author,
- Acknowledgment of the individuals who contributed to the preparation of the manuscript but who do not fulfil the authorship criteria.

Abstract: Abstract with subheadings should be written as structured abstract in submitted papers except for Review Articles and Letters to the Editor. Please check Table 1 below for word count specifications (250 words).

Keywords: Each submission must be accompanied by a minimum of three to a maximum of six keywords for subject indexing at the end of the abstract. The keywords should be listed in full without abbreviations.

Manuscript Types

Original Articles: This is the most important type of article since it provides new information based on original research. A structured abstract is required with original articles and it should include the following subheadings: Objective, Materials and Methods, Results and Conclusion. The main text of original articles should be structured with Introduction, Materials and Methods, Results, Discussion, and Conclusion subheadings. Please check Table 1 for the limitations of Original Articles.

Statistical analysis to support conclusions is usually necessary. Statistical analyses must be conducted in accordance with international statistical reporting standards. Information on statistical analyses should be provided with a separate subheading under the Materials and Methods section and the statistical software that was used during the process must be specified.

Units should be prepared in accordance with the International System of Units (SI).

Short Communications: Short communication is for a concise, but independent report representing a significant contribution to Biology. Short communication is not intended to publish preliminary results. But if these results are of exceptional interest and are particularly topical and relevant will be considered for publication.

Short Communications should include an abstract and should be structured with the following subheadings: "Introduction", "Materials and Methods", "Results and Discussion".

Editorial Comments: Editorial comments aim to provide a brief critical commentary by reviewers with expertise or with high reputation in the topic of the research article published in the journal. Authors are selected and invited by the journal to provide such comments. Abstract, Keywords, and Tables, Figures, Images, and other media are not included.

Review Articles: Reviews prepared by authors who have extensive knowledge on a particular field and whose scientific background has been translated into a high volume of publications with a high citation potential are welcomed. These authors may even be invited by the journal. Reviews should describe, discuss, and evaluate the current level of knowledge of a topic in clinical practice and should guide future studies. The main text should contain Introduction, Experimental and Clinical Research Consequences, and Conclusion sections. Please check Table 1 for the limitations for Review Articles.

Letters to the Editor: This type of manuscript discusses important parts, overlooked aspects, or lacking parts of a previously published article. Articles on subjects within the scope of the journal that might attract the readers' attention, particularly educative cases, may also be submitted in the form of a "Letter to the Editor." Readers can also present their comments on the published manuscripts in the form of a "Letter to the Editor." Abstract, Keywords, and Tables, Figures, Images, and other media should not be included. The text should be unstructured. The manuscript that is being commented on must be properly cited within this manuscript.

Tables

Tables should be included in the main document, presented after the reference list, and they should be numbered consecutively in the order they are referred to within the main text. A descriptive title must be placed above the tables. Abbreviations used in the tables should be defined below the tables by footnotes (even if they are defined within the main text). Tables should be created using the "insert table" command of the word processing software and they should be arranged clearly to provide easy reading. Data presented in the tables should not be a repetition of the data presented within the main text but should be supporting the main text.

Figures and Figure Legends

Figures, graphics, and photographs should be submitted as separate files (in TIFF or JPEG format) through the submission system. The files should not be embedded in a Word document or the main document. When there are figure subunits, the subunits should not be merged to form a single image. Each subunit should be submitted separately through the submission system. Images should not be labeled (a, b, c, etc.) to indicate figure sub-

Table 1. Limitations for each manuscript type

Type of manuscript	Word limit	Abstract word limit	Reference limit	Table limit	Figure limit
Original Article	4500	250 (Structured)	No limit	6	Maximum 10
Short Communication	2500	200	30	3	4
Review Article	5500	250	No limit	5	6
Letter to the Editor	500	No abstract	5	No tables	No media

nits. Thick and thin arrows, arrowheads, stars, asterisks, and similar marks can be used on the images to support figure legends. Like the rest of the submission, the figures too should be blind. Any information within the images that may indicate an individual or institution should be blinded. The minimum resolution of each submitted figure should be 300 DPI. To prevent delays in the evaluation process, all submitted figures should be clear in resolution and large in size (minimum dimensions: 100 × 100 mm). Figure legends should be listed at the end of the main document.

All acronyms and abbreviations used in the manuscript should be defined at first use, both in the abstract and in the main text. The abbreviation should be provided in parentheses following the definition.

When a drug, chemical, product, hardware, or software program is mentioned within the main text, product information, including the name of the product, the producer of the product, and city and the country of the company (including the state if in USA), should be provided in parentheses in the following format: "Discovery St PET/CT scanner (General Electric, Milwaukee, WI, USA)"

All references, tables, and figures should be referred to within the main text, and they should be numbered consecutively in the order they are referred to within the main text.

Limitations, drawbacks, and the shortcomings of original articles should be mentioned in the Discussion section before the conclusion paragraph.

References

While citing publications, preference should be given to the latest, most up-to-date publications. If an ahead-of-print publication is cited, the DOI number should be provided. Authors are responsible for the accuracy of references. Journal titles should be abbreviated in accordance with the journal abbreviations in Index Medicus/ MEDLINE/PubMed. When there are six or fewer authors, all authors should be listed. If there are seven or more authors, the first six authors should be listed followed by "et al." In the main text of the manuscript, references should be cited using Arabic numbers in parentheses. The reference styles for different types of publications are presented in the following examples.

Journal Article: Rankovic A, Rancic N, Jovanovic M, Ivanović M, Gajo-ović O, Lazić Z, et al. Impact of imaging diagnostics on the budget – Are we spending too much? *Vojnosanit Pregl* 2013; 70: 709-11.

Book Section: Suh KN, Keystone JS. Malaria and babesiosis. Gorbach SL, Barlett JG, Blacklow NR, editors. *Infectious Diseases*. Philadelphia: Lippincott Williams; 2004.p.2290-308.

Books with a Single Author: Sweetman SC. *Martindale the Complete Drug Reference*. 34th ed. London: Pharmaceutical Press; 2005.

Editor(s) as Author: Huizing EH, de Groot JAM, editors. *Functional reconstructive nasal surgery*. Stuttgart-New York: Thieme; 2003.

Conference Proceedings: Bengissson S, Sothemin BG. Enforcement of data protection, privacy and security in medical informatics. In: Lun KC, Degoulet P, Piemme TE, Rienhoff O, editors.

MEDINFO 92. Proceedings of the 7th World Congress on Medical Informatics; 1992 Sept 6-10; Geneva, Switzerland. Amsterdam: North-Holland; 1992. pp.1561-5.

Scientific or Technical Report: Cusick M, Chew EY, Hoogwerf B, Agrón E, Wu L, Lindley A, et al. Early Treatment Diabetic Retinopathy Study Research Group. Risk factors for renal replacement therapy in the Early Treatment Diabetic Retinopathy Study (ETDRS), *Kidney Int*: 2004. Report No: 26.

Thesis: Yılmaz B. Ankara Üniversitesindeki Öğrencilerin Beslenme Durumları, Fiziksel Aktiviteleri ve Beden Kitle İndeksleri Kan Lipidleri Arasındaki İlişkiler. H.Ü. Sağlık Bilimleri Enstitüsü, Doktora Tezi. 2007.

Epub Ahead of Print Articles: Cai L, Yeh BM, Westphalen AC, Roberts JP, Wang ZJ. Adult living donor liver imaging. *Diagn Interv Radiol*. 2016 Feb 24. doi: 10.5152/dir.2016.15323. [Epub ahead of print].

Manuscripts Published in Electronic Format: Morse SS. Factors in the emergence of infectious diseases. *Emerg Infect Dis* (serial online) 1995 Jan-Mar (cited 1996 June 5): 1(1): (24 screens). Available from: URL: [http:// www.cdc.gov/ncidod/EID/cid.htm](http://www.cdc.gov/ncidod/EID/cid.htm).

REVISIONS

When submitting a revised version of a paper, the author must submit a detailed "Response to the reviewers" that states point by point how each issue raised by the reviewers has been covered and where it can be found (each reviewer's comment, followed by the author's reply and line numbers where the changes have been made) as well as an annotated copy of the main document. Revised manuscripts must be submitted within 30 days from the date of the decision letter. If the revised version of the manuscript is not submitted within the allocated time, the revision option may be cancelled. If the submitting author(s) believe that additional time is required, they should request this extension before the initial 30-day period is over.

Accepted manuscripts are copy-edited for grammar, punctuation, and format. Once the publication process of a manuscript is completed, it is published online on the journal's webpage as an ahead-of-print publication before it is included in its scheduled issue. A PDF proof of the accepted manuscript is sent to the corresponding author and their publication approval is requested within 2 days of their receipt of the proof.

Editor in Chief: Prof. Sehnaz BOLKENT

Address: Istanbul University, Faculty of Science, Department of Biology, 34134 Vezneciler, Fatih, Istanbul, TURKEY

Phone: +90 212 4555700 (Ext. 15079)

Fax: +90 212 5280527

E-mail: sbolkent@istanbul.edu.tr

Contents

Research Articles

- 1** **The Effects of Ghrelin on Renal Complications in Newborn Diabetic Rats**
Ayse Karatug Kacar, Ozlem Sacan, Neslihan Ozicli, Sehnaz Bolkent, Refiye Yanardag, Sema Bolkent
- 7** **Gross Morphology, Histology and Ultrastructure of the Nymphal Ileum of *Conocephalus (Xiphidion) fuscus fuscus* (Fabricius, 1793) (Orthoptera, Tettigoniidae)**
Damla Amutkan Mutlu, Irmak Polat, Zekiye Suludere
- 14** **A Fourier Transform Infrared Spectroscopic Investigation of *Macrovipera lebetina lebetina* and *M. l. obtusa* Crude Venoms**
Nasit Igci, Fatma Duygu Ozel Demiralp
- 23** ***In vitro* Antidiabetic Activity of Seven Medicinal Plants Naturally Growing in Turkey**
Ebru Deveci, Gulsen Tel-Cayan, Mehmet Emin Duru
- 29** **Antioxidative Effects of Mash Beans Depending on Gender and High Fat Intake in a Model Organism**
Eda Gunes, Gulsum Rabia Sahin
- 36** **Apoptosis Signaling Pathway Regulates the Gene Expression in the Yeast Retrotransposons Ty1 and Ty2**
Ceyda Colakoglu, Sezai Türkel
- 43** **Conserved Protein YpmR of Moderately Halophilic *Bacillus licheniformis* has Hydrolytic Activity on p-Nitrophenyl Laurate**
Abdoulie O. Touray, Ayse Ogan, Kadir Turan

Review Article

- 51** **Caspase-1: Past and Future of this Major Player in Cell Death and Inflammation**







Elif Eren, Nesrin Ozoren

Short Communication

- 62** **Comparison of the Anti-Legionella Fill Material against Standard Polypropylene Fill Material in Model Cooling Tower Water System**

Irfan Turetgen, Cansu Vatansever

The Effects of Ghrelin on Renal Complications in Newborn Diabetic Rats

Ayse Karatug Kacar¹ , Ozlem Sacan² , Neslihan Ozicli³ , Sehnaz Bolkent¹ ,
Refiye Yanardag² , Sema Bolkent³ 

¹Istanbul University, Faculty of Science, Department of Biology, Istanbul, Turkey

²Istanbul University-Cerrahpasa, Faculty of Engineering, Department of Chemistry, Istanbul, Turkey

³Istanbul University-Cerrahpasa, Cerrahpasa Faculty of Medicine, Department of Medical Biology, Istanbul, Turkey

ORCID IDs of the authors: A.K.K. 0000-0001-6032-470X; O.S. 0000-0001-6503-4613; N.O. 0000-0001-9991-3421; S.B. 0000-0002-1112-5162; R.Y. 0000-0003-4185-4363; S.B. 0000-0001-8463-5561

Please cite this article as: Karatug Kacar A, Sacan O, Ozicli N, Bolkent S, Yanardag R, Bolkent S. The Effects of Ghrelin on Renal Complications in Newborn Diabetic Rats. Eur J Biol 2020; 79(1): 1-6. DOI: 10.26650/EurJBiol.2020.0043

ABSTRACT

Objective: Ghrelin is an orexigenic hormone mainly released from the stomachs of rats and takes a significant part in the development of newborn rats. Ghrelin has been shown to possess antioxidant, anti-apoptotic, and anti-inflammatory properties. In this study, we aimed to examine microscopical and biochemical parameters in the kidney of newborn non-treated diabetic and ghrelin-treated diabetic rats.

Materials and Methods: Wistar-type newborn rats were divided into four groups. First group: control rats given physiological saline for four weeks; second group: control animals given ghrelin from the third day to the fourth week; third group: diabetic rats given streptozotocin (STZ) on the second day after birth as a single dose; fourth group: diabetic rats given ghrelin from the third day to the fourth week.

Results: There was no microscopic difference between the kidney tissues of non-treated diabetic and ghrelin-treated diabetic rats. Lipid peroxidation levels decreased, while superoxide dismutase, catalase activities, and glutathione levels increased in the diabetic group given ghrelin. Serum urea, uric acid, creatinine levels, myeloperoxidase, and xanthine oxidase activities decreased in diabetic rats treated with ghrelin.

Conclusion: It can be said that the ghrelin given exogenously has a protective effect in some degree on renal complications in newborn diabetic rats.

Keywords: Diabetes, ghrelin, kidney

INTRODUCTION

The pancreas has four main types of endocrine cells. The first one of them is alpha cells, which synthesize glucagon, the second one is beta cells, which synthesize insulin, the third one is delta cells, which synthesize somatostatin, the fourth one is pancreatic polypeptide (PP) cells, which synthesize pancreatic polypeptide (1-3), and the fifth type is ghrelin cells, which synthesize ghrelin in mammalian pancreatic islet cells (4,5). Ghrelin cells are the most important source of ghrelin in the fetal peri-

od (6). Their number increases during this period, and these cells are located around pancreatic islands (4,5). It has been shown that when the number of beta cells decreases, the number of ghrelin cells increases in experimental mouse models (5). Ghrelin controls glucose metabolism (7). Ghrelin levels decrease in type 2 diabetes individuals and healthy offspring of them (8-10). There is a relationship between ghrelin and insulin levels. The authors demonstrated that insulin plays an important role in inhibition of nutrition-related ghrelin as a modu-



Corresponding Author: Ayse Karatug Kacar

E-mail: akaratug@istanbul.edu.tr

Submitted: 18.11.2019 • **Revision Requested:** 27.12.2019 • **Last Revision Received:** 21.01.2020 •

Accepted: 28.01.2020 • **Published Online:** 11.03.2020

© Copyright 2020 by The Istanbul University Faculty of Science • Available online at <http://ejb.istanbul.edu.tr> • DOI: 10.26650/EurJBiol.2020.0043

lator of plasma ghrelin (11,12). Furthermore, the hyperglycemic and lowering effect also occurred when ghrelin is given to a healthy human. These findings reveal effects of ghrelin on insulin secretion and glucose metabolism (13,14).

Diabetes mellitus is a chronic metabolic disease. Prolonged hyperglycemia causes damage to some tissues, such as kidney tissue, and an increase in oxidative stress. This situation induces renal damage. Therefore, kidney damage is associated with increased oxidative stress (15). Renal failures are the cause of diabetic nephropathy. One of the mortalities caused in patients who have insulin-dependent and non-insulin-dependent diabetes is renal disease (16). Diabetic nephropathy is a major problem in diabetic patients (17). Reactive oxygen species (ROS) has an important role in diabetic pathogenesis (18). Antioxidants protect cells and tissues from oxidative damage (19). The kidney damage caused by oxidative stress is reduced by increased antioxidant levels. Ghrelin may be an important antioxidant agent with increasing antioxidant enzyme activities (20,21). Increased ROS levels and decreased antioxidant levels are observed in diabetes (22). Then, free radicals come into play, and this situation occurs with nonenzymatic glycation of proteins, oxidation of glucose, increase of lipid peroxidation (LPO), and the development of insulin resistance (23). Oxidative stress emerges from an imbalance between the formed radicals and the level of antioxidants. It has been shown in many studies that complications that occur in diabetes cause the development of oxidative stress (18,24,25). Ghrelin has an antioxidant effect and is a strong lipolytic hormone (26). Fujimura et al. demonstrated that ghrelin has a significant role in the decrease of ROS levels in angiotensin II-induced renal damage in mice (27).

In the present study, it was purposed to reveal the anti-proliferative and antioxidants effects of ghrelin microscopically and biochemically in the kidney of newborn normal and STZ-induced diabetic rats following exogenous administration of ghrelin.

MATERIAL AND METHODS

Animals

The Local Ethics Committee on Animal Research of Istanbul University approved for all the experimental procedures. In this study, newborn Wistar albino female and male rats were divided into four groups (n=5 per group, totally 20 rats in histological and immunohistochemical assays; n=13 for control and ghrelin control groups, n=9 for diabetic and diabetic group given ghrelin, totally 44 rats in biochemical assays). In the first group, which was the control group, physiological saline was given intraperitoneally for four weeks. Ghrelin (AnaSpec, Fremont, CA, USA, 24160) was given subcutaneously as 100 µg/kg/day from the third day to the fourth week to the second group rats. Rats in the third group, which was the diabetic group, were treated with a single dose of 100 mg/kg streptozotocin (STZ) on the second day after birth to induce newborn diabetes, intraperitoneally. Ghrelin after STZ injection was given to the rats in the last group. At the end of the experiment, the rats were sacrificed. Their blood samples were taken for biochemical analysis,

and kidney tissues were taken for examining microscopical and biochemical parameters.

Histological and Immunohistochemical Assays

Kidney tissues fixed in Bouin's solution for 24 hours at room temperature were used. After the series of ethanol and xylene for dehydration and cleaning, the kidney tissues were embedded in paraffin. The embedded kidney tissues were cut as a 5 µm section for a histological assay and a 4 µm section for an immunohistochemical assay. The kidney tissues were stained with a Periodic Acid Schiff reagent for microscopy analysis. The poly-L-lysine was used to coat microscope slides. The sections were placed on these slides for the immunohistochemical assay. Caspase-3 and proliferating cell nuclear antigen (PCNA) were investigated for immunohistochemical assay. The paraffin was removed by keeping the sections in toluene. After this stage, the sections were incubated with hydrogen peroxide (3%) to block the endogenous peroxidase activity. The Histostain Plus Broad Spectrum Kit (Zymed, 85-9743, South San Francisco, CA), PCNA antibody (Ab-1 MS-106-P, Neomarkers, Fremont, CA, dilution 1:50, 30 minutes at room temperature), and caspase-3 (Millipore AB3623, Bedford, MA, USA; dilution 1:50, overnight at +4°C) were utilized for immunohistochemical labeling by employing the streptavidin-biotin-peroxidase technique. The 3-amino-9-ethyl carbazole was used to detect of immunoreactivity. Mayer's hematoxylin was used for counterstain of the sections and mounted using glycerol vinyl alcohol mounting medium.

Histological and immunohistochemical assays were conducted by using an X40 objective and X10 ocular system of the Olympus CX-45 microscope as Microscopic analysis. The results were explained by the histological score with a grade from 0 to 3 as negative (0), weak (1), moderate (2), and strong (3). PCNA immunopositive cells were counted for each slide at a minimum of ten random fields.

Biochemical Assays

In the previous study, blood glucose levels were measured, and Turk et al. decided that the rats were diabetic (28). Creatinine, uric acid, and serum urea levels were investigated by the methods of Jaffe reaction (29), Caraway (30), and acetylmonoxime (31), respectively. Cold 0.9% NaCl and glass equipment were used for homogenization of kidney tissues. 10% (w/v) homogenate was obtained. It was centrifuged. Clear supernatants were utilized for protein, glutathione (GSH), and LPO levels and antioxidant enzyme analysis. GSH levels were determined in accordance with the Beutler method using Ellman's reagent (32). LPO levels were investigated by Ledwozyw's method in kidney homogenates (33). Catalase (CAT) activity was determined in accordance with Aebi (34), superoxide dismutase (SOD) activity in accordance with Mylroie's method (35), myeloperoxidase (MPO) activity in accordance with Wei and Frenkel (36), and xanthine oxidase (XO) activity in accordance with Corte and Stirpe with a number of modifications (37). The protein level was determined by employing the method of Lowry in the supernatants. The bovine serum albumin was used as standard for this method (38).

Statistical Analysis

The Mann-Whitney U tests and the two-way ANOVA using GraphPad Prism version 4.0 computer package were used for analysis of the histological and immunohistochemical data. The unpaired Student's *t*-test and one-way ANOVA using the NCSS statistical computer package were used for the biochemical results. The results were presented as mean±SE for histological and immunohistochemical assays; as mean±SD for biochemical assays. P values less than 0.05 were considered significant.

RESULTS

Histological and Immunohistochemical Assays

Degenerative changes such as expansion in the capsular spaces of glomeruli, ruptures at the brush border in apical, desquamated nuclei and cytoplasmic debris in the lumen of proximal tubules, necrotic areas, moderate cytoplasmic vacuolar degeneration, and hyperemia in the kidney tissue of rats given STZ were determined. These changes were not changed in the kidney tissue of the diabetic animals given ghrelin (Figure 1).

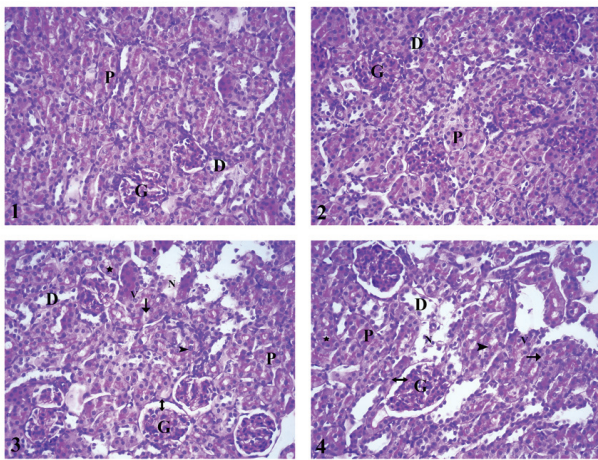


Figure 1. A normal histological appearance was observed in the kidney tissue of the control (1), control group given ghrelin (2), STZ group (3), diabetic group given ghrelin (4). G: Glomeruli, P: Proximal tubules, D: Distal tubules, N: Necrotic area, V: Vacuolar degeneration, ►: Ruptures at the brush border in apical, *: Cytoplasmic debris and ►: Desquamated nuclei in the lumen of proximal tubules, ↔: Expansion in capsular spaces of glomeruli. Periodic Acid Schiff (PAS) staining technique. 400x magnification

PCNA immune⁺ cell number as cell proliferation increased in the diabetic group given STZ compared to both the control groups. In the diabetic group given ghrelin, cell proliferation decreased compared to the control group given ghrelin, while it decreased in comparison with the diabetic group. PCNA immune⁺ cell number (Figures 2A and 2B) was observed. Caspase-3 immune⁺ cell number did not exhibit a difference between the four groups statistically (Data not shown).

Biochemical Assays

The serum uric acid and urea levels in the diabetic group were determined to have increased significantly in comparison with the control group (*p*<0.001; *p*<0.05). Ghrelin caused a significant decrease in creatinine, uric acid, and urea levels in the diabetic group (*p*<0.0001; *p*<0.001; *p*<0.05) (Table 1).

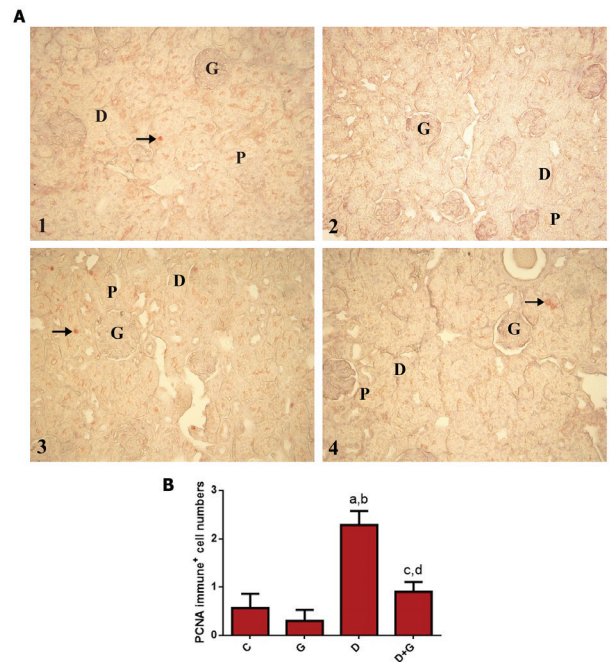


Figure 2. A) PCNA immune⁺ cells (►) are observed with immunohistochemistry in kidney tissue of the control group (1), control group given ghrelin (2), STZ group (3), diabetic group given ghrelin (4). G: Glomeruli, P: Proximal tubules, D: Distal tubules. B) PCNA immune⁺ cell number for all groups. **p*<0.05 versus control group, ^b*p*<0.01 versus ghrelin group, ^c*p*<0.05 versus ghrelin group, ^d*p*<0.01 versus diabetic group. 400x magnification

Table 1. Serum urea, creatinine and uric acid levels of all groups

Group	Urea (mg/dL)*	Creatinine (mg/dL)*	Uric Acid (mg/L)*
Control	59.84±7.48	1.32±0.15	4.23±0.22
Control+Ghrelin	76.19±26.14	0.65±0.23 ^c	3.39±0.67 ^a
Diabetic	106.41±20.41 ^a	1.42±0.02 ^d	5.14±0.39 ^f
Diabetic+Ghrelin	72.79±5.84 ^b	0.51±0.03 ^e	3.20±0.67 ^g
P _{ANOVA}	0.041	0.0001	0.0001

*Mean±SD; ^a*p*<0.05 versus control group, ^b*p*<0.05 versus diabetic group, ^c*p*<0.0001 versus control group, ^d*p*>0.05 versus control group, ^e*p*<0.0001 versus diabetic group, ^f*p*<0.001 versus control group and ^g*p*<0.001 versus diabetic group.

Table 2. Kidney glutathione (GSH) and lipid peroxidation (LPO) levels of all groups

Group	GSH (nmol GSH/mg protein)*	LPO (nmol MDA/mg protein)*
Control	10.46±3.56	0.39±0.03
Control+ Ghrelin	9.64±2.63	0.41±0.04
Diabetic	2.73±1.15 ^a	0.65±0.05 ^c
Diabetic+ Ghrelin	11.31±2.21 ^b	0.37±0.07 ^d
P _{ANOVA}	0.0001	0.0001

*Mean ± SD; ^ap<0.0001 versus control group, ^bp<0.0001 versus diabetic group, ^cp<0.001 versus control group and ^dp<0.001 versus diabetic group.

A significant reduction in GSH levels was determined in the diabetic group in comparison with the control groups (p<0.0001). Ghrelin administered to the diabetic rats induced a significant increase in GSH levels in the kidney (p<0.0001). LPO levels was increase significantly in the diabetic rats compared to the control groups (p<0.001). There was a decrease in LPO levels in the kidney with given ghrelin to STZ-diabetic rats (p<0.001) (Table 2).

A significant reduction in kidney CAT and SOD activities were determined in the diabetic group in comparison with the control groups (p<0.0001). However, MPO and XO activities significantly increased in the diabetic group compared to the control group (p<0.001; p<0.05) (Table 3). The exogenously administered ghrelin induced an increase in kidney CAT and SOD activities (p<0.001; p<0.005), and a decrease in kidney MPO and XO activities in the diabetic rats (p<0.05; p<0.0001) (Table 3).

Table 3. Kidney catalase (CAT), superoxide dismutase (SOD), myeloperoxidase (MPO) and xanthine oxidase (XO) activities of all groups

Group	CAT (U/mg protein)*	SOD (U/g protein)*	MPO (U/g tissue)*	XO (U/g protein)
Control	291.45±41.44	15.05±4.57	41.57±5.87	1.89±0.67
Control+Ghrelin	218.32±86.91 ^a	11.60±4.84	44.07±11.91	1.31±0.82
Diabetic	211.83±36.69 ^b	7.47±0.88 ^b	83.10±14.84 ^e	2.60±0.28 ^a
Diabetic+Ghrelin	269.01±8.82 ^c	9.66±1.41 ^d	38.03±14.63 ^f	1.73±0.19 ^g
P _{ANOVA}	0.003	0.001	0.001	0.001

*Mean ± SD; ^ap<0.05 versus control group, ^bp<0.0001 versus control group, ^cp<0.001 versus diabetic group, ^dp<0.005 versus diabetic group, ^ep<0.001 versus control group, ^fp<0.05 versus diabetic group and ^gp<0.0001 versus diabetic group.

DISCUSSION

The blood glucose levels decreased in diabetic rats given ghrelin compared to non-treated diabetic rats (28). Ghrelin administration inhibits the diabetic effects as a result of reducing the blood glucose levels in newborn diabetic rats. Brouwers et al. showed that kidney damage occurred as a result of administering 250 mg/kg STZ doze to mice (39). They have observed disruption of the brush border, the loss of nucleus in proximal tubule cells, dilatation of non-proximal tubules, and moderate acute tubular injury. Koyuturk et al. found that ghrelin reduced cell proliferation and caspase 8 activity, while caspase-3 activity did not change in the liver tissue of ghrelin-administrated dia-

betic rats (40). Renal damage caused by ischemia/reperfusion or cisplatin showed that ghrelin administration reduced apoptosis (41,42). In the present study, some degenerative changes in the STZ treated kidney tissue of newborn rats were determined. Ghrelin did not reverse these changes in diabetic animals. Ghrelin did not affect the renal injury of experimental diabetic rats microscopically. However, PCNA immune+ cell number decreased with the administration of ghrelin in diabetic rats. Proximal tubule epithelial cells start to proliferate to prevent acute injury (43,44). Proliferation increases in the proximal tubule after injury. Therefore, the occurred cell number decrease by cell death is compensated (45). Danilewicz and Wagrowska-Danilewicz suggest that cell proliferation was inhibited by ghrelin in control kidney tissues and non-proliferative glomerulopathies. The lack or low level of this protein in proliferative glomerulopathies was observed (46). It was thought that when the cells were damaged, it increased the number of cells to prevent damage. Therefore, PCNA immune+ cell number increased in the diabetic group. It decreased because of reduced damage with the administration of ghrelin.

Necrotic areas in the kidney tissue of the experimental group were determined by histochemical staining, and it was desired to investigate caspase-3 activity to determine apoptosis, a form of cell death. There were no changes in caspase-3 between the four groups. We thought that cell death might occur in the diabetic group. However, apoptotic cell death did not occur with the administration of STZ, statistically.

Creatinine levels decreased with the administration of ghrelin in renal damage caused by cisplatin (42). In another study, creatinine levels were shown to be higher compared to the control group in diabetic nephropathy (47,48). Van Ginhoven et al. have shown that urea levels increased after reperfusion (49). However, there were no changes between both the control group and the group given ghrelin. Furthermore, uric acid, urea, and creatinine levels increased in an experimental model of diabetic nephropathy compared to the control group (50). In our study, uric acid, creatinine, and serum urea levels reduced in the diabetic group given ghrelin. It can be said that ghrelin takes a significant part in the prevention of renal damage.

Ghrelin increases antioxidant activity. Therefore, it has antioxidant properties in the rat kidney tissue (51). The authors indicated that SOD and GSH levels reduced in the kidney tissue in the diabetic group compared to the control group (52). In another similar study, CAT, SOD activities and GSH levels reduced, while malondialdehyde levels increased in diabetic nephropathy in comparison with the control group (50). Sudhakara et al., have shown that LPO and XO levels increased in the kidney tissue of diabetic rats (53). Sacan et al., has shown that LPO, CAT, SOD, MPO, and XO significantly increased, while GSH levels reduced in lung tissues in diabetic rats in comparison with the control group (54). In our study, kidney GSH level, SOD, and CAT activities significantly increased, while XO and MPO activities and LPO level significantly reduced in the diabetic group given ghrelin. Ghrelin reversed biochemical changes in diabetic rats.

CONCLUSION

The biochemical results showed that ghrelin provides recovery of complications in kidney tissue in newborn diabetic rats. Ghrelin treatment partially reversed the renal injury of experimental diabetic rats because of the antioxidant properties of ghrelin.

Peer-review: Externally peer-reviewed.

Author Contributions: Conception/Design of study: S.B., N.O.; Data Acquisition: A.K.K., O.S., R.Y.; Data Analysis/Interpretation: A.K.K., O.S., R.Y.; Drafting Manuscript: A.K.K.; Critical Revision of Manuscript: A.K.K., O.S., S.B., R.Y., S.B.; Final Approval and Accountability: A.K.K., O.S., S.B., R.Y., S.B.; Technical or Material Support: S.B., O.S., R.Y., S.B.; Supervision: S.B.

Conflict of Interest: The authors declare that they have no conflicts of interest to disclose.

Financial Disclosure: This work was supported by Scientific Research Project Coordination Unit of Istanbul University. Project No. B.Y.P-36942.

REFERENCES

1. Edlund H. Developmental biology of the pancreas. *Diabetes* 2001; 50(Suppl 1): S5-S9.
2. Brissova M, Fowler MJ, Nicholson WE, Chu A, Hirshberg B, Harlan DM, et al. Assessment of human pancreatic islet architecture and composition by laser scanning confocal microscopy. *J Histochem Cytochem* 2005; 53: 1087-97.
3. Cabrera O, Berman DM, Kenyon NS, Ricordi C, Berggren PO, Caicedo A. The unique cytoarchitecture of human pancreatic islets has implications for islet cell function. *Proc Natl Acad Sci USA* 2006; 103: 2334-9.
4. Wierup N, Svensson H, Mulder H, Sundler F. The ghrelin cell: a novel developmentally regulated islet cell in the human pancreas. *Regul Pept* 2002; 107: 63-9.
5. Prado CL, Pugh-Bernard AE, Elghazi L, Sosa-Pineda B, Sussel L. Ghrelin cells replace insulin-producing beta cells in two mouse models of pancreas development. *Proc Natl Acad Sci USA* 2004; 101: 2924-9.
6. Chanoine JP, Wong AC. Ghrelin gene expression is markedly higher in foetal pancreas compared with foetal stomach: effect of maternal fasting. *Endocrinology* 2004; 145: 3813-20.
7. O. Ukkola, Ghrelin and metabolic disorders. *Curr Protein Pept Sc* 2009; 10-1: 2-7.
8. Ostergard T, Hansen TK, Nyholm B, Gravholt CH, Djurhuus CB, Hosoda H, et al. Circulating ghrelin concentrations are reduced in healthy offspring of type 2 diabetic subjects, and are increased in women independent of a family history of type 2 diabetes. *Diabetologia* 2003; 46-1: 134-6.
9. Poikko SM, Kellokoski E, Horkkoe S, Kauma H, Kesäniemi YA, Ukkola O. Low plasma ghrelin is associated with insulin resistance, hypertension, and the prevalence of type 2 diabetes. *Diabetes* 2003; 52-10: 2546-53.
10. Barazzoni R, Zanetti M, Ferreira C, Vinci P, Pirulli A, Mucci M, et al. Relationships between desacylated and acylated ghrelin and insulin sensitivity in the metabolic syndrome. *J Clin Endocrinol Metab* 2007; 92: 3935-40.
11. McCowen KC, Maykel JA, Bistran BR, Ling PR. Circulating ghrelin concentrations are lowered by intravenous glucose or hyperinsulinemic euglycemic conditions in rodents. *J Endocrinol* 2002; 175: R7-R11.
12. Saad MF, Bernaba B, Hwu CM, Jinagouda S, Fahmi S, Kogosov E, et al. Insulin regulates plasma ghrelin concentration. *J Clin Endocrinol Metab* 2002; 87: 3997-4000.
13. Broglio F, Arvat E, Benso A, Gottero C, Muccioli G, Papotti M, et al. Ghrelin, a natural GH secretagogue produced by the stomach, induces hyperglycemia and reduces insulin secretion in humans. *J Clin Endocrinol Metab* 2001; 86: 5083-6.
14. Broglio F, Gottero C, Prodham F, Gauna C, Muccioli G, Papotti M, et al. Non-acylated ghrelin counteracts the metabolic but not the neuroendocrine response to acylated ghrelin in humans. *J Clin Endocrinol Metab* 2004; 89: 3062-5.
15. Nasri H, eian-Kopaei MR. Protective effects of herbal antioxidants on diabetic kidney disease. *J Res Med Sci* 2014; 82-3.
16. Cooper ME. Pathogenesis, prevention, and treatment of diabetic nephropathy. *Lancet* 1998; 352: 213-9.
17. Winegrad AL. Banting lecture 1986. Does a common mechanism induce the diverse complications of diabetes? *Diabetes* 1987; 36(3): 396-406.
18. Baynes, J.W. Role of oxidative stress in development of complications in diabetes. *Diabetes* 1991; 40: 405-12.
19. Freeman BA, Crapo JD. Biology of disease: free radicals and tissue injury. *Lab Invest* 1982; 47(5): 412-26.
20. Obay BD, Tasdemir E, Tumer C, Bilgin H, Atmaca M. Dose dependent effects of ghrelin on pentylenetetrazole-induced oxidative stress in a rat seizure model. *Peptides* 2008; 29: 448-55.
21. Zwirska-Korczala K, Adamczyk-Sowa M, Sowa P, Pilc K, Suchanek R, Pierzchala K, et al. Role of leptin, ghrelin, angiotensin II and orexins in 3T3 L1 preadipocyte cells proliferation and oxidative metabolism. *J Physiol Pharmacol* 2007; 58: 53-64.
22. Wiernsperger NF. Oxidative stress as a therapeutic target in diabetes: revisiting the controversy. *Diabetes Metab* 2003; 29: 579-85.
23. Maritim AC, Sanders RA, Watkins III JB. Diabetes, oxidative stress, and antioxidants: a review. *J Biochem Mol Toxicol* 2003; 17: 24-38.
24. Monnier L, Colette C, Mas E, Michel F, Cristol JP, Boegner C, et al. Regulation of oxidative stress by glycaemic control: evidence for an independent inhibitory effect of insulin therapy. *Diabetologia* 2009; 53: 562-71.
25. Aslam F, Iqbal S, Nasir M, Anjum AA. White sesame seed oil mitigates blood glucose level, reduces oxidative stress, and improves biomarkers of hepatic and renal function in participants with type 2 diabetes mellitus. *J Am Coll Nutr* 2018; 27: 1-12.

26. Korbonits M, Goldstone AP, Gueorguiev M, Grossman AB. Ghrelin a hormone with multiple functions. *Front Neuroendocrinol* 2004; 25(1): 27-68.
27. Fujimura K, Wakino S, Minakuchi H, Hasegawa K, Hosoya K, Komatsu M et al. Ghrelin protects against renal damages induced by angiotensin-II via an antioxidative stress mechanism in mice. *PLoS One* 2014; 9(4): e94373.
28. Turk N, Dagistanli FK, Sacan O, Yanardag R, Bolkent S. Obestatin and insulin in pancreas of newborn diabetic rats treated with exogenous ghrelin. *Acta Histochem* 2012; 114(4): 349-57.
29. Bonsnes RW, Taussky HH. On the colorimetric determination of creatinine by the Jaffe reaction. *J Biol Chem* 1945; 158: 581-91.
30. Caraway WT. Determination of uric acid in serum by a carbonate method. *Am J Clin Pathol* 1955; 25(7): 840-5.
31. Barker SB. The direct colorimetric determination of urea in blood and urine. *J Biol Chem* 1944; 152: 453-63.
32. Beutler E. Glutathione in red cell metabolism. In: *A Manual of Biochemical Methods*. New York: Grune and Stratton 1975; pp. 112-4.
33. Ledwozyw A, Michalak J, Stepień A, Kadziolka A. The relationship between plasma triglycerides, cholesterol, total lipids and lipid peroxidation products during human atherosclerosis. *Clin Chim Acta* 1986; 155: 275-83.
34. Aebi H. Catalase in vitro. *Methods Enzymol* 1984; 105: 121-6.
35. Mylorie AA, Collins H, Umbles C, Kyle J. Erythrocyte superoxide dismutase activity and other parameters of copper status in rats ingesting lead acetate. *Toxicol Appl Pharmacol* 1986; 82: 512-20.
36. Wei H, Frenkel K. In vivo formation of oxidized DNA bases in tumor promoter-treated mouse skin. *Cancer Res* 1991; 51(16): 4443-9.
37. Corte ED, Stirpe F. Regulation of xanthine oxidase in rat liver: Modifications of the enzyme activity of rat liver supernatant on storage at 20 degrees. *Biochem J* 1968; 108: 349-51.
38. Lowry OH, Rosebrough NJ, Farr AL, Randall RJ. Protein measurement with the Folin phenol reagent. *J Biol Chem* 1951; 193: 265-75.
39. Brouwers B, Pruniau VP, Cauwelier EJ, Schuit F, Lerut E, Ectors N, et al. Phlorizin pretreatment reduces acute renal toxicity in a mouse model for diabetic nephropathy. *J Biol Chem* 2013; 288(38): 27200-7.
40. Koyuturk M, Sacan O, Karabulut S, Turk N, Bolkent S, Yanardag R, et al. The role of ghrelin on apoptosis, cell proliferation and oxidant-antioxidant system in the liver of neonatal diabetic rats. *Cell Biol Int* 2015; 39(7): 834-41.
41. Takeda R, Nishimatsu H, Suzuki E, Satonaka H, Nagata D, Oba S, et al. Ghrelin improves renal function in mice with ischemic acute renal failure. *J Am Soc Nephrol* 2006; 17(1): 113-21.
42. Nojiri T, Hosoda H, Kimura T, Tokudome T, Miura K, Takabatake H, et al. Protective effects of ghrelin on cisplatin-induced nephrotoxicity in mice. *Peptides* 2016; 82: 85-91.
43. Cuppage FE, Neagoy DR, Tate A. Repair of the nephron following temporary occlusion of the renal pedicle. *Lab Invest* 1967; 17: 660-74.
44. Witzgall R, Brown D, Schwarz C, Bonventre JV. Localization of proliferating cell nuclear antigen, vimentin, c-Fos, and clusterin in the postischemic kidney. Evidence for a heterogenous genetic response among nephron segments, and a large pool of mitotically active and dedifferentiated cells. *J Clin Invest* 1994; 93: 2175-88.
45. Guo JK, Cantley LG. Cellular maintenance and repair of the kidney. *Annu Rev Physiol* 2010; 72: 357-76.
46. Danilewicz M, Wagrowska-Danilewicz M. Renal immunorepression of ghrelin is attenuated in human proliferative glomerulopathies. *Nefrologia* 2010; 30(6): 633-8.
47. Li Y, Liu J, Liao G, Zhang J, Chen Y, Li L, et al. Early intervention with mesenchymal stem cells prevents nephropathy in diabetic rats by ameliorating the inflammatory microenvironment. *Int J Mol Med* 2018; 41(5): 2629-39.
48. Wang D, Zhang G, Chen X, Wei T, Liu C, Chen C, et al. Sitagliptin ameliorates diabetic nephropathy by blocking TGF- β 1/Smad signaling pathway. *Int J Mol Med* 2018; 41(5): 2784-92.
49. van Ginhoven TM, Huisman TM, van den Berg JW, Ijzermans JN, Delhanty PJ, de Bruin RW. Preoperative fasting induced protection against renal ischemia/reperfusion injury is independent of ghrelin in mice. *Nutr Res* 2010; 30(12): 865-9.
50. Yarıbeygi H, Mohammadi MT, Rezaee R, Sahebkar A. Fenofibrate improves renal function by amelioration of NOX-4, IL-18, and p53 expression in an experimental model of diabetic nephropathy. *J Cell Biochem* 2018; 119(9): 7458-69.
51. Neamati S, Alirezaei M, Kheradmand A. Ghrelin Acts as an Antioxidant Agent in the Rat Kidney. *Int J Pept Res Ther* 2011; 17-3: 239-45.
52. Elsherbiny NM, Zaitone SA, Mohammad HMF, El-Sherbiny M. Renoprotective effect of nifuroxazide in diabetes-induced nephropathy: impact on NF κ B, oxidative stress, and apoptosis. *Toxicol Mech Method* 2018; 28-6: 467-473.
53. Sudhakara G, Ramesh B, Mallaiiah P, Sreenivasulu N, Saralakumari D. Protective effect of ethanolic extract of *Commiphora mukul* gum resin against oxidative stress in the brain of streptozotocin induced diabetic Wistar male rats. *Excli J* 2012; 11: 576-92.
54. Sacan O, Turkyilmaz IB, Bayrak BB, Mutlu O, Akev N, Yanardag R. Zinc supplementation ameliorates glycoprotein components and oxidative stress changes in the lung of streptozotocin diabetic rats. *Biometals* 2016; 29(2): 239-48.

Gross Morphology, Histology and Ultrastructure of the Nymphal Ileum of *Conocephalus (Xiphidion) fuscus fuscus* (Fabricius, 1793) (Orthoptera, Tettigoniidae)

Damla Amutkan Mutlu¹ , Irmak Polat² , Zekiye Suludere¹ 

¹Gazi University, Faculty of Science, Department of Biology, Ankara, Turkey

²Çankırı Karatekin University, Faculty of Science, Department of Biology, Çankırı, Turkey

ORCID IDs of the authors: D.A.M. 0000-0002-4780-8520; I.P. 0000-0001-7230-4589; Z.S. 0000-0002-1207-5814

Please cite this article as: Amutkan Mutlu D, Polat I, Suludere Z. Gross Morphology, Histology and Ultrastructure of the Nymphal Ileum of *Conocephalus (Xiphidion) fuscus fuscus* (Fabricius, 1793) (Orthoptera, Tettigoniidae). Eur J Biol 2020; 79(1): 7-13. DOI: 10.26650/EurJBiol.2020.0040

ABSTRACT

Objective: The alimentary canal is composed of the foregut, the midgut, and the hindgut in insects. The hindgut is the region where the reabsorption of the water and some ions occur and the feces are generated. The hindgut is generally divided into 3 parts as the ileum, the colon and the rectum in insects. The morphological and fine structures of these parts can be used as the taxonomical character. The aim of this study is to investigate the fine structure and morphology of the ileum in the last instar nymph of *Conocephalus (Xiphidion) fuscus fuscus* (Fabricius, 1793) (Orthoptera, Tettigoniidae).

Materials and Methods: In this study, morphology, histology, and ultrastructure of the ileum in the last instar nymphal *C. fuscus fuscus* were examined by stereomicroscope, light microscope, scanning electron microscope, and transmission electron microscope.

Results: Ileum is a tube-like structure, which is situated between the midgut and the colon. The wall of the ileum is composed of muscle tissue, connective tissue, epithelial tissue, and cuticular intima from the outermost to the innermost. Those single-layered epithelial cells have globular nuclei, and some granulated endoplasmic reticulum can be observed in photographs. Besides, the regenerative cells groups called regenerative nidi are clear in some basal regions of the epithelial layer.

Conclusion: The general morphology and structure of the nymphal ileum in *C. fuscus fuscus* have some differences with the insects belonging to Orthoptera orders, but its histological, cytological, and fine structure are very alike.

Keywords: Digestive system, hindgut, ileum, light microscope, electron microscope

INTRODUCTION

The alimentary system of the insect is a structure which continues from the mouth to the end of the anus. The digestive system is basically divided into three regions in insects. These regions are the foregut, the midgut, and the hindgut (1-13). The foregut contains the esophagus, the pharynx, the crop, and the proventriculus. The midgut consists of the gastric caecum and the ventriculus. The hindgut is divided into three parts: the ileum, the colon, and the rectum. The ileum has an ectodermal origin, and the inside of the epithelium is lined by a cuticle (14-18).

The Malpighian tubules and the hindgut interoperate in excretory system of terrestrial insects. The primary isosmotic filtrate is produced by the Malpighian tubule cells, and then it is discharged in the lumen of ileum. The volume and composition of this filtrate starts to modify in the ileum lumen. The main role of the ileum in insects, as the intermediate step of the excretory system, is secretion, food digestion, and reabsorption of the water, ions, and metabolic residues (16,18-31). Besides, in some insects such as *Schistocerca gregaria* (Orthoptera: Acrididae), the ileum contributes to the osmoregulation (32).

Corresponding Author: Damla Amutkan Mutlu E-mail: damlamutkan@gazi.edu.tr

Submitted: 08.11.2019 • **Revision Requested:** 05.12.2019 • **Last Revision Received:** 23.01.2020 •

Accepted: 30.01.2020 • **Published Online:** 20.03.2020

© Copyright 2020 by The Istanbul University Faculty of Science • Available online at <http://ejb.istanbul.edu.tr> • DOI: 10.26650/EurJBiol.2020.0040



Conocephalus (Xiphidion) fuscus fuscus (Fabricius, 1793) (Tettigoniidae), which can be found in parts of France, Sweden, Kazakhstan, Northern Africa, Bulgaria, Germany, Romania, Spain, Iran, Pakistan, Switzerland, Italy, Middle Asia, the Netherlands, and Turkey, is a species that belongs to Orthoptera order. The increase in the global climate in recent years has had a highly significant impact on the spread of this species. *C. fuscus fuscus* is a phytophagous species which feeds primarily on grasses (33,34).

Since the studies regarding the histology and ultrastructure of the ileum in insects are very limited, we aimed to examine the structure of the ileum of the nymphal *C. fuscus fuscus*, whose digestive system has not been studied at the level of light and electron microscopy. We hope that the data obtained in this study will contribute to various experimental taxonomical, histological, and ultrastructural studies about insect tissues.

MATERIALS AND METHODS

The 10 male and 10 female last instar nymphal individuals of *C. fuscus fuscus* (Fabricius, 1793) (Orthoptera, Tettigoniidae) were collected from the terrains around the Ankara-Çankırı road in June 2017-2018. Samples brought to laboratory were anesthetized with ethyl acetate fumes first and the digestive canal was dissected out in physiological water under the stereomicroscope (Olympus SZX7).

For the scanning electron microscope (SEM) examinations, specimens were fixed in 5% glutaraldehyde. After fixation, the specimens, washed with phosphate buffer, were dehydrated in an ascending series of ethanol. Then, they were dried with a critical point dryer (Polaron CPD 7501), taken on SEM stubs, and coated with gold in a sputter coater (Polaron SC 502). The coated specimens were examined with JEOL JSM 6060 SEM at 10kV at Gazi University, Faculty of Science.

For the transmission electron microscope (TEM) examinations, specimens were post-fixed in 1% OsO₄ after pre-fixation in 5% glutaraldehyde. After rinsing with phosphate buffer, the specimens were dehydrated in ascending ethanol concentrations, and then embedded in Araldite. Ultra-thin sections were cut with Leica EM UC6 ultramicrotome and stained with lead citrate and uranyl acetate. The sections were examined with JEOL JEM 1400 TEM at 80 kV and photographed Gazi University, Faculty of Science.

For the light microscopy (LM), semi-thin sections were cut with ultramicrotome from Araldite blocks prepared for TEM examinations and stained with 1% methylene blue. The stained sections were observed under a light microscope (Olympus BX51) and photographed.

RESULTS

The alimentary canal in the last instar nymphal *C. fuscus fuscus* is composed of three main parts as the foregut, the midgut, and the hindgut (Figure 1). The hindgut is divided into three regions called ileum, colon and rectum. The ileum is a short and thick tubular structure and located between midgut and colon (Figure 2). The

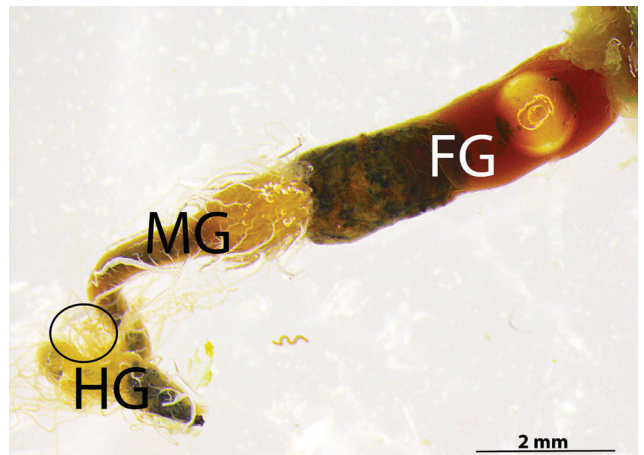


Figure 1. The general view of the alimentary canal in *C. fuscus fuscus*. Foregut (FG), midgut (MG), hindgut (HG) and Malpighian tubules (encircled) (Stereomicroscope).

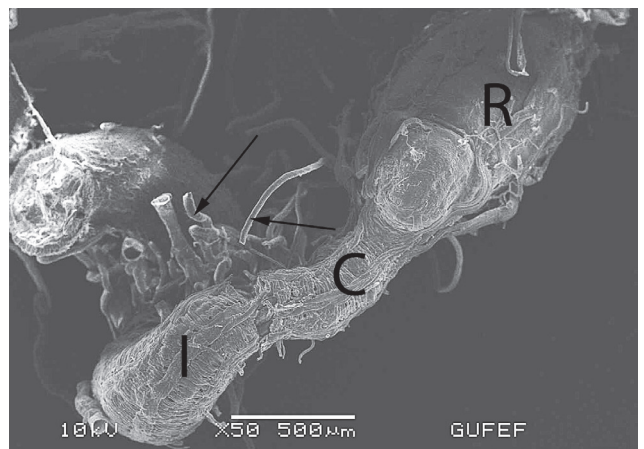


Figure 2. The general view of the hindgut in *C. fuscus fuscus*. Ileum (I), colon (C), rectum (R) and Malpighian tubules (arrows). SEM

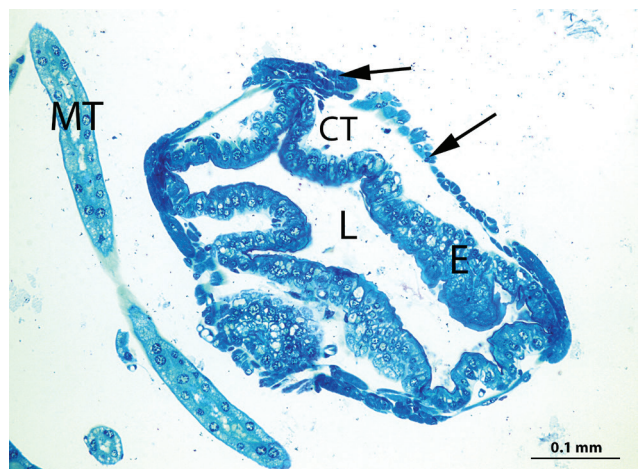


Figure 3. The semi-thin section of the ileum. Epithelial layer (E), muscle tissue (arrows), Malpighian tubules (MT), connective tissue (CT) and lumen (L). Light microscope, Methylene blue, x200

Malpighian tubules are connected to the alimentary canal at the region where the midgut-ileum junction is (Figures 1 and 2).

In the cross-sections, it was seen that the ileum wall consists of single layer cubic epithelial tissue as the innermost, connective tissue in the middle, and muscle tissue as the outermost (Figures 3-7). There is a thin cuticular intima layer surrounding the lumen, the innermost above the epithelial layer (Figures 4-7).

Rather large and rounded nuclei are found in the middle of the epithelial cells (Figures 4, 7 and 8). Besides, granulated endoplasmic reticulum in the cytoplasm is visible in TEM photographs (Figure 8). It is observed that there is a connection between the outer membrane of the nucleus and granulated endoplasmic reticulum (Figure 8).

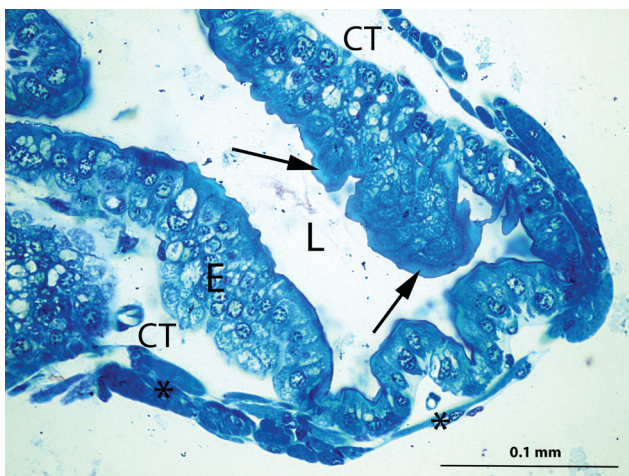


Figure 4. The semi-thin section of the ileum. Epithelial layer (E), muscle tissue (asterix), cuticular intima (arrows), connective tissue (CT) and lumen (L). Light microscope, Methylene blue, x400

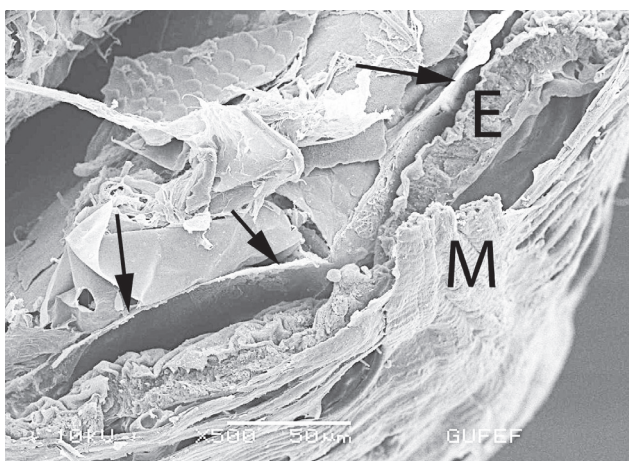


Figure 5. SEM photograph of the ileum in *C. fuscus fuscus*. Epithelial tissue (E), muscle tissue (M) and cuticular intima (arrows).

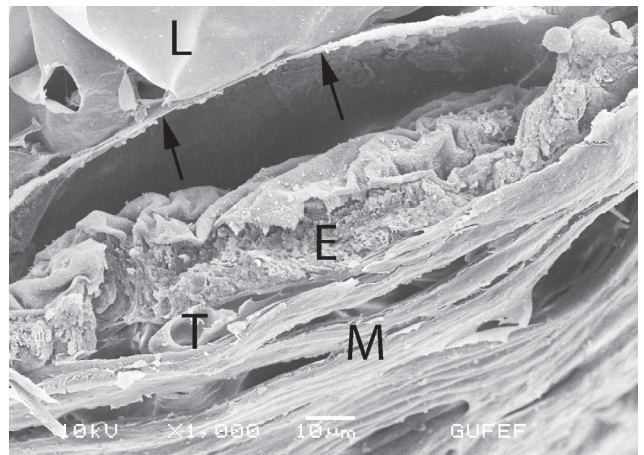


Figure 6. SEM photograph of the ileum in *C. fuscus fuscus*. Epithelial tissue (E), muscle tissue (M), lumen (L), trachea (T) and cuticular intima (arrows).

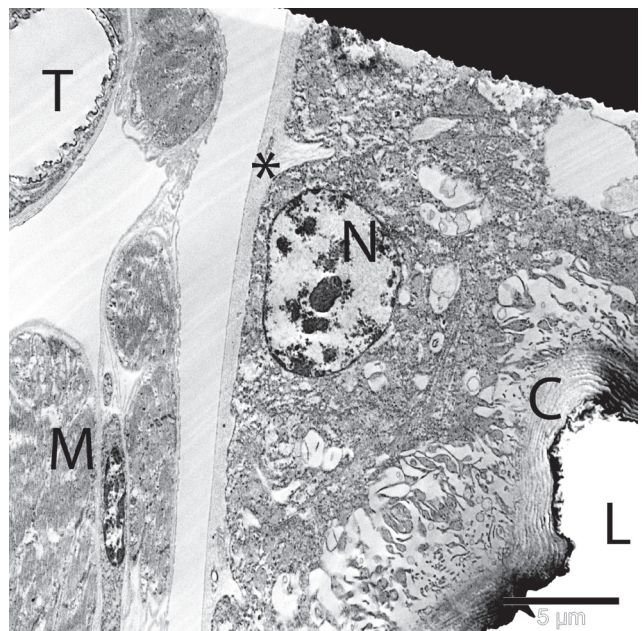


Figure 7. The thin section of the ileum. Nucleus (N), cuticular intima (C), lumen (L), basal lamina (asterix), muscle tissue (M) and trachea (T). TEM

In SEM photographs, the apical side of the epithelial cells looks undulated and indented (Figures 9 and 10) and have numerous knobby protrusions on the surface facing the cuticular intima (Figure 10). In TEM photographs, this structure looks as if it has some dispersed and nonuniform invaginations going toward the cytoplasm above the cuticular intima (Figure 11).

The nidi, which are regenerative cell groups, are located in basal region of epithelial layer. The regenerative cells have denser cytoplasm as regards electron comparing to the epithelial cells

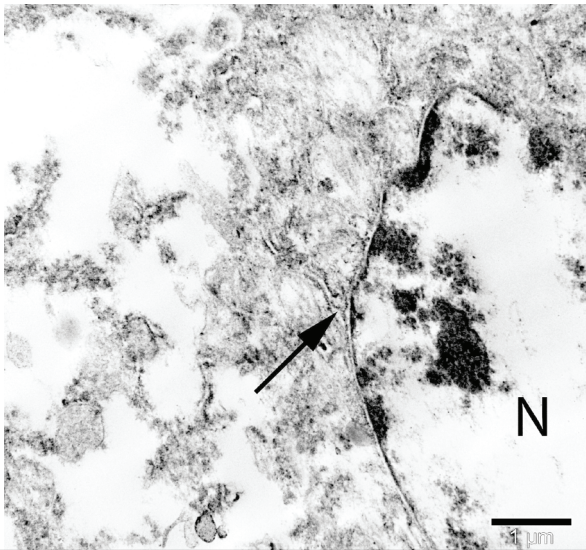


Figure 8. The thin section of the ileum. Nucleus (N) and the connection between the granulated endoplasmic reticulum and the outer membrane of the nucleus (arrow) in the epithelial cell. TEM

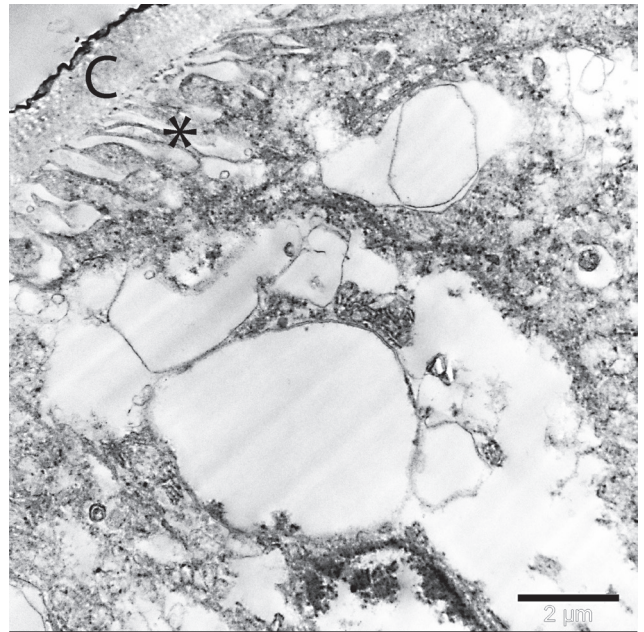


Figure 11. Dispersed and nonuniform invaginations (asterisk) go toward the cytoplasm above the cuticular intima (C). SEM

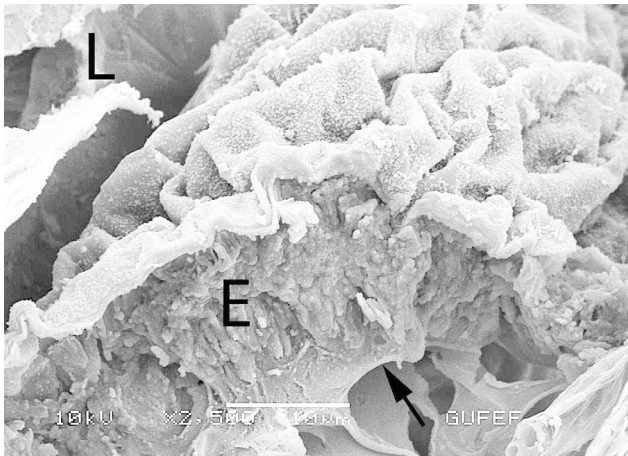


Figure 9. SEM photograph of the ileum wall. Epithelial layer (E), basal lamina (arrow) and lumen (L).

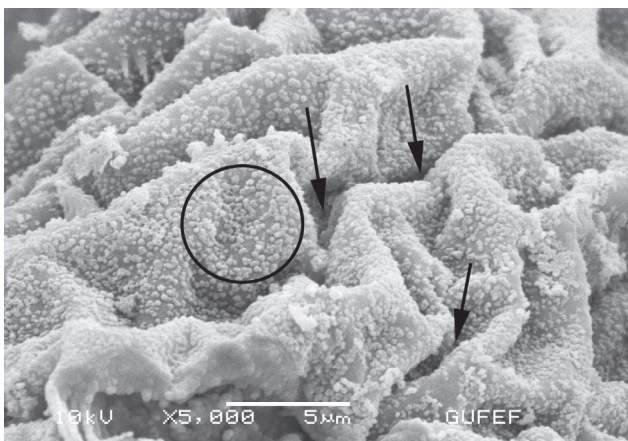


Figure 10. The apical surface of the epithelial layer. Undulated areas of apical region (arrows) and knobby protrusions (encircled). SEM

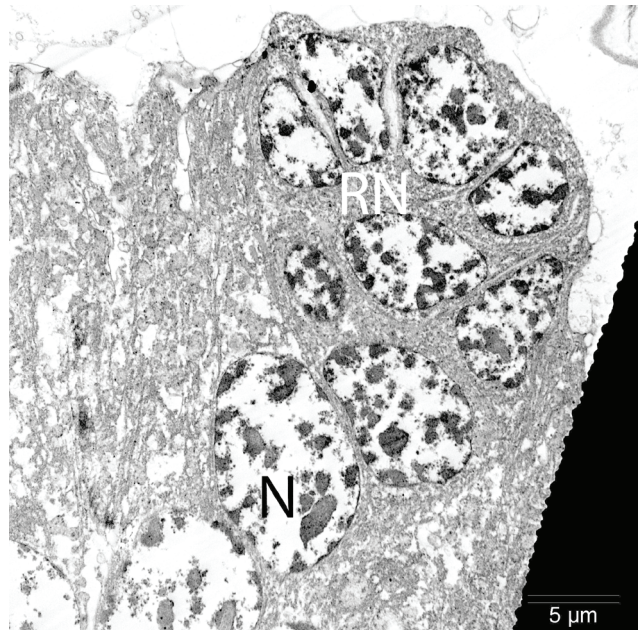


Figure 12. The thin section of the ileum showing the regenerative cell nidi (RN), which is composed of several regenerative cells and nucleus (N) in epithelial cells. TEM

(Figure 12). The connective tissue recesses into the epithelial layer and thus the epithelial layer gains undulated structure (Figures 3 and 4). Epithelial cells rest on a thin basal lamina (Figures 7 and 9). The thin muscle tissue surrounds the outer surface of the ileum (Figures 4, 5 and 7). The trachea, which is situated in the connective tissue and outer side of the muscle tissue, can be observed in the cross sections of the ileum (Figures 6 and 7).

DISCUSSION

In the insects, the digestive system consists of three regions: the foregut, the midgut, and the hindgut, while each region can be divided within itself (13,17). The hindgut generally consists of the ileum, the colon, and the rectum (17,35). However, in some insects such as *Catopsilla pomona* (Fabricius, 1758) (Lepidoptera: Pieridae) the hindgut is composed of two subparts as the ileum and the rectum (29). The ileum, which is the first part of the hindgut, can be divided into different parts in different insect groups (36). For example, in *Formica nigricans* (Hymenoptera, Formicidae), the ileum is divided into proximal, middle, and distal ileum (37). In *Cephalodesmius armiger* (Coleoptera, Scarabaeidae), larvae of *Anticarsia gemmatalis* (Lepidoptera, Noctuidae), *Melanogryllus desertus* (Orthoptera, Gryllidae), *Poecilimon cervus* (Orthoptera, Tettigoniidae) and *Graphosoma lineatum* (Heteroptera, Pentatomidae), the ileum consists of a single region (2,17,18,35,37,38). When the ileum morphology of the last instar nymphal *C. fuscus fuscus* (Orthoptera) is compared with the other species, there is no compartment.

The ileum in *Cenocorixa bifida* (Hung.) (Hemiptera, Corixidae) is composed of two distinct areas that can be observed in TEM photographs of cross sections of the ileum. These areas are a ventral squamous epithelium and a dorsolateral columnar epithelium consisted of extremely large cells. The arrangement of the columnar epithelium forms a structure called as ileac pad. Although, the ileum in the last instar nymphal *C. fuscus fuscus* has no structure as in *C. bifida* (39).

In the cross sections of the ileum in the last instar nymphal *C. fuscus fuscus* the epithelial layer has infoldings on the apical side of the epithelium that can also be observed in *Locusta migratoria* (Orthoptera, Acrididae) and *C. bifida*. The epithelial cell layer also has finger-like invaginations into the lumen in *M. desertus* (18,20,39).

In some insects, the ileum has symbiotic bacteria (40,41). It has been thought that the presence of bacteria in the ileum contributes to digestion by increasing digestibility of carbohydrates. The symbiotic bacteria localized on invaginations which at the apical side facing the lumen of the epithelial layer in the ileum of *Gryllus bimaculatus* (Orthoptera, Gryllidae) and *Acheta domestica* (Orthoptera, Gryllidae) was described in the studies of Ulrich et al. (1981) and Woodring and Lorenz (2007) (42,43). In our study, we couldn't observe the symbiotic bacteria of the ileum lumen in the last instar nymphal *C. fuscus fuscus*.

The ileum epithelium of different species has different cell types. While the proximal ileum of *F. nigricans* has simple pyramidal epithelial cells, the middle ileum of the same species has simple cubic epithelial cells (36). Although the ileum epithelium has a single layer of cylindrical cell type in *M. desertus*, *L. migratoria*, and *C. armiger*, the ileum structure of larvae of *A. gemmatalis* consists of squamous epithelial cells (2,17,20,37). The cells of the nymphal *C. fuscus fuscus* have a monolayer cubic epithelium similar to the ileum epithelium of *P. cervus* (35).

In general, the regenerative cells groups, called nidi, are shown in the midgut epithelium in insects. The new cells that grow from small regenerative cells in the midgut can replace cells lost through age, wear, and loss through apocrine or holocrine secretion (35,44-46). Regenerative cells lie near the base of the epithelial cells in larval Diptera, Lepidoptera, and Orthoptera. On the other hand, in some orders as Coleoptera, these cell groups are located at the apical side of the mature cells through the gut muscle layers (47). In our results, regenerative cell nidi were observed at the basal side of the epithelial layer of ileum in the last instar nymphs of *C. fuscus fuscus*. This may be due to the high requirement for regeneration of the ileum due to being in one of the stages of development.

The innermost layer of the ileum of nymphal *C. fuscus fuscus* shows an intima which has a cuticular layer and is folded along the epithelial cell layer. The cuticular intima layer is similar to the one observed in the ileum of *P. cervus*, *C. bifida*, *Apis mellifera* (Hymenoptera, Apidae), *L. migratoria*, *Pylaemenes mitratus* (Phasmatodea, Heteropterygidae), and *C. pomona*, which were compared in this study. The cuticular layer is thin in the last instar nymphal *C. fuscus fuscus*, *Cephalotes pusillus* (Hymenoptera, Formicidae), *Cephalotes clypeatus* (Hymenoptera, Formicidae), and *Cephalotes atratus* (Hymenoptera, Formicidae). The thickness of the cuticular layer is related to the roles of the ileum in absorption in these insects (13,16,20,29,35,39,48).

The outer surface of the epithelial cell layer is surrounded by layers of circular and longitudinal muscles in *C. fuscus fuscus*, *C. pusillus*, *C. clypeatus*, and *C. atratus*; however, while the muscle tissue of ileum in *C. pusillus*, *C. clypeatus*, and *C. atratus* is thick, the one in the last instar nymphal *C. fuscus fuscus* is rather thin in some regions, and other regions have medium thickness. The ileum in *M. desertus* has only circular muscle layer surrounding the ileum wall (16,18).

CONCLUSION

This study was conducted to provide a fundamental knowledge about the last instar nymphal *C. fuscus fuscus*. This species will contribute to the data on the families of Orthoptera and the other orders. Future comparative taxonomical, histological, and ultrastructural studies about the alimentary canals of insects can be conducted between other species of different insect orders.

Peer-review: Externally peer-reviewed.

Author Contributions: Conception/Design of study: D.A.M., I.P., Z.S.; Data Acquisition: D.A.M., I.P., Z.S.; Data Analysis/Interpretation: D.A.M., I.P., Z.S.; Drafting Manuscript: D.A.M., I.P., Z.S.; Critical Revision of Manuscript: D.A.M., I.P., Z.S.; Final Approval and Accountability: D.A.M., I.P., Z.S.; Technical or Material Support: Z.S.; Supervision: Z.S..

Conflict of Interest: The authors declare that they have no conflicts of interest to disclose.

Financial Disclosure: There are no funders to report for this submission.

Acknowledgements: We express our thanks to Prof. Dr. Mustafa ÜNAL (Bolu Abant İzzet Baysal University, Faculty of Arts and Sciences, Biology Department) for helping in the species diagnosis and to Gazi University Academic Writing and Research Center for their help and support in the proofreading of the current study.

REFERENCES

1. Lee WY, Chen ME, Lin TL. Morphology and ultrastructure of the alimentary canal of oriental fruit fly *Bactrocera dorsalis* (Hendel) (Diptera: Tephritidae) (I): the structure of the foregut and cardia. *Zool Stud* 1998; 1(37): 95-101.
2. Levy SM, Falleiros ÂM, Moscardi F, Gregório EA, Toledo LA. Morphological study of the hindgut in larvae of *Anticarsia gemmatilis* Hübner (Lepidoptera: Noctuidae). *Neotrop Entomol* 2004; 33(4): 427-31.
3. Levy SM, Falleiros ÂM, Moscardi F, Gregório EA, Toledo LA. Ultrastructure of digestive tract of *Anticarsia gemmatilis* (Hübner, 1818) (Lepidoptera: Noctuidae) at final larval development. *Semina: Ciências Agrárias* 2008; 29(2): 313-21.
4. Bution ML, Caetano FH, Britto FB, Gomes GT, Zara FJ. Histology and histochemistry of the ventriculus of *Dolichoderus (=Monacis) bispinosus* (OLIVIER, 1792) (Hymenoptera: Formicidae). *Micron* 2006; 37(3): 249-54.
5. Boonsriwong W, Sukontason K, Olson JK, Vogtsberger RC, Chaitong U, Kuntalue B, et. al. Fine structure of the alimentary canal of the larval blow fly *Chrysomya megacephala* (Diptera: Calliphoridae). *Parasitol Res* 2007; 100(3): 561-74.
6. Rubio G, José D, Bustillo P, Alex E, Vallejo E, Luis F, et. al. Alimentary canal and reproductive tract of *Hypothenemus hampei* (Ferrari) (Coleoptera: Curculionidae, Scolytinae). *Neotrop Entomol* 2008; 37(2): 143-51.
7. Serrão JE, Ronnau M, Neves CA, Campos LA, Zanuncio JC. Ultrastructure of anterior midgut region of corbiculate bees (Hymenoptera: Apidae). *Ann Entomol Soc Am* 2008; 101(5): 915-21.
8. Fialho MD, Zanuncio JC, Neves CA, Ramalho FS, Serrão JE. Ultrastructure of the digestive cells in the midgut of the predator *Brontocoris tabidus* (Heteroptera: Pentatomidae) after different feeding periods on prey and plants. *Ann Entomol Soc Am* 2009; 102(1): 119-27.
9. Santos CG, Neves CA, Zanuncio JC, Serrão JE. Postembryonic development of rectal pads in bees (Hymenoptera, Apidae). *Anat Rec* 2009; 292(10): 1602-11.
10. De Sousa G, Scudeler EL, Abrahão J, Conte H. Functional morphology of the crop and proventriculus of *Sitophilus zeamais* (Coleoptera: Curculionidae). *Ann Entomol Soc Am* 2013; 106(6): 846-52.
11. Gonçalves WG, Fernandes KM, Barcellos MS, Silva FP, Magalhaes-Junior MJ, Zanuncio JC, et. al. Ultrastructure and immunofluorescence of the midgut of *Bombus morio* (Hymenoptera: Apidae: Bombini). *Comptes Rendus Biologies* 2014; 337(6): 365-72.
12. Polat I, Suludere S, Candan S. Histological and ultrastructural features of the rectum in *Poecilimon cervus* Karabağ, 1950 (Orthoptera: Tettigonidae). *Microsc Res Techniq* 2017; 80: 195-201.
13. Harris MN, Azman S, Nurul Wahida O. Gross anatomy and histology of alimentary system of stick insect, *Pylaemenes mitratus* (Phasmid: Basillidae). *Serangga* 2019; 24(1): 151-8.
14. Wigglesworth VB. *The Principles of Insect Physiology*. 7th ed. London: Chapman and Hall; 1972.
15. Nation JL. *Insect Physiology and Biochemistry*. CRC Press Boca Raton FL; 2002.
16. Bution ML, Caetano FH. Ileum of the Cephalotes ants: A specialized structure to harbor symbionts microorganisms. *Micron* 2008; 39: 897-909.
17. Çakıcı Ö. Histological and Ultrastructural Investigations on the Digestive System of *Melanogryllus desertus* Pallas (Orthoptera: Gryllidae). E.Ü. Fen Bilimleri Enstitüsü, Doktora Tezi. 2008.
18. Çakıcı Ö, Ergen G. Histological and ultrastructural investigations on hindgut of *Melanogryllus desertus* (Pallas, 1771) (Orthoptera: Gryllidae). *German J Zool Res* 2013; 1(1): 1-6.
19. Beams HW, Tahmisian TN, Devine RL. Electron microscope studies on the cells of the Malpighian tubules of the grasshopper (Orthoptera, Acrididae). *J. Biophysic Biochem Cytol* 1955; 1(3): 197-214.
20. Peacock AJ. Ultrastructure of the ileum of *Locusta migratoria*. *J Morphol* 1986; 188: 191-201.
21. Irvine B, Audsley N, Lechleitner R, Meredith J, Thomson B, Phillips J. Transport properties of locust ileum *in vitro*: effects of cyclic AMP. *J Exp Biol* 1988; 137: 361-85.
22. Prado MA, Montuenga LM, Villaro AC, Etayo JC, Polak JM, Sesma MP. A novel granular cell type of locust Malpighian tubules: ultrastructural and immunocytochemical study. *Cell Tissue Res* 1992; 268(1): 123-30.
23. Gaino E, Rebora M. The duct connecting Malpighian tubules and gut: an ultrastructural and comparative analysis in various Ephemeroptera nymphs (Pterygota). *Zoomorphol* 2000; 120(2): 99-106.
24. Acar G. *Melanogryllus desertus* (Pallas, 1771) (Orthoptera: Gryllidae)'ta Malpighi Tüpcüklerinin Morfoloji ve Histolojisi. E.Ü. Fen Bilimleri Enstitüsü, Yüksek Lisans Tezi. 2009.
25. Conti B, Berti F, Mercati D, Giusti F, Dallai R. The ultrastructure of Malpighian tubules and the chemical composition of the cocoon of *Aeolothrips intermedius* Bagnall (Thysanoptera). *J Morphol* 2010; 271(2): 244-54.
26. De Azeredo-Oliveira MT, da Silva TL, Mello ML. Mg²⁺-dependent ATPase activity in Malpighian tubules of *Triatoma infestans* Klug. *Micron* 2012; 43(2-3): 298-304.
27. Ferreira RA, Zacarin EC, Malaspina O, Bueno OC, Tomotake ME, Pereira AM. Cellular responses in the Malpighian tubules of *Scaptotrigona postica* (Latreille, 1807) exposed to low doses of fipronil and boric acid. *Micron* 2013; 46: 57-65.
28. Pal R, Kumar K. Malpighian tubules of adult flesh fly, *Sarcophaga ruficornis* Fab. (Diptera: Sarcophagidae): an ultrastructural study. *Tissue Cell* 2013; 45(5): 312-7.
29. Poolprasert P, Mongkolchaichana E, Senarat S, Kettratad J, Yenchum W, Angsirijinda W. Light microscopic observations of the mesentero-proctodeal regions in adult *Catopsilla pomona* (Fabricius, 1758) (Lepidoptera: Pieridae). *Suranaree J Sci Technol* 2015; 22(1): 99-103.
30. Giglio A, Perrotta ID, Brandmayr P. Exosomes: Ultrastructural evidence in epithelial cells of Malpighian tubules. *Micron* 2017; 100: 34-7.
31. Rivera-Vega L, Mikó I. Know your insect: Malpighian tubules in *Trichoplusia ni* (Lepidoptera: Noctuidae). *Res Ideas Outcomes*. 2017 Feb 01. doi: 10.3897/rio.3.e11827 e11827.
32. Gullan PJ, Cranston PS, editors. *İç anatomi ve fizyoloji. Böcekler: entomolojinin ana hatları*. Ankara: Nobel; 2012.
33. Ragge DR. *Grasshoppers, Crickets and Cockroaches of the British Isles*. London: F Warne and Co; 1965.

34. Sadiq S, Panhwar WA, Sultana R, Saeed M, Wagan SA, Ahmed S. New record of *Conocephalus (Anisoptera) fuscus* (Fabricius, 1793) (Conocephalinae: Tettigoniidae: Orthoptera) from Pakistan. *J Entomol Zool Stud* 2017; 5(3): 1431-4.
35. Polat I. The ultrastructural features of the digestive, excretory, female and male reproductive systems of *Poecilimon cervus* Karabag, 1950. G.Ü. Fen Bilimleri Enstitüsü, Doktora Tezi. 2016.
36. Villaro AC, Garayoa M, Lezaun MJ, Sesma P. Light and electron microscopic study of the hindgut of the ant (*Formica nigricans*, Hymenoptera): I. structure of the ileum. *J Morphol* 1999; 242(3): 189-204.
37. Lopez-Guerrero Y. Anatomy and histology of the digestive system of *Cephalodesmus armiger* Westwood (Coleoptera, Scarabaeidae, Scarabaeinae). *Coleop Bull* 2002; 56(1): 97-107.
38. Amutkan D, Suludere Z, Candan S. Ultrastructure of digestive canal of *Graphosoma lineatum* (Linnaeus, 1758) (Heteroptera: Pentatomidae). *J Entomol Res Soc* 2015; 17(3): 75-96.
39. Jarial MS; Scudder GGE. The morphology and ultrastructure of the Malpighian tubules and hindgut in *Cenocorixa bifida* (Hung.) (Hemiptera, Corixidae). *Z Morphol Oekol Tiere* 1970; 68(4): 269-99.
40. Chapman RF. *The Insects: Structure and Function*. 5th ed. New York: Cambridge University Press; 2013.
41. Klowden MJ. *Physiological Systems in Insects*. 3rd ed. London: Academic Press; 2013.
42. Ulrich RG, Buthala DA, Klug MJ. Microbiota associated with the gastrointestinal tract of the common house cricket, *Acheta domestica*. *Appl Environ Microbiol* 1981; 41(1): 246-54.
43. Woodring J, Lorenz MW. Feeding, nutrient flow, and functional gut morphology in the cricket *Gryllus bimaculatus*. *J Morphol* 2007; 268: 815-25.
44. Illa-Bochaca I, Montuenga LM. The regenerative nidi of the locust midgut as a model to study epithelial cell differentiation from stem cells. *J Exp Biol* 2006; 209: 2215-23.
45. Park MS, Park P, Takeda M. Starvation induces apoptosis in the midgut nidi of *Periplaneta americana*: a histochemical and ultrastructural study. *Cell Tissue Res* 2009; 335: 631-8.
46. Çakıcı Ö, Ergen G. Histologic description of midgut in *Melanogryllus desertus* (Pallas, 1771) (Orthoptera: Gryllidae). *Biharean Biol* 2012; 6(2): 108-111.
47. Nation JL. *Insect Physiology and Biochemistry*. 2nd ed. Florida: CRC Press; 2008.
48. Gonçalves WG, Fernandes KM, Santana WC, Martins GF, Zanuncio JC, Serrão JE. Post-embryonic changes in the hindgut of honeybee *Apis mellifera* workers: Morphology, cuticle deposition, apoptosis, and cell proliferation. *Dev Biol* 2017; 431(2): 194-204.

A Fourier Transform Infrared Spectroscopic Investigation of *Macrovipera lebetina lebetina* and *M. l. obtusa* Crude Venoms*

Nasit Igci^{1,2} , Fatma Duygu Ozel Demiralp^{3,4} 

¹Nevşehir Hacı Bektaş Veli University, Faculty of Science and Arts, Department of Molecular Biology and Genetics, Nevşehir, Turkey

²Nevşehir Hacı Bektaş Veli University, Science and Technology Application and Research Center, Nevşehir, Turkey

³Ankara University, Biotechnology Institute, Ankara, Turkey

⁴Ankara University, Faculty of Engineering, Department of Biomedical Engineering, Ankara, Turkey

ORCID IDs of the authors: N.I. 0000-0001-6151-808X; F.D.O.D. 0000-0002-1798-7951

Please cite this article as: Igci N, Ozel Demiralp FD. A Fourier Transform Infrared Spectroscopic Investigation of *Macrovipera lebetina lebetina* and *M. l. obtusa* Crude Venoms. Eur J Biol 2020; 79(1): 14-22. DOI: 10.26650/EurJBiol.2020.0039

ABSTRACT

Objective: Snake venoms are rich sources of bioactive molecules and have been investigated using various bioanalytical methods. Fourier transform infrared (FTIR) spectroscopy is a sensitive method that can be used to analyze biological samples. The aim of this study is to apply the FTIR spectroscopy method for the characterization of snake venom.

Materials and Methods: The study characterized the lyophilized crude venoms of *Macrovipera lebetina lebetina* and *M. l. obtusa* by FTIR spectroscopy coupled with attenuated total reflectance (ATR) method in the mid-infrared region and compared the spectra between the two subspecies. The band area and intensity values were calculated for comparison and wavenumbers were detected by automated peak picking. Additionally, the study analyzed the secondary structure of venom proteins by using the second derivative spectra.

Results: The study detected fourteen major and minor peaks in absorbance spectra which were assigned to various biomolecules such as proteins, carbohydrates, and nucleic acids. Four major sub-bands were observed in the second derivative spectra of Amide I-II region indicating different protein secondary structures. It was observed that there are some quantitative differences and peak shifts between the spectra of venoms of two subspecies, indicating the alteration of biomolecules.

Conclusion: To the best of our knowledge, this is the first report of the use of the FTIR-ATR spectroscopy method focusing solely on the characterization of crude snake venoms in literature, accompanied with detailed peak assignment and protein secondary structure analysis. As a preliminary reference study, the results showed the usefulness of FTIR-ATR spectroscopy for the physicochemical characterization of lyophilized snake venom.

Keywords: Fourier transform infrared spectroscopy, snake venom, viper, *Macrovipera lebetina*

INTRODUCTION

Snake venoms are complex molecular cocktails consisting mainly of bioactive peptides and proteins including enzymes (such as serine and metalloproteinase, phospholipase A₂, hyaluronidase, L-amino acid oxidase, nucleotidase), non-enzymatic proteins (e.g. cysteine-rich secretory protein, disintegrin, vascular endothelial growth factor, nerve growth factor, C-type lectin) and smaller peptides (e.g. bradykinin-potentiating peptides,

protease inhibitor peptides) (1-3). Snake venoms also contain some minor compounds such as carbohydrates, nucleosides, biogenic amines, various carboxylic acids and inorganic elements (4,5). Snake venoms, an important source of bioactive proteins, have attracted researchers in the past. Drugs and diagnostic kits were developed using snake venom peptides and proteins (2,6-8).

Macrovipera lebetina (Serpentes: Viperidae: Viperinae) is a relatively big viper species which could reach up to

* This paper was produced from the M.Sc. thesis of the first author. Part of this paper was presented at 16th National Biotechnology Congress (13-16 December 2009, Antalya, Turkey).

Corresponding Author: Nasit Igci

E-mail: igcinasit@yahoo.com.tr

Submitted: 06.11.2019 • **Revision Requested:** 13.12.2019 • **Last Revision Received:** 10.03.2020 • **Accepted:** 11.03.2020

© Copyright 2020 by The Istanbul University Faculty of Science • Available online at <http://ejb.istanbul.edu.tr> • DOI: 10.26650/EurJBiol.2020.0039



2 meters long and has a wide geographical range from northern Africa to Pakistan and Kashmir, reaching to Kazakhstan and Dagestan (southwestern Russia) in the North, including Turkey and Cyprus (9-11). Although the taxonomic status of some subspecies is still in question, it is accepted that nominate taxon *M. l. lebetina* (Linnaeus, 1758) inhabits Cyprus (11-13). The southern and southeastern Anatolia populations were treated as *M. l. euphratica* (Martin, 1838) in the past but this name is generally synonymized under *M. l. obtusa* (Dwigubsky, 1832) today (12). *M. l. obtusa* has a geographical range from Mersin to south-eastern, southern, and northeastern Anatolia in Turkey while *M. l. lebetina* is restricted to Cyprus island (10-13). *M. lebetina* is largely responsible for the harmful snakebite-cases in its world-wide range as well as in Turkey and it is the only venomous viper species occurring in Cyprus (12,14,15).

Fourier transform infrared (FTIR) spectroscopy is a fast, robust, sensitive, and widely-used vibrational spectroscopy method. The working principle is the formation of different vibrational modes of the chemical groups in molecules after absorbing infrared radiation (16,17). Due to the non-destructive and non-invasive nature of infrared radiation, this method is widely applied to biological and biomedical studies today (18-21). Each vibration type has its specific frequency of absorption which can be associated with various bioorganic molecules in biological samples. The amounts of biomolecules can be assessed in a comparative manner using the band intensities and areas (18,19). Moreover, information regarding the secondary structures of proteins can be obtained by spectral interpretation (17,19,20,22).

Since the major elements of crude snake venoms are proteins and peptides, researchers have been focusing on their proteomic characterization using various bioanalytical methods suitable for protein separation and analysis such as polyacrylamide gel electrophoresis, liquid chromatography, and mass spectrometry (3,23-28). Venom of the subspecies of *M. lebetina* has also been an important source in many studies aimed to purify proteins and make proteomic and biological characterization (3,25,29). Major protein families of *M. lebetina* venom are metalloproteinase, serine proteinase, phospholipase A₂, L-amino acid oxidase, hyaluronidase, disintegrin, C-type lectin, cysteine-rich secretory protein, vascular endothelial growth factor, nerve growth factor, bradykinin-potentiating peptides, and protease inhibitor peptides (3,25,29). These proteins give the venom its unique pharmacological properties such as anti-coagulant, cytotoxic and antimicrobial activities.

The Fourier Transform Infrared Spectroscopy method was used to analyze the secondary structures of purified snake venom toxins (30-33) and their complexes with nanomaterials (34,35). In one study, the FTIR spectrum of *Echis carinatus* venom was published together with its chitosan nanoparticle complex but the results were used for comparative purposes to assess the loading efficiency and it was not aimed to make a venom characterization (36). Another study, by Shafiga and Huseyn (37), reported some IR peaks of *M. l. obtusa* venom as a part of their results but their data was limited. There is no detailed

published study focusing solely on the application of FTIR spectroscopy for the characterization of crude snake venoms which provides detailed band assignments, to the best of authors' knowledge. The present study aimed to make physicochemical characterization of crude snake venoms by FTIR-ATR spectroscopy using the venoms of *M. l. lebetina* and *M. l. obtusa* as representative materials and assess the method's usefulness in the field of toxinology.

MATERIALS AND METHODS

Venom Samples

In this study, we used the pooled venoms of two adult *M. l. lebetina* and two adult *M. l. obtusa* individuals collected from The Turkish Republic of Northern Cyprus (Selvilitpe and Dikmen) and southeast Turkey (Egil/Diyarbakir and Suruc/Sanlıurfa), respectively. The venom samples were extracted from vipers using a paraffin-covered laboratory beaker and without applying any pressure on the venom glands. Authors had ethical permission for venom extraction at the time of the study (Ege University Animal Experiments Ethics Committee, permit number 2010-43). After extraction, venom samples were centrifuged at 2000 × g for 10 min at 4°C. Supernatants were collected, frozen at -80°C and then lyophilized by using a bench-top freeze-dryer (Millrock Technology, Kingston, NY, USA). Lyophilized samples were kept at 4°C until used.

FTIR Data Collection and Evaluation

Lyophilized venom samples were measured using a universal attenuated total reflectance (ATR) cell (Pike Technologies, Wisconsin, USA) connected to an FTIR device (Bruker Tensor 27, Bruker Optics GmbH, Ettlingen, Germany) equipped with a liquid nitrogen cooled photovoltaic mercury cadmium telluride detector. High-purity nitrogen gas was purging during all the measurements. Air was subtracted automatically before all sample measurements. Spectra of the venom samples were recorded in the mid-infrared region, between 4500-850 cm⁻¹ wavenumbers and interferograms were accumulated for 50 scans at 4 cm⁻¹ resolutions at room temperature in the single-bounce ATR mode. A small amount of the sample, enough to cover the ZnSe ATR crystal, were placed and compressed with a clamp. Each sample was measured in triplicate and the average spectra was used for analyses.

Spectral data interpretation was performed by OPUS 5.5 software (Bruker). Automated peak picking was performed in order to determine wavenumber values. Min-max normalization was applied with respect to the Amide I peak (at 1644 cm⁻¹) for illustrative purposes. Spectra were baselined using an automated multipoint method and band areas were calculated by integration. Band areas were normalized by dividing the value of each band to the total spectrum area in order to minimize technical variation (21). Second derivatives of the absorbance spectra, in which absorption maxima appear as minima, were calculated using Savitzky-Golay algorithm. Relative intensity values of the second derivative peaks in the Amide I-II region (1700-1500 cm⁻¹) were used to assign protein secondary structures (20-22,

38). Relative intensities were calculated using the arbitrary unit values on the y-axis after lining a reference baseline at the minimum point of the spectrum in Amide I-II region.

RESULTS

As a result of the FTIR measurements, 14 significant peaks were detected in the spectrum of *M. l. obtusa* and *M. l. lebetina* venom in the mid-infrared region between 4500-850 cm^{-1} (Figure 1). A majority of the characteristic peaks were observed between 1800 and 850 cm^{-1} wavenumbers. The wavenumber of each peak was determined by automated peak picking and the areas under the bands were calculated by integration (Table 1). Table 1 also includes the definitions of the spectral assignments for each major absorbance peak observed in the present study, with their wavenumbers (see the Discussion section for a detailed explanation of the peak assignment process).

The characteristic peaks arising from the protein backbone such as Amide A, B, I, II and III were observable on the spectra of *M. lebetina* venom (Figure 1, Table 1). The major bands with the highest intensities were Amide I at 1644 cm^{-1} and Amide II at 1543 cm^{-1} wavenumbers (Figure 1, Table 1). Sub-bands were obtained by derivatization (second derivative) in the Amide I-II region, ranging between 1700-1500 cm^{-1} to obtain information about the protein secondary structures. Two major sub-bands and three minor shoulders were observed in this region after derivatization in the present study (Figure 1). The wavenumbers were assigned to the secondary structures of the proteins by comparing the data previously published in the literature (see Discussion) and presented in Table 1 with their intensity values. According to our results, overall venom proteins of *M. lebetina* subspecies predominantly have α -helix and unordered (random coil) secondary structures. The second derivative spectra in the

Amide I-II region of two subspecies were similar. However, some quantitative differences and band shifts were observed (Table 1, Figure 1), which will be discussed in the next section.

DISCUSSION

We characterized crude venoms of two subspecies of *M. lebetina* (*M. l. lebetina* and *M. l. obtusa*) by using FTIR spectroscopy coupled with the ATR method. As a fast, robust, and sensitive analytical method, FTIR has been used not only in chemistry but also in biological and biomedical studies (18). In the present study, a majority of the characteristic peaks were observed between 1800 and 850 cm^{-1} wavenumbers, which is considered a fingerprint region in FTIR spectroscopy (18-21). All the absorbance peaks were assigned to various vibrational modes associated with biomolecules such as proteins, nucleic acids, and carbohydrates comparing the frequencies with those in the related literature previously published elsewhere (18,20-22, 39-46). This is a routine and widely-accepted procedure for the FTIR spectroscopic investigation of biological materials, relying on information obtained from published literature (18,42,46). As a result of scientific research in this field, very detailed reference papers as well as textbooks are available today (18,19,22,38-53).

Peak assignment in FTIR spectroscopic studies includes two steps: The peaks observed in an FTIR spectrum gives information about the vibrational modes of specific functional groups. Absorbance peaks of many of the functional groups in the IR spectrum were characterized in previous studies (generally using pure model molecules) and this information can be found in published papers and textbooks (18,20-22,39-46). Associating the vibrational definitions to particularly more complex molecules (such as bioorganic macromolecules) is the second step and depends on the sample. If one knows that the analyte is a biological sample, peaks can be assigned to functional groups of major and minor biomolecules. Since the most abundant macromolecules in cells and biological fluids are proteins, carbohydrates, nucleic acids and lipids, the major peaks observed in the FTIR spectrum generally arise from various functional groups of these macromolecules (18,19,40,42,46). Snake venom is a secretion of cells covering the lumen of the venom gland, a biological fluid consisting mainly of proteins. Carbohydrates, biological amines, nucleotides, and nucleic acids can also be found as minor constituents (5). In the light of this knowledge, peaks in the FTIR spectrum of a snake venom can be assigned to these molecules using previously published papers in which FTIR peak information of tissue or cells is available.

Among the observed peaks in the present study, asymmetric and symmetric C-H stretching vibrations of CH_3 and CH_2 groups give rise in the region between 2950-2860 cm^{-1} wavenumbers, which originate from proteins and lipids in biological samples (18,20,21,39-42,46). Peaks around 1446-1443 cm^{-1} can be assigned to CH_2 and CH_3 bending of lipids and amino acid side chains of proteins, respectively (40,42,46). Since snake venom predominantly consists of proteins, these bands can be assigned mainly to proteins rather than lipids for snake venoms.

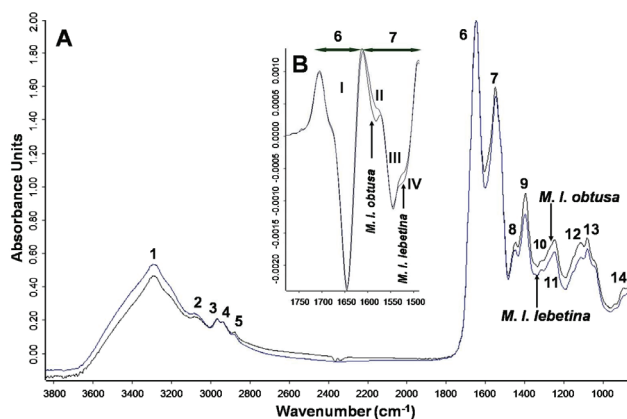


Figure 1. Overlaid FTIR spectra of *Macrovipera lebetina lebetina* and *M. l. obtusa* venoms showing absorbance spectra between 3800–850 cm^{-1} wavenumbers and second derivative spectra of Amide I and II peaks demonstrated as sub-bands. Arabic numbers correspond to the peaks in the absorbance spectrum while roman numerals refer to the sub-peaks of the second derivative spectrum (see Table 1 for peak assignments)

Table 1. Assignments of the FTIR peaks of venom samples with their chemical bond definitions. Band area values were given for the absorbance peaks (1-14), whereas relative intensity values were used for the second derivative peaks (I-IV).

Peak Number	Wavenumber, cm^{-1} (<i>lebetina/obtusa</i>)	Normalized Area or Intensity* (<i>lebetina/obtusa</i>)	Definition of the Spectral Assignment	Related Bioorganic Molecules in Snake Venom	Reference
1	3289/3287	0.232/0.210	Amide A, N-H stretching of proteins and amines (mainly), with contribution from O-H stretching of carbohydrates	Proteins (mainly), carboxylic acids, carbohydrates	(18,20,40,41,45,46)
2	3080/3081	0.032/0.027	Amide B, N-H stretching	Proteins (mainly)	(18,40,45,46)
3	2964/2963	0.017/0.012	CH_3 asymmetric stretching	Proteins	(39–41,46)
4	2938/2939	0.015/0.013	Asymmetric CH_2 stretching	Proteins	(42,46)
5	2879/2876	0.009/0.007	Symmetric CH_3 stretching	Proteins (mainly)	(18,39,41,46)
6	1644/1644	0.168/0.174	Amide I; 80% C=O stretching, 10% N-H bending, 10% C-N stretching	Proteins	(18,20,21,38-41,45,46)
7	1543/1543	0.154/0.171	Amide II; 60% N-H bending, 40% C-N stretching	Proteins	(18,20,21,38,40,41,45,46)
8	1446/1443	0.037/0.034	CH_3 asymmetric bending	Proteins	(40,42,46)
9	1395/1393	0.065/0.075	CH_3 symmetric bending	Amino acid side chains, methyl groups of proteins	(18,20,40,41)
10	1313/1313	NC**	Amide III; C-N stretching (30%), N-H bending (30%), C=O stretching (10%), O=C-N bending (10%)	Proteins	(21,40,45,46)
11	1246/1246	0.093/0.097	PO_2^- antisymmetric stretching (non H-bonded)	Nucleic acids (mainly), phospholipids, phosphorylated proteins	(18,20,21,40,42,46)
12	1110/1111	0.060/0.067	C-O stretching, C-C stretching (ring)	Carbohydrates, nucleic acids	(40,42)
13	1077/1077	0.079/0.077	PO_2^- symmetric stretching (fully H-bonded)	Nucleic acids, nucleotides	(18,21,40,41,42,46)
14	893/892	0.034/0.030	Different modes of phosphodiester bonds, C-C, C-O stretching	Nucleic acids	(20,40,42,46)
I-shoulder	1683/1683	NC**	β -sheet, β -turns and bends	Proteins	(38,44-46)
I	1645/1646	0.095e-3/0.150e-3	Disordered structure (random coils), overlaps with α -helical structure	Proteins	(38,44-46)
II	1580/1580	0.023e-3/0.041e-3	Amino acid side chains	Proteins	(45)
III	1544/1543	0.063e-3/0.103e-3	α -helix, random coils	Proteins	(44,45)
IV	1516/1516	0.071e-3/0.048e-3	Amino acid side chains	Proteins	(45,46)

* Area values were used for absorbance peaks while intensity values for second derivative peaks; ** NC: Not calculated; because these peaks/shoulders were too weak.

Similarly, a peak at 1446 cm^{-1} was assigned to CH_3 bending of amino acid side chains. Two peaks at 1246 and 1077 cm^{-1} arise from PO_2 stretching modes of nucleotides and nucleic acids and phosphoproteins in biological samples (18,20,21,40,41,42,46).

Detailed studies on the FTIR spectroscopic characterization of proteins in H_2O and D_2O revealed band patterns which can be used to identify proteins, secondary structures, and amino acid side chains (18,22,38,42-46). The major absorption bands in an IR spectrum of pure proteins are mainly associated with their amide group (i.e. peptide bond). The characteristic bands of proteins arise from C=O, C-N, N-H stretching, N-H bending and O-C-N bending modes of their amide groups and therefore labelled as *Amide* bands (e.g. Amide I-VII, A, B) (17-21). The Amide I band originates from C=O stretching (80%), N-H bending (10%) and C-N stretching (10%) modes of proteins. Similarly, the Amide II band arises from N-H bending (60%) and C-N stretching (40%) vibrations of amide groups and takes a significant contribution from proteins (18,20,21,38,41,44-46). The percentages written in parentheses were calculated by the potential energy distribution approach in previous studies, reflecting the relative contribution of a specific mode to the total change in potential energy during vibration (54). A strong band rising from N-H stretching vibrations between 3310 - 3270 cm^{-1} is referred to as Amide A band of proteins (45,46) and a weaker band rising again from N-H stretching modes between 3100 - 3030 cm^{-1} is named Amide B band (45,46). A weak band near 1300 cm^{-1} originates from C-N stretching (30%), N-H bending (30%), C=O stretching (10%) and O=C-N bending (10%) modes of proteins is called the Amide III band (44-46). These bands were also observable in the IR spectrum of *M. lebetina* venom.

Sub-bands obtained by derivatization (e.g. second derivative) in the Amide I-II region, ranging between 1700 - 1500 cm^{-1} provides information about the protein secondary structures. The Amide I band is generally preferred for analyzing protein structures but the Amide II band can also be used for the same purpose (38,43-46). It is a widely-applied procedure to obtain information about secondary structures of proteins by spectral interpretation using FTIR data since previous studies using pure peptides and proteins provided knowledge for this practice by relating specific frequencies to particular protein secondary structures (38,43-46,54). Exact frequencies of sub-bands in the Amide I-II region depend on the H-bonding, involving the amide group, which is determined by the secondary structure (46). In the present study, wavenumbers were assigned to the secondary structures of proteins by comparing the reference data previously published in the literature (38,44-46).

Analyzing biological samples gives insight about the unique biomolecular content and provides information about the amounts of these compounds, as well as molecular alterations (19,42,46). This method also provides an opportunity to analyze the protein secondary structures and structural changes (38,46). There are many published papers on the use of FTIR spectroscopy coupled with multivariate statistical analysis for the elucidation of molecular mechanisms and the diagnosis of various diseases such as

cancers, (21,47,48) metabolic disorders (20,41), the classification of microorganisms (49,50), plants (51), and food products (52,53).

In the field of toxinology, FTIR spectroscopy has been used to analyze the secondary structure of purified snake venom proteins (30-33) but there is scarce data on the physicochemical characterization of crude snake venoms. In one study, the influence of ecological factors on the venom of *M. l. obtusa* (from Azerbaijan) was investigated by radiobiological and biophysical (spectroscopic) methods (37). The researchers also made an IR spectroscopic characterization using the KBr pellet method, but they presented neither a detailed assignment list associated to venom molecules nor protein secondary structure information. Moreover, the resolution of spectrum figures did not allow an investigation of spectral patterns and the spectrum in two out of three figures seemed too noisy, making clear peak picking not possible. The study reported peaks at 3300 , 3100 , 3020 , 2570 , 2100 - 2260 , 1480 , 1460 , 1350 , 1100 cm^{-1} wavenumbers. It assigned peaks above 3000 cm^{-1} to N-H stretching, while others to various C-H modes. It also identified peaks between 3100 - 3700 cm^{-1} as an indication of the presence of S atoms, but characteristic bands of S containing groups lie below 2600 cm^{-1} (46). Possible S-H stretching peaks in this region are generally too weak to observe. The research data contained significant differences when compared to the results of this study. The most important protein bands (i.e. Amide I, II) were lacking in the previous study's reported peaks, which was surprising since the major component of snake venom is protein. Moreover, that study did not report any peak assigned to PO_2 stretching modes. This current study presents a more comprehensive and complete FTIR spectroscopic characterization of both *M. l. obtusa* and *M. l. lebetina*.

In another study, chitosan nanoparticles alone and loaded with *Echis carinatus* venom were measured by FTIR spectroscopy but the spectrum was dominated by peaks originated from chitosan nanoparticles so that it was not possible to obtain information from snake venom (35). After this study, the same group investigated the efficiency of *E. carinatus* venom loaded chitosan nanoparticles as antigen carrier for antivenom production and they provided the FTIR spectrum of *E. carinatus* venom obtained by the KBr pellet method together with chitosan, chitosan nanoparticles and *E. carinatus* venom loaded chitosan nanoparticles in the same figure (36). It was not easy to discriminate the venom spectrum from the figure published in the results and it only reported that a venom sample showed peaks around 3305 , 1650 and 1541 cm^{-1} wavenumbers which correspond to the Amide A, Amide I and Amide II peaks, respectively. These peaks were also visible in the FTIR spectrum of *M. lebetina* venom obtained in the present study with slightly shifted wavenumbers, due to the protein-based nature of snake venoms. Since the aim of the study by Mirzaei et al. (36) was to investigate the formation of venom loaded nanoparticles, the researchers focused on the spectra of nanoparticles and did not provide a detailed FTIR spectroscopy-based biomolecular characterization of the venom sample. With the use of state-of-the-art *-omics* technologies and approaches such as genomics, transcriptomics, proteomics and metabolomics in toxinology, the characterization of unex-

explored animal venoms can be done faster and more reliably today. Within the context of systems biology and *-omics* approach, FTIR spectroscopy has the potential to provide complementary information for the characterization of snake venoms.

This study optimized the FTIR-ATR procedure, which allowed us to detect absorbance peaks characterizing the major and minor biomolecules in venom samples. Moreover, information about the overall protein secondary structures was obtained by analyzing a second derivative spectrum of the Amide I and Amide II region. As a result, major structures were found as random coil and α -helix, taking contributions from β -sheet structures. This finding is concordant with three dimensional structures of snake venom C-type lectins (55), phospholipase A₂s (56), metalloproteinases (57), and serine proteinases (58), which are also the most abundant proteins in the venom of *M. lebetina* (3,25,59). Each species has a unique combination of proteins in their venoms and this method can be used to obtain information reflecting the dominant secondary structures of abundant venom proteins, as well as to make comparisons between different species and individuals. The study found that the absorbance spectra of two subspecies were quite similar, as an expected result of the research. However, there were some quantitative, qualitative alterations and peak shifts in both absorbance and second derivative spectra. The Peak II and Peak IV in second derivative spectra originating from amino acid side chains clearly showed a difference between subspecies (Figure 1) and this result emphasized the potential of second derivative spectrum in Amide I-II region for the differentiation of venom samples.

Differences in the area or intensity values of the bands indicate that the amount of venom compounds show variation between subspecies. Inter and intraspecies variation in snake venoms is a well-known phenomenon (60) which can explain the differences we observed in the present study. Moreover, the venom proteins of *M. l. lebetina* and *M. l. obtusa* were previously compared by using two-dimensional polyacrylamide gel electrophoresis (2D-PAGE) method and results showed that there was a variation between these two taxa (3). Although the FTIR spectroscopy method gives resulting peaks rising from different vibrational modes of overall molecules in the sample, the results of the present study showed that its sensitive measurement can provide data especially in the second derivative spectrum in Amide I-II region to uncover the venom variation between different taxa.

Major absorbance peaks observed in the present study such as Amide A, B, I, II and III arise from proteins (Table 1), which was an expected result since snake venoms mainly consist of proteins and peptides (1-3). Additionally, some other peaks were observable originating from other biological macromolecules such as nucleic acids and carbohydrates. The main bioactive compounds responsible for the pharmacological properties of snake venoms are proteins and peptides but the other molecules such as amines, nucleosides, carbohydrates and inorganic elements, which can be referred to as minor components, contribute to the activity of these proteins (4). The Fourier

transform infrared spectroscopy method provides information about all the bioorganic molecules allowing the researchers to analyze minor components of crude venoms. There was little information in the literature about the aforementioned minor components of snake venom, except some very old research. Recently, in a study by Villar-Briones and Aird (5), small metabolites and peptides were screened in the venom of 15 different taxa belonging to Elapidae, Viperinae and Crotalinae by using liquid chromatography-mass spectrometry (LC-MS) which revisited the small organic molecule content of snake venoms. They detected carboxylic acids, purine nucleosides and their bases, neurotransmitters, amines, amino acid residues, and peptides as abundant small organic molecules.

We observed C-O and C-C stretching vibration modes originating from carbohydrates. Although old publications reported the presence of sugars such as galactose, glucose, mannose and fucose in some Viperid and Elapid species (61), observed peaks may also arise from the carbohydrate moieties of nucleosides, nucleotides (4,5) and venom glycoproteins (5,62). Polysaccharides are not reported from snake venoms. This research also detected peaks characterizing PO₂⁻ stretching modes mainly arising from nucleic acids and nucleotides. The presence of nucleosides in snake venom and its role in toxicity was documented but there was limited information on free nucleotides (4,5). However, it is known that snake venom contains ribonucleic acid (RNA) (63,64) and deoxyribonucleic acid (DNA) (65,66), which comes from the cells covering the lumen of the venom gland. In line with this information, it is highly possible that peaks originating from PO₂⁻ stretching vibrations in the FTIR spectrum arise mainly from nucleic acid backbone and nucleosides. Phosphate groups of phosphorylated proteins may also contribute to these bands. Stretching vibration peaks of CH₂ and CH₃ groups were also observed which may originate from proteins and lipids but there is scarce information on the occurrence of lipids in snake venom (4) and more studies should be conducted on this topic.

CONCLUSION

In conclusion, we applied the FTIR-ATR method for crude snake venom analysis and obtained the molecular fingerprint spectrum of *M. l. lebetina* and *M. l. obtusa* venom samples in the mid-IR region. This method is fast, sensitive to molecular alterations and does not require time-consuming sample preparation, which is suitable for the direct measurement of lyophilized venom samples. It provides rapid information about not only proteins, but also minor constituents of snake venoms. Although this method is not sufficient alone to fully characterize an unexplored venom, once the spectral libraries including data from different known species is obtained it may be possible to classify and identify venom samples using multivariate statistical analyses such as hierarchical cluster analysis and principal component analysis coupled with linear discriminant analysis, as well as to make quality control and stability testing of crude venom products. These kinds of classifications of biological samples were successfully achieved by FTIR spectroscopy (47-

52). Moreover, this method can be used to assess the individual venom variation. The results of this study show the usefulness and feasibility of this method in the field of toxinology. It also provides a peak assignment table which will be useful for other similar studies as a reference list. Although the absorbance spectra of two subspecies were almost identical (except some quantitative differences), the second derivative spectra showed differences in the Amide I-II region. Therefore, the second derivative spectra should be taken in consideration in similar studies. The sample size of this study was not enough to perform statistical analyses but this approach deserves further studies including more individual venom samples from different species and families to test the sensitivity and specificity of the method supported with univariate and multivariate statistics. Such studies will reveal the potential of this method for classifying crude venoms by using chemometric analyses.

Acknowledgement: We greatly acknowledge and dedicate this article to late Prof. Dr. Bayram GÖÇMEN who passed away tragically on 22 March 2019, for his great contributions to the field herpetology and his invaluable support to the studies related to snake venoms in Turkey by providing venom samples. We also thank Assoc. Prof. Mehmet Zülfü YILDIZ (Adiyaman University Department of Biology), Assoc. Prof. Bahadır AKMAN (İğdır University) and Assoc. Prof. Deniz YALÇINKAYA (Toros University) for their helps in the field studies.

Peer-review: Externally peer-reviewed.

Author Contributions: Conception/Design of study: N.I., F.D.O.D.; Data Acquisition: N.I.; Data Analysis/Interpretation: N.I.; Drafting Manuscript: N.I., F.D.O.D.; Critical Revision of Manuscript: N.I., F.D.O.D.; Final Approval and Accountability: D N.I., F.D.O.D.; Technical or Material Support: F.D.O.D.; Supervision: F.D.O.D.

Conflict of Interest: The authors declare that they have no conflicts of interest to disclose.

Financial Disclosure: There are no funders to report for this submission.

REFERENCES

1. Tu AT. Overview of snake venom chemistry. Singh BR, Tu AT, editors. Natural Toxins II. New York: Plenum Press; 1996. pp. 37–62.
2. Chippaux JP. Snake venoms and envenomations. 1st ed. Florida: Krieger Publishing Company; 2006.
3. Igci N, Ozel Demiralp D. A preliminary investigation into the venom proteome of *Macrovipera lebetina obtusa* (Dwigubsky, 1832) from Southeastern Anatolia by MALDI-TOF mass spectrometry and comparison of venom protein profiles with *Macrovipera lebetina lebetina* (Linnaeus, 1758) from Cyprus by 2D-PAGE. Arch Toxicol 2012; 86(3): 441–51.
4. Bieber AB. Metal and Nonprotein Constituents of Snake Venoms. Lee CY, editor. Snake venoms. Handbook of experimental pharmacology. Berlin, Heidelberg: Springer; 1979. pp. 295–306.
5. Villar-Briones A, Aird SD. Organic and peptidyl constituents of snake venoms: The picture is vastly more complex than we imagined. Toxins 2018; 10(392): 1–49.
6. Lewis RJ, Garcia ML. Therapeutic potential of venom peptides. Nat Rev Drug Discov 2003; 2(10): 790–802.
7. Vetter I, Davis JL, Rash LD, Anangi R, Mobli M, Alewood PF, et al. Venomics: a new paradigm for natural products-based drug discovery. Amino Acids 2011; 40(1): 15–28.
8. Vonk FJ, Jackson K, Doley R, Madaras F, Mirtschin PJ, Vidal N. Snake venom: From fieldwork to the clinic: Recent insights into snake biology, together with new technology allowing high-throughput screening of venom, bring new hope for drug discovery. Bioessays 2011; 33(4): 269–79.
9. Atatür MK, Göçmen B. Kuzey Kıbrıs'ın kurbağa ve sürüngenleri-amphibians and reptiles of Northern Cyprus. 1st ed. Izmir: Ege Üniversitesi Yayınları Fen Fakültesi Kitaplar Serisi No: 170; 2001.
10. Mallow D, Ludwig D, Nilson G. True vipers: Natural history and toxinology of old world vipers. 1st ed. Florida: Krieger Publishing Company; 2003.
11. Budak A, Göçmen B. Herpetoloji. 2nd ed. Izmir: Ege Üniversitesi Yayınları Fen Fakültesi Yayın No: 194; 2008.
12. Stümpel N, Joger U. Recent advances in phylogeny and taxonomy of Near and Middle Eastern Vipers – an update. ZooKeys 2009; 31: 179–91.
13. Göçmen B, Atatür MK, Budak A, Bahar H, Yıldız MZ, Alpagut-Keskin N. Taxonomic notes on the snakes of Northern Cyprus, with observations on their morphologies and ecologies. Anim Biol 2009; 59: 1–30.
14. Swaroop S, Grab B. Snakebite mortality in the World. Bull World Health Organ 1954; 10(1): 35–76.
15. Cesaretli Y, Ozkan O. Snakebites in Turkey: epidemiological and clinical aspects between the years 1995 and 2004. J Venom Anim Toxins Incl Trop Dis 2010; 16(4): 579–86.
16. Sherman Hsu CP. Infrared Spectroscopy. Settle FA, editor. Handbook of instrumental techniques for analytical chemistry. New Jersey: Prentice Hall; 1997. pp. 247–83.
17. Özel Demiralp FD, İgci N, Peker S, Ayhan B. Temel proteomik stratejiler. 1st ed. Ankara: Ankara Üniversitesi Yayınevi; 2014.
18. Severcan F, Akkas SB, Turker S, Yuçel R. Methodological approaches from experimental to computational analysis in vibrational spectroscopy and microspectroscopy. Severcan F, Haris PI, editors. Vibrational spectroscopy in diagnosis and screening. Amsterdam: IOS Press; 2012. pp. 12–52.
19. Baker MJ, Trevisan J, Bassan P, Bhargava R, Butler HJ, Dorling KM, et al. Using fourier transform IR spectroscopy to analyze biological materials. Nat Protoc 2014; 9(8): 1771–91.
20. Igci N, Sharafi P, Ozel Demiralp D, Demiralp CO, Yuce A, Dokmeci Emre S. Application of Fourier transform infrared spectroscopy to biomolecular profiling of cultured fibroblast cells from Gaucher disease patients: A preliminary investigation. Adv Clin Exp Med 2017; 26(7): 1053–61.
21. Bozdag G, Igci N, Calis P, Ayhan B, Ozel Demiralp D, Mumusoglu S, et al. Examination of cervical swabs of patients with endometriosis using Fourier transform infrared spectroscopy. Arch Gynecol Obstet 2019; 299(5): 1501–08.
22. Haris PI, Severcan F. FTIR spectroscopic characterization of protein structure in aqueous and non-aqueous media. J Mol Catal B Enzym 1999; 7(1–4): 207–21.
23. Bazaa A, Marrakchi N, El Ayeb M, Sanz L, Calvete JJ. Snake venomics: comparative analysis of the venom proteomes of the Tunisian snakes *Cerastes cerastes*, *Cerastes vipera* and *Macrovipera lebetina*. Proteomics 2005; 5(16): 4223–35.
24. Arıkan H, Göçmen B, Kumlutaş Y, Alpagut-Keskin N, Ilgaz Ç, Yıldız MZ. Electrophoretic characterisation of the venom samples obtained from various Anatolian snakes (Serpentes: Colubridae, Viperidae, Elapidae). North-West J Zool 2008; 4(1): 16–28.

25. Sanz L, Ayzvazyan N, Calvete JJ. Snake venomomics of the Armenian mountain vipers *Macrovipera lebetina obtusa* and *Vipera raddei*. J Proteomics 2008; 71: 198–209.
26. Calvete JJ, Sanz L, Angulo Y, Lomonte B, Gutiérrez JM. Venomomics, antivenomics. FEBS Lett 2009; 583(11): 1736–43.
27. Nalbantsoy A, Hempel BF, Petras D, Heiss P, Göçmen B, İğci N, Yıldız MZ, Süßmuth RD. Combined venom profiling and cytotoxicity screening of the Radde's mountain viper (*Montivipera raddei*) and mount bulgar viper (*Montivipera bulgardaghica*) with potent cytotoxicity against human A549 lung carcinoma cells. Toxicon 2017; 135: 71–83.
28. Petras D, Hempel BF, Göçmen B, Karis M, Whiteley G, Wagstaff SC, et al. Intact protein mass spectrometry reveals intraspecies variations in venom composition of a local population of *Vipera kaznakovi* in north eastern Turkey. J Proteomics 2019; 199: 31–50.
29. Siigur J, Aaspõllu A, Siigur E. Biochemistry and pharmacology of proteins and peptides purified from the venoms of the snakes *Macrovipera lebetina* subspecies. Toxicon 2019; 158: 16–32.
30. Aird SD, Middaugh CR, Kaiser II. Spectroscopic characterization of textilotoxin, a presynaptic neurotoxin from the venom of the Australian eastern brown snake (*Pseudonaja t. textilis*). Biochim Biophys Acta Protein Struct Mol Enzymol 1989; 997(3): 219–23.
31. Lamthanh H, Léonetti M, Nabedryk E, Ménez A. CD and FTIR studies of an immunogenic disulphide cyclized octadecapeptide, a fragment of a snake curaremimetic toxin. Biochim Biophys Acta Protein Struct Mol Enzymol 1993; 1203(2): 191–8.
32. Cecchini AL, Soares AM, Cecchini R, Oliveira AHC, Ward RJ, Giglio JR, et al. Effect of crotoptin on the biological activity of Asp49 and Lys49 phospholipases A₂ from *Bothrops* snake venoms. Comp Biochem Physiol C Toxicol Pharmacol 2004; 138(4): 429–36.
33. Oliveira KC, Spencer PJ, Ferreira Jr RS, Nascimento N. New insights into the structural characteristics of irradiated crotoamine. J Venom Anim Toxins Incl Trop Dis 2015; 21: 14.
34. Bhowmik T, Saha PP, Sarkar A, Gomes A. Evaluation of cytotoxicity of a purified venom protein from *Naja kaouthia* (NKCT1) using gold nanoparticles for targeted delivery to cancer cell. Chem Biol Interact 2017; 261: 35–49.
35. Mohammadpour Dounighi M, Mehrabi M, Avadi MR, Zolfagharian H, Rezayat M. Preparation, characterization and stability investigation of chitosan nanoparticles loaded with the *Echis carinatus* snake venom as a novel delivery system. Arch Razi Inst 2015; 70(4): 269–77.
36. Mirzaei F, Mohammadpour Dounighi N, Avadi MR, Rezayat M. A new approach to antivenom preparation using chitosan nanoparticles containing *Echis carinatus* venom as a novel antigen delivery system. Iran J Pharm Res 2017; 16(3): 858–67.
37. Shafiga T, Huseyn A. Radiobiological and biophysical showing of venom of *Macrovipera lebetina obtusa*. IJREH 2017; 1(3): 1–12.
38. Adigüzel Y, Haris PI, Severcan F. Screening of proteins in cells and tissues by vibrational spectroscopy. Severcan F, Haris PI, editors. Vibrational spectroscopy in diagnosis and screening. Amsterdam: IOS Press; 2012. pp. 53–108.
39. Severcan F, Toyran N, Kaptan N, Turan B. Fourier transform infrared study of the effect of diabetes on rat liver and heart tissues in the C–H region. Talanta 2000; 53(1): 55–9.
40. Movasaghi Z, Rehman S, Rehman I. Fourier transform infrared (ftir) spectroscopy of biological tissues. Appl Spectrosc Rev 2008; 43(2): 134–79.
41. Severcan F, Bozkurt O, Gurbanov R, Gorgulu G. FT-IR spectroscopy in diagnosis of diabetes in rat animal model. J Biophotonics 2010; 3(8–9): 621–31.
42. Rehman I, Movasaghi Z, Rehman S. Vibrational spectroscopy for tissue analysis. 1st ed. Florida: CRC Press, 2013.
43. Jackson M, Mantsch HH. The use and misuse of FTIR spectroscopy in the determination of protein structure. Crit Rev Biochem Mol Biol 1995; 30(2): 95–120.
44. Goormaghtigh E, Ruyschaert J-M, Raussens V. Evaluation of the information content in infrared spectra for protein secondary structure determination. Biophys J 2006; 90(8): 2946–57.
45. Barth A. Infrared spectroscopy of proteins. Biochim Biophys Acta 2007; 1767(9): 1073–101.
46. Stuart B. Biological applications of infrared spectroscopy. 1st ed. West Sussex: John Wiley & Sons, 1997.
47. Cheung KT, Trevisan J, Kelly JG, Ashton KM, Stringfellow HF, Taylor SE, et al. Fourier-transform infrared spectroscopy discriminates a spectral signature of endometriosis independent of inter-individual variation. Analyst 2011; 136(10): 2047–55.
48. Bellisola G, Sorio C. Infrared spectroscopy and microscopy in cancer research and diagnosis. Am J Cancer Res 2012; 2(1): 1–21.
49. Garip S, Bozoglu F, Severcan F. Differentiation of mesophilic and thermophilic bacteria with fourier transform infrared spectroscopy. Appl Spectrosc 2007; 61(2): 186–92.
50. Maity JP, Kar S, Lin C-M, Chen C-Y, Chang Y-F, Jean J-S, et al. Identification and discrimination of bacteria using Fourier transform infrared spectroscopy. Spectrochim Acta A Mol Biomol Spectrosc 2013; 116: 478–84.
51. Turker Gorgulu S, Dogan M, Severcan F. The characterization and differentiation of higher plants by fourier transform infrared spectroscopy. Appl Spectrosc 2007; 61(3): 300–8.
52. Gok S, Severcan M, Goormaghtigh E, Kandemir I, Severcan F. Differentiation of Anatolian honey samples from different botanical origins by ATR-FTIR spectroscopy using multivariate analysis. Food Chem 2015; 170: 234–40.
53. Deniz E, Güneş Altuntaş E, Ayhan B, İğci N, Özel Demiralp D, Candoğan K. Differentiation of beef mixtures adulterated with chicken or turkey meat using FTIR spectroscopy. J Food Process Preserv 2018; 42: e13767.
54. Krimm S, Bandekar J. Vibrational spectroscopy and conformation of peptides, polypeptides and proteins. Anfinsen CB, Edsall JT, Richards FM, editors. Advances in protein biochemistry, vol. 38. New York: Academic Press; 1986. pp. 181–364.
55. Jebali J, Fakhfekh E, Morgen M, Srairi-Abid N, Majdoub H, Gargouri A, et al. Lebecin, a new C-type lectin like protein from *Macrovipera lebetina* venom with anti-tumor activity against the breast cancer cell line MDA-MB231. Toxicon 2014; 86: 16–27.
56. Tonello F, Rigoni M. Cellular Mechanisms of Action of Snake Phospholipase A₂ Toxins. In: Gopalakrishnakone P, Inagaki H, Vogel CW, Mukherjee A, Rahmy T, editors. Snake Venoms. Dordrecht: Springer, 2017: 49–65.
57. Takeda S. ADAM and ADAMTS family proteins and snake venom metalloproteinases: A structural overview. Toxins 2016; 8(155): 1–38.
58. Zeng F, Shen B, Zhu Z, Zhang P, Ji Y, Niu L, et al. Crystal structure and activating effect on RyRs of AhV_TL-I, a glycosylated thrombin-like enzyme from *Agkistrodon halys* snake venom. Arch Toxicol 2013; 87(3): 535–45.
59. İğci N, Özel Demiralp FD, Yıldız MZ. Cytotoxic activities of the crude venoms of *Macrovipera lebetina lebetina* from Cyprus and *M. l. obtusa* from Turkey (Serpentes: Viperidae) on human umbilical vein endothelial cells. Comm J Biol 2019; 3(2): 110–3.
60. Chippaux JP, Williams V, White J. Snake venom variability: Methods of study, results and interpretation. Toxicon 1991; 29(11): 1279–303.

61. Devi A. The protein and nonprotein constituents of snake venoms. Bücherl W, Buckley EE, Deulofeu V, editors. Venomous animals and their venoms. New York: Academic Press; 1968. pp. 119–65.
62. Gowda DC, Davidson EA. Structural features of carbohydrate moieties in snake venom glycoproteins. Biochem Biophys Res Commun 1992; 182(1): 294–301.
63. Currier RB, Calvete JJ, Sanz L, Harrison RA, Dowley PD, Wagstaff SC. Unusual stability of messenger RNA in snake venom reveals gene expression dynamics of venom replenishment. PLoS ONE 2012; 7(8): e41888.
64. Modahl CM, Mackessy SP. Full-length venom protein cDNA sequences from venom-derived mRNA: Exploring compositional variation and adaptive multigene evolution. PLoS Negl Trop Dis 2016; 10(6): e0004587.
65. Pook CE, McEwing R. Mitochondrial DNA sequences from dried snake venom: a DNA barcoding approach to the identification of venom samples. Toxicon 2005; 46(7): 711-5.
66. Smith CF, McGlaughlin ME, Mackessy SP. DNA barcodes from snake venom: a broadly applicable method for extraction of DNA from snake venoms. Biotechniques 2018; 65(6): 339–45.

***In vitro* Antidiabetic Activity of Seven Medicinal Plants Naturally Growing in Turkey**

Ebru Deveci¹ , Gulsen Tel-Cayan² , Mehmet Emin Duru³ 

¹Konya Technical University, Department of Chemistry and Chemical Processing Technologies, Konya, Turkey

²Muğla Sıtkı Koçman University, Department of Chemistry and Chemical Processing Technologies, Muğla, Turkey

³Muğla Sıtkı Koçman University, Faculty of Science, Department of Chemistry, Muğla, Turkey

ORCID IDs of the authors: E.D. 0000-0002-2597-9898; G.T.C. 0000-0002-1916-7391; M.E.D. 0000-0001-7252-4880

Please cite this article as: Deveci E, Tel-Cayan G, Duru ME. *In vitro* Antidiabetic Activity of Seven Medicinal Plants Naturally Growing in Turkey. Eur J Biol 2020; 79(1): 23-28. DOI: 10.26650/EurJBiol.2020.0011

ABSTRACT

Objective: Diabetes mellitus is a worldwide metabolic/endocrine disease that causes major medical problems. One of the most important strategies used in the therapy of the diabetes mellitus is the use of inhibition of α -glucosidase and α -amylase enzymes. Therefore, this study aimed to investigate antidiabetic activities of the hexane and methanol extracts of the medicinal plants from Turkey.

Materials and Methods: The hexane and methanol extracts of *Euphorbia helioscopia*, *Ferula elaeochoytris*, *Sideritis albiflora*, *Sideritis stricta*, *Sideritis pisdica*, *Sideritis leptoclada*, *Salvia chionantha* plants were prepared at room temperature. Antidiabetic activities of the extracts on α -glucosidase and α -amylase enzymes were determined.

Results: *S. pisdica* hexane extract exhibited higher α -amylase inhibitory activity than acarbose (96.60±0.08 %) used as a standard with an inhibition value of 97.99±0.79 % at 1000 μ g/mL concentration. In terms of α -glucosidase inhibitory activities, the extracts were ranked in the following order: *F. elaeochoytris* hexane extract > *S. leptoclada* hexane extract > *S. stricta* hexane extract > *E. helioscopia* hexane extract.

Conclusion: In this study, antidiabetic activities of the extracts on α -glucosidase and α -amylase enzymes of the studied medicinal plants were screened for the first time. It has been suggested that *S. pisdica* hexane extract can be used as antidiabetic agent.

Keywords: Medicinal plants, antidiabetic activity, extracts, α -amylase, α -glucosidase

INTRODUCTION

Diabetes mellitus, which is a carbohydrate metabolism disease, causes complications by increasing the risk of neuropathy, retinopathy, and cardiovascular disease if left untreated (1,2). In a report of the World Health Organization, it is reported that these diseases and complications cause direct medical costs, loss of work and wage losses and significant economic losses (3). Type 2 diabetes is more common among cases of diabetes mellitus and occurs mainly in adults; however, it is becoming increasingly popular in adolescents. Type 2 diabetes, which is caused by insulin resistance

or loss of function of pancreatic β -cells, is estimated to affect around 150 million people worldwide (4). Endogenous factors, such as genetic and metabolic abnormalities, and exogenous factors, such as behavior and the environment, constitute the pathogenesis of type 2 diabetes (5). Type 2 diabetes causes increased blood sugar levels in diabetic patients. Today, the most widely accepted method in the treatment of type 2 diabetes is monitoring and controlling hyperglycemia. Digestive enzymes such as α -amylase, and α -glucosidase have a key role in determining blood sugar levels. α -Amylase is involved in the breakdown of long-chain carbohydrates, while α -glucosidase directly converts carbohy-



Corresponding Author: Gulsen Tel-Cayan

E-mail: gulsentel@mu.edu.tr

Submitted: 26.02.2020 • **Revision Requested:** 02.03.2020 • **Last Revision Received:** 23.03.2020 • **Accepted:** 02.04.2020

© Copyright 2020 by The Istanbul University Faculty of Science • Available online at <http://ejb.istanbul.edu.tr> • DOI: 10.26650/EurJBiol.2020.0011

drates into glucose in the small intestine (6,7). α -Glucosidase and α -amylase inhibitors delay the digestion of carbohydrates and slow the rate of glucose absorption. This reduces the level of glucose in the blood cells. For the control of postprandial hyperglycemia as well as type 2 diabetes, inhibition of these enzymes has been considered therapeutically (8). Therefore, simultaneous administration of α -amylase and α -glucosidase inhibitors via food is a potential and feasible method for the control of type 2 diabetes (9).

Artificial inhibitors such as voglibose, acarbose and miglitol are used clinically for the treatment of type 2 diabetes. However, due to the observation of side effects of these synthetic inhibitors, such as gas compression in the stomach, hepatotoxicity, diarrhea, abdominal pain and liver diseases, studies focusing on the discovery of new and non-side effects inhibitors from natural sources and plants are being conducted (10-13). Many studies have shown that some plants used in traditional medicine have therapeutic effects on diabetic patients (14,15). More than 400 plants worldwide have been documented as beneficial in the treatment of diabetes (16-19).

Salvia and *Sideritis* genus are the main species belonging to the Lamiaceae family (20). The *Sideritis* genus contains more than 150 species, while the *Salvia* genus is represented by over 900 species in the world (20,21). Both these species are mostly consumed as tea, and used in the treatment of various diseases (22,23). Previous studies have revealed that the *Sideritis* species has various biological properties such as antioxidant, anti-inflammatory, antifeedant, antimicrobial, antiviral, antinociceptive and antiulcer (24,25). The *Salvia* species is the medically important plant species due to having numerous pharmacological activities such as antitumor, antioxidant and wound healing, insecticidal, herbicidal, antifungal, antimicrobial and cytotoxic (26). The *Ferula* genus, an important member of the Apiaceae family, consists of more than 170 species. In folk medicine, the *Ferula* species is used in the treatment of indigestion, whooping cough, cramps, inflammation, epilepsy, pain, cholera, flatulent colic and infertility (27). Also, it has been determined that this species has anti-fertility, antifungal, anti-inflammatory, antispasmodic, antitumor, antiviral, antiulcerogenic, cancer chemopreventive and antioxidant effects (28). The *Euphorbia* genus, the most well-known of the Euphorbiaceae family, is represented by approximately 2150 taxa in the world (29). Anti-inflammatory, antiarthritic, antiviral, antitussives, antitumor, antiallergic, antiasthma and antioxidant activities of the *Euphorbia* species have been reported in earlier investigations (30). As a result of the studies carried out so far, it is obvious that these species are included in the class of aromatic plants that are considered biologically and medically important.

The interest of different scientific fields in natural compounds has increased in recent years. Medicinal plants are considered to be rich sources of biologically active compounds, such as terpenes, alkaloids and phenolics, and are responsible for multifunctional biological effects including anti-inflammatory, antimicrobial, antioxidant and antitumor (31). Also, an inverse re-

lationship between the consumption of fruits, vegetables, and plants in diets and the risk of developing chronic illness such as cancer, diabetes, and cardiovascular diseases has been reported. Therefore, this study aimed to investigate antidiabetic activities on α -amylase and α -glucosidase enzymes of the hexane and methanol extracts of *Euphorbia helioscopia*, *Ferula elaeochoytris*, *Sideritis stricta*, *Sideritis leptoclada*, *Sideritis albiflora*, *Sideritis pisidica*, and *Salvia chionantha*. [*Euphorbia helioscopia* (EHH, EHM), *Ferula elaeochoytris* (FEH, FEM), *Sideritis stricta* (SSH, SSM), *Sideritis leptoclada* (SLH, SLM), *Sideritis albiflora* (SAH, SAM), *Sideritis pisidica* (SPH, SPM), and *Salvia chionantha* (SCH, SCM)]

MATERIALS AND METHODS

Plant Materials

Euphorbia helioscopia was collected from Artvin, Turkey; *Ferula elaeochoytris* from Bayburt, Turkey; *Sideritis stricta*, *Sideritis leptoclada*, *Sideritis albiflora*, *Sideritis pisidica* from Muğla, Turkey; and *Salvia chionantha* from Burdur, Turkey. The specimens with voucher numbers have been deposited at Natural Products Laboratory of Muğla Sıtkı Koçman University Herbarium.

Extraction

The dried and powdered aerial parts of plants were extracted with *n*-hexane (4 x 24h) at room temperature. After filtration, the solvent was evaporated on a vacuum by an evaporator to produce hexane extracts. The plant residue was dried and then extracted with methanol (4 x 24h) at room temperature. After filtration, the solvent was evaporated on a vacuum by an evaporator to produce methanol extracts. The hexane and methanol extracts were stored at +4°C for further tests.

Determination of α -Amylase Inhibitory Activity

α -Amylase inhibitory activity of the extracts was tested by using the method previously reported by Quan et al. with slight modifications (31). 25 μ L sample solution and 50 μ L α -amylase solution (0.1 units/mL) in phosphate buffer (20 mM pH=6.9 phosphate buffer prepared with 6 mM NaCl) were mixed in a 96-well microplate. The mixture was pre-incubated for 10 min. at 37 °C. After pre-incubation, 50 μ L starch solution (0.05 %) was added and incubated for 10 min. at 37 °C. The reaction was completed by addition of 25 μ L HCl (0.1 M) and 100 μ L Lugol solutions. A 96-well microplate reader was used to measure absorbance at 565 nm. Acarbose was used as the standard compound. α -Amylase inhibitory activity results are stated as inhibition percentage (%) of the enzyme at 1000 μ g/mL concentration of the extracts and 50 % inhibition concentration (IC_{50}).

Determination of α -Glucosidase Inhibitory Activity

α -Glucosidase inhibitory activity of the extracts was performed using the method previously reported by Kim et al. with slight modifications (32). 50 μ L phosphate buffer (0.01 M pH=6.9), 25 μ L PNPG (4-N-nitrophenyl- α -D-glucopyranoside) in phosphate buffer (0.01 M pH=6.9), 10 μ L sample solution and 25 μ L α -glucosidase (0.1 units / mL) in phosphate buffer (0.01 M pH=6.0) were mixed in a 96-well microplate. The mixture was incubated for 20 min. at 37 °C. To stop reaction, 90 μ L sodium carbonate (0.1 M) was added and a 96-well microplate reader was

used to measure absorbance at 400 nm. Acarbose was used as the standard compound. α -Glucosidase inhibitory activity results are stated as inhibition percentage (%) of the enzyme at 500 $\mu\text{g/mL}$ concentration of the extracts and as 50 % inhibition concentration (IC_{50}).

Statistical Analysis

All data on the antidiabetic activities were determined as the averages of three parallel sample measurements. The data were registered as the mean \pm S.E.M. Student's t test was used to evaluate important differences between the means, and p values <0.05 were accepted as substantial.

RESULTS

The hexane and methanol extracts of *E. helioscopia*, *F. elaeochytris*, *S. albiflora*, *S. stricta*, *S. pisidica*, *S. leptoclada*, *S. chionantha* plants were prepared at room temperature. α -Amylase and α -glucosidase inhibitory activities of the extracts were tested spectrophotometrically. Acarbose was used as the standard compound. Table 1 shows α -amylase and α -glucosidase inhibitory activities of the extracts of the studied plant species. The inhibitory activities on α -amylase of the hexane extracts of the plant species are given in Figure 1. The inhibitory activities on α -glucosidase of the hex-

ane extracts of the plant species are given in Figure 2. The hexane extracts showed higher inhibitory activity on α -amylase than the methanol extracts. The highest inhibitory activities on α -amylase at 1000 $\mu\text{g/mL}$ concentration were observed in *S. pisidica* hexane

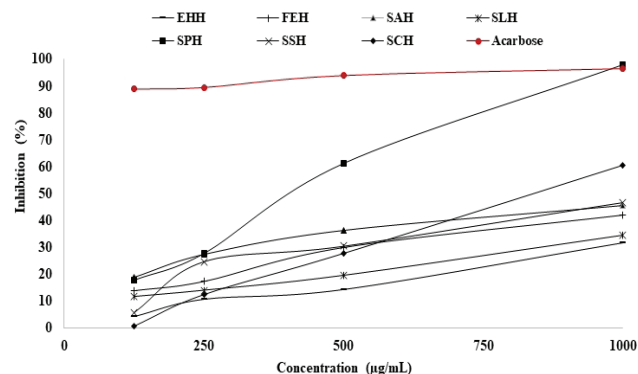


Figure 1. α -Amylase inhibitory activities of the hexane extracts of plant species. EHH: *E. helioscopia* hexane extract, FEH: *F. elaeochytris* hexane extract, SAH: *S. albiflora* hexane extract, SLH: *S. leptoclada* hexane extract, SPH: *S. pisidica* hexane extract, SSH: *S. stricta* hexane extract, SCH: *S. chionantha* hexane extract

Table 1. α -Amylase and α -glucosidase inhibitory activities of the extracts of plant species^a

Plants species	Extracts	Code	α -Amylase Inhibitory Activity		α -Glucosidase Inhibitory Activity	
			Inhibition (%) (at 1000 $\mu\text{g/mL}$)	IC_{50} ($\mu\text{g/mL}$)	Inhibition (%) (at 500 $\mu\text{g/mL}$)	IC_{50} ($\mu\text{g/mL}$)
<i>E. helioscopia</i>	Hexane	EHH	31.58 \pm 0.17	>1000	1.95 \pm 0.06	>500
	Methanol	EHM	11.85 \pm 0.56	>1000	NA ^b	>500
<i>F. elaeochytris</i>	Hexane	FEH	42.14 \pm 0.30	>1000	14.24 \pm 0.82	>500
	Methanol	FEM	8.62 \pm 0.00	>1000	NA ^b	>500
<i>S. albiflora</i>	Hexane	SAH	45.45 \pm 0.22	>1000	NA ^b	>500
	Methanol	SAM	21.94 \pm 0.95	>1000	NA ^b	>500
<i>S. leptoclada</i>	Hexane	SLH	34.68 \pm 0.34	>1000	11.08 \pm 0.73	>500
	Methanol	SLM	20.09 \pm 0.05	>1000	NA ^b	>500
<i>S. pisidica</i>	Hexane	SPH	97.99 \pm 0.79	413.53 \pm 0.18	NA ^b	>500
	Methanol	SPM	17.11 \pm 0.15	>1000	NA ^b	>500
<i>S. stricta</i>	Hexane	SSH	46.77 \pm 1.04	>1000	7.10 \pm 0.81	>500
	Methanol	SSM	18.21 \pm 0.70	>1000	NA ^b	>500
<i>S. chionantha</i>	Hexane	SCH	60.68 \pm 0.04	>1000	NA ^b	>500
	Methanol	SCM	6.35 \pm 0.11	>1000	NA ^b	>500
Standard	Acarbose		96.60 \pm 0.08	21.63 \pm 0.01	67.01 \pm 2.28	378.66 \pm 0.14

^a Values represent the means \pm SEM of three parallel sample measurements ($p < 0.05$).

^b NA: not active.

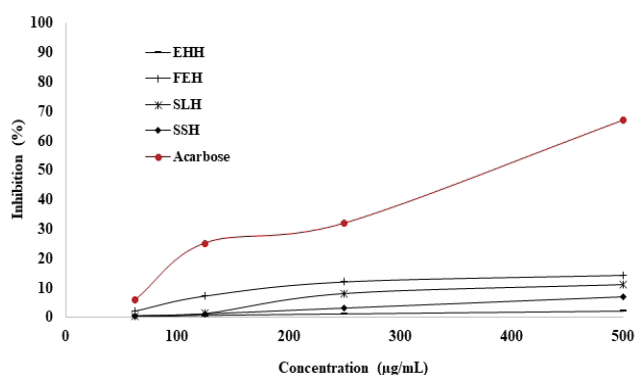


Figure 2. α -Glucosidase inhibitory activities of the hexane extracts of plant species. EHH: *E. helioscopia* hexane extract, FEH: *F. elaeochoytris* hexane extract, SLH: *S. leptoclada* hexane extract, SSH: *S. stricta* hexane extract

extract (SPH) (97.99 ± 0.79 %), *S. chionantha* hexane extract (SCH) (60.68 ± 0.04 %), *S. stricta* hexane extract (SSH) (46.77 ± 1.04 %) and *S. albiflora* hexane extract (SAH) (45.45 ± 0.22 %), respectively (Table 1). Also, against α -amylase, SPH extract was found to be more active than acarbose (96.60 ± 0.08 %) with an inhibition value of 97.99 ± 0.79 % at $1000 \mu\text{g/mL}$ concentration. In terms of inhibitory activities on α -glucosidase enzyme, the extracts were ranked in the following order: *F. elaeochoytris* hexane extract (FEH) > *S. leptoclada* hexane extract (SLH) > *S. stricta* hexane extract (SSH) > *E. helioscopia* hexane extract (EHH). The other extracts showed no α -glucosidase inhibitory activity. The highest activity of the hexane extracts is considered to be related to the non-polar compounds contained.

DISCUSSION

Enzyme inhibition, considered a significant area of pharmaceutical research, has allowed the discovery of a wide variety of drugs that have previously been useful in a number of diseases. The activity of the enzymes is blocked by the interaction of their specific inhibitors. Enzyme inhibitors, which have been used to treat a wide range of physiological conditions, are of great importance as drugs (33). Currently, one of the therapeutic methods used in the therapy of type 2 diabetes is the inhibition of α -amylase and α -glucosidase to reduce the reabsorption of glucose in the intestine. α -Amylase is the enzyme responsible for the initial stage of hydrolysis of complex carbohydrates to an oligosaccharide and disaccharide mixture in the intestinal mucosa. These sugars are broken down into monosaccharides by the effect of α -glucosidase (34).

Medicinal plants are extremely important natural resources for discovering new drug molecules due to the pharmacologic properties such as antioxidants, cytotoxic, antimicrobial, anti-inflammatory and antidiabetic activities (35,36). In this current research, *in vitro* inhibitory activities on α -amylase and α -glucosidase enzymes of the hexane and methanol extracts of *E. helioscopia*, *F. elaeochoytris*, *S. stricta*, *S. leptoclada*, *S. albiflora*,

S. pisidica, *S. chionantha* were evaluated. According to the obtained results, when SPH extract displayed the highest α -amylase inhibitory activity, FEH extract showed the best α -glucosidase inhibitory activity. The hexane extracts were found to have higher antidiabetic activity when compared to the methanol extracts. This highest activity of the hexane extracts is considered to be related to the non-polar compounds contained.

In a previous report of Adimclar et al. IC_{50} value of *S. chionantha* methanol extract was calculated as $43.3 \pm 2.5 \mu\text{g/mL}$ in α -glucosidase inhibitory assay (37). α -Amylase and α -glucosidase inhibitory activities of the water, methanol and dichloromethane extracts of *Salvia modesta* were investigated. The dichloromethane extract showed the highest antidiabetic activity with a mean value of 0.64 and 9.48 mmol ACAE/g sample on α -amylase and α -glucosidase, respectively (38). Water, ethyl acetate and methanol extracts of *Salvia cadmica* were tested to evaluate their α -amylase and α -glucosidase inhibitory activities. The methanol extract exhibited considerable α -amylase inhibitory activity ($102.28 \pm 2.09 \mu\text{mol ACEs/g}$ dry plant) and α -glucosidase inhibitory activity ($869.21 \pm 19.55 \mu\text{mol ACEs/g}$ dry plant) (39). The methanol extracts of *Euphorbia denticulata* parts (mix of aerial part, stem, flowers, leaf) were used to evaluate inhibitory activities on α -glucosidase and α -amylase enzymes by Zengin et al. (40). *E. denticulata* flower extract indicated the highest activity in the α -glucosidase assay with an inhibition value of $10.59 \pm 0.01 \text{ mmol ACAE/g}$ while *E. denticulate* mix extract was found to be the most active extract in α -amylase with an inhibition value of $0.77 \pm 0.04 \text{ mmol ACAE/g}$. α -Glucosidase and α -amylase inhibitory activities of dichloromethane and methanol extracts of *Euphorbia milli* aerial and root parts were investigated in the study of Sallem et al. (41). For α -glucosidase inhibition, both aerial methanol ($1.9 \pm 0.01 \text{ mmol ACAE/g}$ extract) and root methanol ($1.79 \pm 0.02 \text{ mmol ACAE/g}$ extract) extracts exhibited higher inhibitory potential than dichloromethane extracts. In the case of α -amylase, dichloromethane extracts ($0.62 \pm 0.02 \text{ mmol ACAE/g}$ extract for aerial part, $0.55 \pm 0.01 \text{ mmol ACAE/g}$ extract for root part) showed higher inhibition than the methanol extracts. Inhibitory activities on α -glucosidase and α -amylase enzymes of the methanol, acetone and chloroform extracts of *Ferula halophila* were investigated. When the chloroform extract demonstrated the highest α -amylase inhibitory activity ($1.04 \pm 0.04 \text{ mmol ACAE/g}$ extract), the methanol extract expressed potent α -glucosidase inhibitory activity ($43.02 \pm 0.45 \text{ mmol ACAE/g}$ extract) (42). In another study, the highest α -amylase inhibitory ($0.71 \pm 0.02 \text{ mmol ACE/g}$ extract) and α -glucosidase inhibitory ($5.66 \pm 0.04 \text{ mmol ACE/g}$ extract) activities were observed in *Sideritis galatica* petroleum ether extract (43). α -Glucosidase and α -amylase inhibitory activities of the ethyl acetate, methanol and water extracts of *Sideritis ozturkii* were evaluated by Zengin et al. (44). The higher inhibitory activity on glucosidase was found for the methanol ($13.33 \text{ mmol ACAE/g}$ extract) and ethyl acetate ($13.81 \text{ mmol ACAE/g}$ extract) extracts, while the water extract (3.60 mmol ACAE/g extract) was the least active. α -Amylase inhibitory activities of *S. ozturkii* extracts ranged between 0.11 and 0.63

mmol ACAE/g extract. α -Glucosidase and α -amylase enzymes were used for assessing the antidiabetic activities of the hexane, chloroform and methanol extracts of *Calamintha origanifolia*, *Satureja thymbra*, *Prangos asperula*, *Sideritis perfoliata*, *Asperula glomerata*, *Hyssopus officinalis*, *Erythraea centaurium*, *Marrubium radiatum* and *Salvia acetabulosa*. Among the studied plant species, *M. radiatum* methanol extract exerted the highest inhibitory activity against both α -amylase and α -glucosidase with IC_{50} values of 61.1 and 68.8 μ g/mL, respectively (45). Ekin et al. (46) had described antidiabetic activities of the ethanol extracts of *Lamium purpureum* var. *purpureum*, *Origanum onites*, *Salvia sclarea*, *Salvia virgata* and *Thymus zygoides* var. *lycaonicus* at 2000 μ g/mL concentration. α -Glucosidase inhibitory activities of the extracts followed the order: *T. zygoides* var. *lycaonicus* (85.28 \pm 0.89%)> *O. onites* (77.39 \pm 0.76%)> *S. sclarea* (leaves) (72.95 \pm 1.0%)> *S. sclarea* (flowers) (64.72 \pm 1.06%)> *S. virgata* (61.15 \pm 2.03 %) > *L. purpureum* var. *purpureum* (46.75 \pm 1.54%). α -Amylase inhibitory activity of all tested extracts were found between 2.30 \pm 0.21 and 8.93 \pm 1.73% (46). The obtained antidiabetic activity results are in agreement with the literature.

When the literature studies are examined, it is seen that there are studies on bioactive properties of *E. helioscopia*, *F. elaeochoytris*, *S. albiflora*, *S. leptoclada*, *S. stricta*, *S. pisidica*, *S. chionantha* species, such as antioxidant, anti-tyrosinase, anticholinesterase, anti-urease, antibacterial, antinociceptive, anti-inflammatory, antimicrobial and anti-pyretic (22,23,47-53). This is the first study on antidiabetic activities of the hexane and methanol extracts of *E. helioscopia*, *F. elaeochoytris*, *S. albiflora*, *S. leptoclada*, *S. pisidica*, and *S. stricta*. The results of this study may be useful in investigating specific enzyme inhibitors from the medicinal plant extracts for efficient management of type 2 diabetes mellitus and relevant complications.

CONCLUSION

In this study, α -glucosidase and α -amylase inhibitory activities of the hexane and methanol extracts of *E. helioscopia*, *F. elaeochoytris*, *S. albiflora*, *S. leptoclada*, *S. stricta*, and *S. pisidica* were screened for the first time. The hexane extracts showed notable α -amylase inhibitory activities. Against α -amylase, *S. pisidica* hexane extract was found to be more active than acarbose used as the standard. This study suggests that the hexane extracts (especially *S. pisidica* hexane extract) can be used in the pharmaceutical industry as a potential α -amylase inhibitor of natural origin.

Peer-review: Externally peer-reviewed.

Author Contributions: Conception/Design of study: E.D., G.T.C., M.E.D.; Data Acquisition: E.D., G.T.C., M.E.D.; Data Analysis/Interpretation: E.D., G.T.C.; Drafting Manuscript: E.D., G.T.C.; Critical Revision of Manuscript: E.D., G.T.C., M.E.D.; Final Approval and Accountability: E.D., G.T.C., M.E.D.; Technical or Material Support: E.D., G.T.C., M.E.D.; Supervision: E.D., G.T.C., M.E.D.

Conflict of Interest: The authors declare that they have no conflicts of interest to disclose.

Financial Disclosure: There are no funders to report for this submission.

REFERENCES

1. Cheng AYY, Fantus IG. Oral antihyperglycemic therapy for type 2 diabetes mellitus, Can Med Assoc J 2005; 172: 213-26.
2. deSales PM, deSouza PM, Simeoni LA, Magalhaes PDA, Silveira D. α -Amylase inhibitors: A review of raw material and isolated compounds from plant source. J Pharm Sci 2012; 15: 141-83.
3. World Health Organization. Global report on diabetes; World Health Organization: Geneva, Switzerland, 2016; 1-88.
4. Quan NV, Xuan TD, Tran HD, Thuy NTD, Trang LT, Huong CT, et al. Antioxidant, α -amylase and α -glucosidase inhibitory activities and potential constituents of *Canarium tramdenum* Bark. Molecules 2019; 24: 605.
5. Wu J, Fang X, Yuan Y, Dong Y, Liang Y, Xie Q, et al. UPLC/Q-TOF-MS profiling of phenolics from *Canarium pimela* leaves and its vasorelaxant and antioxidant activities. Braz J Pharmacog 2017; 27: 716-23.
6. Yao Y, Sang W, Zhou M, Ren G. Antioxidant and α -glucosidase inhibitory activity of colored grains in China. J Agric Food Chem 2010; 58: 770-4.
7. Tundis R, Marrelli M, Conforti F, Tenuta M, Bonesi M, Menichini F, et al. *Trifolium pratense* and *T. repens* (Leguminosae): Edible flower extracts as functional ingredients. Foods 2015; 4: 338-48.
8. Kwon YI, Apostolidis E, Shetty K. *In vitro* studies of eggplant (*Solanum melongena*) phenolics as inhibitors of key enzymes relevant for type 2 diabetes and hypertension. Bioresource Technol 2008; 99: 2981-8.
9. Dias DA, Urban S, Roessner UA. Historical overview of natural products in drug discovery. Metabolites 2012; 2: 303-36.
10. Toeller M. α -Glucosidase inhibitors in diabetes: Efficacy in NIDDM subjects. Eur J Clin Inves 1994; 24: 31-5.
11. Bischoff H. Pharmacology of alpha-glucosidase inhibition. Eur J Clin Inves 1994; 24: 3-10.
12. Hollander, P. Safety profile of acarbose, an alpha-glucosidase inhibitor. Drugs 1992; 44: 47-53.
13. Etxeberria U, de la Garza AL, Campión J, Martínez JA, Milagro FI. Antidiabetic effects of natural plant extracts via inhibition of carbohydrate hydrolysis enzymes with emphasis on pancreatic alpha amylase. Expert Opin Ther Tar 2012; 16: 269-97.
14. Valiathan MS. Healing plants. Curr Sci 1998; 75(11): 1122-7.
15. Sathivelu A, Sangeetha S, Archit R, Mythili S. *In vitro* anti-diabetic activity of aqueous extract of the medicinal plants *Nigella sativa*, *Eugenia jambolana*, *Andrographis paniculata* and *Gymnema sylvestre*. Int J Drug Dev & Res 2013; 5(2): 323-8.
16. Swanson-Flatt SK, Flatt PR, Day C, Bailey CJ. Traditional dietary adjuncts for the treatment of Diabetes mellitus. Proc Nutr Soc 1991; 50: 641-50.
17. Gray AM, Flatt PR. Nature's own pharmacy: The diabetes perspective. Proc Nutr Soc 1997; 56: 507-17.
18. Day C, Bailey CJ. Hypoglycemic agents from traditional plant treatments for diabetes. Int Ind Biotech 1998; 50: 5-8.
19. Sen T, Samanta SK. Medicinal plants, human health and biodiversity: A broad review. Adv Biochem Eng Biotechnol 2015; 147: 59-110.
20. Davis PH. Flora of Turkey and the East Aegean Islands; University Press: Edinburgh, 1998. Vol. 1, p. 1965-85.
21. Lopresti AL. *Salvia* (Sage): A review of its potential cognitive-enhancing and protective effects. Drugs R D 2017; 17: 53-64.
22. Tel G, Öztürk M, Duru ME, Harmandar M, Topçu G. Chemical composition of the essential oil and hexane extract of *Salvia chionantha* and their antioxidant and anticholinesterase activities. Food Chem Toxicol 2010; 48: 3189-93.

23. Deveci E, Tel-Çayan G, Duru ME. Phenolic profile, antioxidant, anticholinesterase and anti-tyrosinase activities of the various extracts of *Ferula elaeochytris* and *Sideritis stricta*. *Int J Food Prop* 2018; 21(1): 771-83.
24. Topcu G, Gören A.C. Biological activity of diterpenoids isolated from Anatolian Lamiaceae plants. *Rec Nat Prod* 2007; 1: 1-16.
25. Gonzalez-Burgos E, Carretero ME, Gomez-Serranillos MP. *Sideritis* spp.: Uses, chemical composition and pharmacological activities-a review. *J Ethnopharmacol* 2011; 135: 209-25.
26. Yılar M, Kadioğlu İ. *Salvia* species and their biological activities naturally distributed in Tokat province. *Sch Bull* 2018; 4: 208-12.
27. Mohammad S, Aftab A, Sarwat S. Asafoetida inhibits early events of carcinogenesis. A chemopreventive study. *Life Sci* 2001; 68: 1913-21.
28. Iranshahy M, Iranshahi M. Traditional uses, phytochemistry and pharmacology of asafoetida (*Ferula assafoetida* oleo-gumresin)-a review. *J Ethnopharmacol* 2011; 134: 1-10.
29. Uzair M, Loothar BA, Choudhary BA. Biological screening of *Euphorbia helioscopia* L. *Pak J Pharm Sci* 2009; 22(2): 184-6.
30. Deveci E, Tel-Çayan G, Duru ME. Investigation of chemical composition, antioxidant, anticholinesterase and anti-urease activities of *Euphorbia helioscopia*. *Int J Sec Metabolite* 2018; 5: 259-69.
31. Quan NV, Tran HD, Xuan TD, Ahmad A, Dat TD, Khanh TD, et al. Momilactones A and B are α -Amylase and α -glucosidase inhibitors. *Molecules* 2019; 24: 482.
32. Kim JS, Kwon CS, Son KH. Inhibition of α -glucosidase and amylase by luteolin, a flavonoid. *Biosci Biotech Bioch* 2010; 64: 2458-61.
33. Amtul Z, Rahman AU, Siddiqui RA, Choudhary MI. Chemistry and mechanism of urease inhibition. *Curr Med Chem* 2002; 9(14): 1323-48.
34. Ecemis CG, Atmaca H. Oral antidiabetic agents. *J Exp Clin Med* 2012; 29: 23-9.
35. Buchholz T, Melzig MF. Polyphenolic compounds as pancreatic lipase inhibitors. *Planta Med* 2015; 81: 771-83.
36. Grochowski DM, Uysal S, Zengin G, Tomczyk M. *In vitro* antioxidant and enzyme inhibitory properties of *Rubus caesius* L. *Int J Environ Health Res* 2018; 12: 1-9.
37. Adımcılar V, Kalaycıoğlu Z, Aydoğdu N, Dirmenci T, Kahraman A, Erim FB. Rosmarinic and carnolic acid contents and correlated antioxidant and antidiabetic activities of 14 *Salvia* species from Anatolia. *J Pharmaceut Biomed* 2019; 175: 112763.
38. Zengin G, Atasagun B, Ameeruddy MZ, Saleemd H, Mollica A, Bahadori MB, et al. Phenolic profiling and *in vitro* biological properties of two Lamiaceae species (*Salvia modesta* and *Thymus argaeus*): A comprehensive evaluation. *Ind Crop Prod* 2019; 128: 308-14.
39. Kocak MS, Sarikurkcü C, Cengiz M, Kocak S, Uren MC, Tepe B. *Salvia cadmica*: Phenolic composition and biological activity. *Ind Crop Prod* 2016; 85: 204-12.
40. Zengin G, Uysal A, Aktumsek A, Mocan A, Mollica A, Locatelli M, et al. *Euphorbia denticulata* Lam.: A promising source of phyto-pharmaceuticals for the development of novel functional formulations. *Biomed Pharmacother* 2017; 87: 27-36.
41. Saleem H, Zengin G, Locatelli M, Mollica A, Ahmad I, Mahomoodally FM, et al. *In vitro* biological propensities and chemical profiling of *Euphorbia milii* Des Moul (Euphorbiaceae): A novel source for bioactive agents. *Ind Crop Prod* 2019; 130: 9-15.
42. Zengin G, Uysal A, Diuzheva A, Gunes E, Jeko J, Cziaky Z, et al. Characterization of phytochemical components of *Ferula halophila* extracts using HPLC-MS/MS and their pharmacological potentials: A multi-functional insight. *J Pharm Biomed* 2018; 160: 374-82.
43. Zengin G, Sarikurkcü C, Aktumsek A, Ceylan R. *Sideritis galatica* Bornm.: A source of multifunctional agents for the management of oxidative damage, Alzheimer's and diabetes mellitus. *J Funct Food* 2014; 11: 538-47.
44. Zengin G, Uğurlu A, Baloglu MC, Diuzheva A, Jeko J, Cziaky Z, et al. Chemical fingerprints, antioxidant, enzyme inhibitory, and cell assays of three extracts obtained from *Sideritis ozturkii* Aytac, & Aksoy: An endemic plant from Turkey. *J Pharmaceut Biomed* 2019; 171: 118-25.
45. Loizzo MR, Saab AM, Tundis R, Menichini F, Bonesi M, Piccolo V, et al. *In vitro* inhibitory activities of plants used in Lebanon traditional medicine against angiotensin converting enzyme (ACE) and digestive enzymes related to diabetes. *J Ethnopharmacol* 2008; 119: 109-16.
46. Ekin HN, Deliorman Orhan D, Erdoğan Orhan İ, Orhan N, Aslan M. Evaluation of enzyme inhibitory and antioxidant activity of some Lamiaceae plants. *J Res Pharm* 2019; 23(4): 749-58.
47. Deveci E, Tel-Çayan G, Yıldırım H, Duru ME. Chemical composition, antioxidant, anticholinesterase and anti-urease activities of *Sideritis pisdica* Boiss. & Heldr. endemic to Turkey. *Marmara Pharm J* 2017; 21(4): 898-905.
48. Deveci E, Tel-Çayan G, Duru ME, Öztürk M. Phytochemical contents, antioxidant effects, and inhibitory activities of key enzymes associated with Alzheimer's disease, ulcer, and skin disorders of *Sideritis albiflora* and *Sideritis leptoclada*. *J Food Biochem* 2019; 14: e13078.
49. Saleem U, Ahmad B, Ahmad M, Hussain K, Bukhari NI. Anti-nociceptive, anti-inflammatory and anti-pyretic activities of latex and leaves methanol extract of *Euphorbia helioscopia*. *Asian Pac J Trop Disease* 2015; 5: 322-8.
50. Awaad AS, Allothman MR, Zain YM, Zain GM, Alqasoumi SI, Hassan DA. Comparative nutritional value and antimicrobial activities between three *Euphorbia* species growing in Saudi Arabia. *Saudi Pharm J* 2017; 25: 1226-30.
51. Askun T, Tumen G, Satil F, Ates M. Characterization of the phenolic composition and antimicrobial activities of Turkish medicinal plants. *Pharm Biol* 2009; 47: 563-71.
52. Dulger B, Gonuz A, Bican T. Antimicrobial studies on three endemic species of *Sideritis* from Turkey. *Acta Biol Cracov Bot* 2005; 47: 153-6.
53. Ayar-Kayali Hulya, Urek Raziye Ozturk, Nakiboglu, Mahmure, Tarhan L. Antioxidant activities of endemic *Sideritis leptoclada* and *Mentha dumetorum* aqueous extracts used in Turkey folk medicine. *J Food Process Pres* 2009; 33: 285-95.

Antioxidative Effects of Mash Beans Depending on Gender and High Fat Intake in a Model Organism

Eda Gunes¹ , Gulsum Rabia Sahin¹ 

¹Konya Necmettin Erbakan University, Faculty of Tourism, Gastronomy and Culinary Arts Department, Konya, Turkey

ORCID IDs of the authors: E.G. 0000-0001-7422-9375; G.R.S. 0000-0002-2904-9575

Please cite this article as: Gunes E, Sahin GR. Antioxidative Effects of Mash Beans Depending on Gender and High Fat Intake in a Model Organism. Eur J Biol 2020; 79(1): 29-35. DOI: 10.26650/EurJBiol.2020.0032

ABSTRACT

Objective: In the study, the aim was to determine the effect of Mash bean, an antioxidant source, against oxidative stress due to gender and high fat intake.

Materials and Methods: For this purpose, local and commercial Mash was added to the fatty and non-fatty diet of the model organism (*Drosophila melanogaster*) which were let to grow. Malondialdehyde and glutathione S-transferase (GST) activities were determined in adult females and males.

Results: According to the results, it was determined that Mash bean increased the GST activity of the insect. Feeding with non-commercial mash bean (NC-MB) and high-fat diet decreased lipid peroxidation (LPO) in females, whereas commercial mash bean (C-MB) had opposite effects.

Conclusion: It was concluded that the NC-MB seeds were more successful in preventing LPO than C-MB. In our study, the nutrition of male individuals with a fat diet or a non-fat diet did not change the amount of LPO.

Keywords: *Drosophila melanogaster*, Mash bean, lipid peroxidation, Glutathione-S-transferase activity, high-fat diet

INTRODUCTION

In recent years, the fact is that carbohydrate and fat-rich diets accelerated aging, increased obesity, diabetes, cancer, and cardiovascular diseases (1). Accordingly, the use of local and natural nutrients and medicinally important herbal content have become widespread and the necessity of being scientifically relevant in the prevention, and treatment of diseases has occurred (2). With the widespread use of herbal therapies, the investigation of functional nutrients has become an important research area in vivo studies with short life forms.

Due to excess nutrient intake (Obesity), aging and an increase in cell lipid levels, oxidative stress-induced complications can develop (3). *Drosophila melanogaster* (Meigen) fed with high-fat diet (HFD) is a model organism used in in vivo nutrition studies for obesity (4-6). The oxidant-antioxidant mechanism, fatty tissue, and digestive system of *D. melanogaster* are similar to

mammals, and due to its advantages in terms of ease of operation, it is frequently preferred in nutrition studies (7-12). It is known that flies fed with HFD have a significant decrease in amino acid and protein levels leading to oxidation (4). Malondialdehyde (MDA) occurs in the biological systems as a result of increased oxidative stress-induced lipid peroxidation (LPO) (13). MDA is an indicator of LPO, and used to determine the LPO grade. Oxidative damage mediated by free radicals caused by many environmental causes and formed during the conversion of nutrients to energy using oxygen as by-products of the metabolism in the body can be prevented by increasing the antioxidant concentration in the tissues (14-17). In many organisms, Glutathione S-transferases (GST) are a family of important detoxification enzymes (18). *Leguminosae* legumes, which are rich in dietary fiber and high nutritional value, show antioxidant activity and its success in preventing oxidation is shown in many studies



Corresponding Author: Eda Gunes

E-mail: egunes@erbakan.edu.tr

Submitted: 27.09.2019 • **Revision Requested:** 04.12.2019 • **Last Revision Received:** 31.01.2020 • **Accepted:** 02.03.2020

© Copyright 2020 by The Istanbul University Faculty of Science • Available online at <http://ejb.ibul.edu.tr> • DOI: 10.26650/EurJBiol.2020.0032

(19-25). Used in many parts of the world and known as mung bean, green gram, urad whole, Mash bean *Vigna radiata* (L.) R. Wilczek is a species belonging to the *Fabaceae* family (26,27). Like other legumes, the high nutritional value of Mash bean is also known, and there are many studies in the literature that determined its antioxidant capacity (28). In spite of this, no study was done to investigate the oxidant-antioxidant effects of Malatya-specific local black Mash bean and commercial Mash bean. In this study, the use of HFD (20% palmitic acid) in the larval period and antioxidant source of Mash bean against oxidative effects on lipid molecules in adult individuals were investigated. The antioxidant effects of non-commercial/local (NC-MB) and commercial (C-MB) mash beans before and after cooking was also compared.

For this purpose, the effect of NC-MB and C-MB was determined in the model organism (*D. melanogaster*) fed with a fat and fat-free diet. In addition to the cooking practices in different products, the possible effect of Mash bean due to fat feeding has been demonstrated.

MATERIALS AND METHODS

Biological Materials

In the study, NC-MB and C-MB (Malatya and Mersin origin) were used (Figure 1). *D. melanogaster's* strain of wild type adult individuals (in 200 ml bottles) were incubated in the laboratory of Necmettin Erbakan University ($25 \pm 2^\circ\text{C}$ and 60-70% relative humidity, 12 hours light, 12 hours dark photoperiod). An artificial diet (potatoes, agar, sucrose, dry yeast, ascorbic acid, and nipagin) prepared with mashed potatoes for culture food was used. This nutrient was also used as an experimental diet and as a control food. Food for the insects in the culture bottles was refreshed every 15 days, and the procedures were made completely under aseptic conditions (29).

Experimental Pattern

In this study, for HFD, palmitic acid was dissolved within Tween-80 and added to 20% of the hot control nutrient (culture food) (30). Commercial and local unprocessed NC-MB and

cooked Mash beans C-MB were added to *D. melanogaster* diet mixed with the food. Similar to the previous study (31), where the upper and lower limits of use were determined, the plant was triturated (unprocessed and cooked) after being held in the incubator for 24 hours at 60°C , and added to the nutrient at $30-40^\circ\text{C}$. For the cooking process (32), 25 minutes was applied. Due to being added to the nutrient and feeding of the insect, the powdered beans (0.21 g) were added to 100 ml of warm food after weighing.

All of the experiments were carried out under conditions where the stock culture of insects was grown. From the culture, the female and male individuals (3 virgin/1 male) were taken for the trial design, and they were mated and the eggs were collected after six hours. *D. melanogaster's* newly hatched larvae (1st stage larvae) were floated in water (taking on blotting paper) as indicated in the experimental pattern, and the larvae were grown up to the adult stage by inoculating on the test nutrients with the fine-tipped brush. Fat containing nutrients were used as a positive control. The larvae of the *D. melanogaster* were grown up to the adult stage with the nutrients indicated in the trial pattern.

Biochemical Analyses

25 female and 25 male adults (33) were used for each trial in the biochemical analysis. Samples were extracted with 1.15% potassium chloride in an ultrasonic homogenizer with a cold homogenization buffer (1.15% potassium chloride, 25 mM dipotassium hydrogen phosphate, 5 mM ethylenediamine tetra acetic acid, 2 mM phenethylsulphonyl, 2 mM dithiollotenitol, pH: 7.4) at $+4^\circ\text{C}$. The samples were stored at -80°C until analysis was carried out.

MDA, the final product of LPO, was measured according to the method used by Jain and Levine (34). GST (EC 2.5.1.18) determination was made according to the method developed by Habig et al. (35). Total protein determination was made according to the Folin-Lowry method to calculate the MDA levels and enzyme specific activity from the obtained supernatants (36).

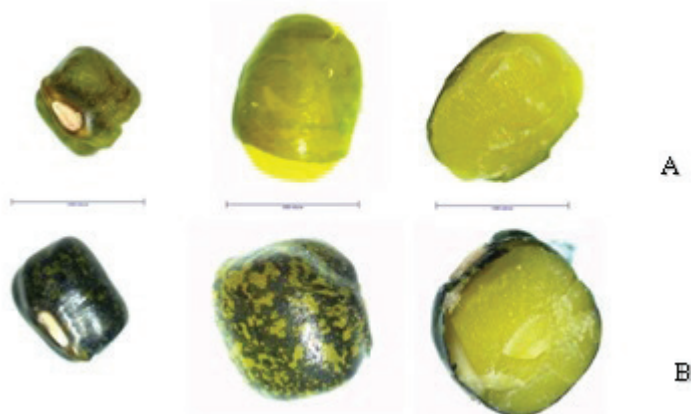


Figure 1. Commercial (A) and non-commercial/local (B) Mash beans (1000 μm).

Table 1. Malondialdehyde (MDA) quantity and glutathione S-transferase (GST) activity in female and male fed with Mash beans

Diets	MDA (nmol/mg protein)		GST (nmol/mg protein/min)	
	Female (Mean* ± S.E) [†]	Male (Mean* ± S.E) [†]	Female (Mean* ± S.E) [†]	Male (Mean* ± S.E) [†]
Control (0.0 [§])	0.43±0.22 ^b	0.73±0.03 ^c	6.03±0.24 ^a	14.83±0.52 ^b
NC-MB cooked	0.28±0.01 ^b	1.60±0.04 ^d	31.08±0.76 ^d	14.99±0.50 ^b
C-MB cooked	0.41±0.01 ^b	0.72±0.01 ^c	30.04±1.01 ^d	4.35±0.26 ^a
NC-MB unprocessed	3.44±0.01 ^e	2.11±0.04 ^e	23.60±0.81 ^c	14.53±0.87 ^b
C-MB unprocessed	1.77±0.02 ^d	4.15±0.05 ^f	46.94±0.64 ^e	22.94±0.23 ^c
NC-MB cooked+ HFD	0.14±0.04 ^a	0.43±0.01 ^b	10.38±0.84 ^b	28.59±0.56 ^d
C-MB cooked + HFD	1.5 ±0.10 ^c	4.47±0.05 ^f	7.79±0.25 ^a	12.63±1.09 ^b
NC-MB unprocessed + HFD	0.12±0.04 ^a	0.41±0.01 ^b	11.85±0.35 ^b	10.16±0.42 ^b
C-MB unprocessed + HFD	3.32±0.12 ^e	0.24±0.01 ^a	5.44±0.77 ^a	30.68±1.00 ^d

*Four experiments were tested, and 25 females and 25 males were used in each trial, [†] Values in the same column with different lowercase letters (a to f) were significantly different by LSD test; b was statistically different from a (p <0.05), c was significantly different from a (p <0.01), d was different from c (p <0.05), e was very significantly different from d (p <0.001), f was very significantly different from e (p <0.001). [§]Control, NC-MB: Non-commercial/local Mash bean, C-MB: Commercial/local Mash bean, HFD: High-fat diet (20% palmitic acid).

Data Analysis

The data were analysed by the statistics package program (SPSS Inc., Chicago, IL, USA). One-way analysis of variance (ANOVA) was used to evaluate data on MDA quantity and GST activity. "LSD test" was used in comparison of diets because the "Duncan's multiple range test" result was homogeneous. Mann Whitney U test was used to determine the changes occurring between male and female adult stages. The significance of the means was evaluated at the 0.05 probability level.

RESULTS

The amount of LPO formed by cooked NC-MB and C-MB in adult female individuals is similar to the negative control, whereas fat supplementation showed that NC-MB reduced LPO (Table 1). It was determined that the amount of MDA increased in the females fed with unprocessed NC-MB and C-MB, and that the unprocessed fatty NC-MB decreased the amount of MDA (Table 1). It was observed that the GST activity of cooked beans increased by about 5 times compared to the control, and that the use of fat increased GST activity by about 4 times compared to the control (Table 1).

Although the activity of GST increased in the cooked beans, it was determined that the resistance was decreased when used with fat, and non-resistant individuals were formed. However, the use of Malatya-origin cooked beans with fat proved its usefulness as it contained low MDA content and GST activity.

The use of unprocessed beans with fat reduced GST activity by more than half. The beans used with the addition of fat reduced the resistance of females, and the beans used without the addition of fat increased the GST activity.

In male subjects, the amount of MDA between control negative and control positive was similar to the negative control with the use of cooked C-MB, but this ratio was increased by 2-fold in the NC-MB and increased by 4-fold and 8-fold in unprocessed products (Table 1). However, the use of beans together with fat decreases the amount of MDA in male subjects. Nonetheless, the use of unprocessed C-MB seeds with fat or fat-free does not differ much in terms of LPO (Table 1). It was observed that there was an inversely proportional relation to the increasing amount of MDA in males and that GST activity decreased in controls, and individual non-resistance was formed. While the GST activity of the cooked NC-MB was statistically similar to the control, it was observed that GST activity decreased in C-MB. This decline can be said to be due to the low amount of MDA. However, when fat was added, the GST activity of insects that eat NC-MB decreased and the resistance of insects that eat C-MB fatty beans increased (Table 1).

LPO of female and male individuals was compared according to their nutritional contents. Fat diet caused oxidation in both, but the female individuals were more affected (Figure 2). Unprocessed NC-MB increased the amount of MDA in females compared to males. In C-MB, it was observed that males had more LPO. In the cooked NC-MB and C-MB, the amount of MDA in females was less than that in males (Figure 2). It was observed that the addition of fat in unprocessed C-MB caused less oxidation in females, the use of cooked NC-MB with fat increased the amount of MDA of males while the amount of MDA in females was higher in the use of fat C-MB (Figure 2).

The use of Mash bean differed in the antioxidant activity of male and female individuals. The combined use of only fat and cooked NC-MB revealed a statistical similarity in males and fe-

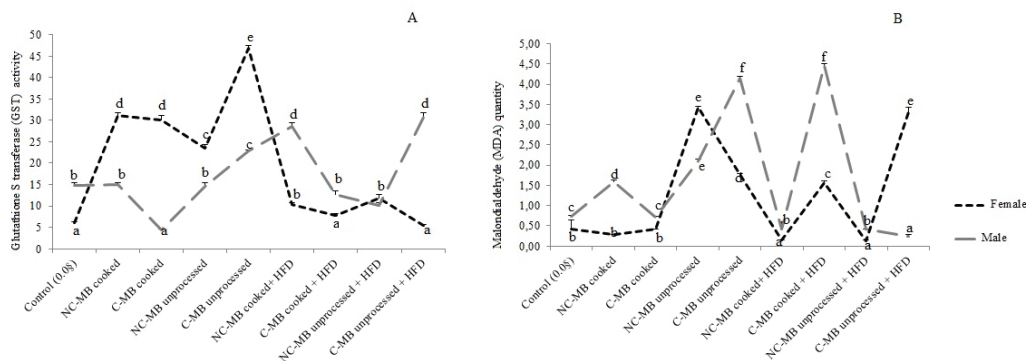


Figure 2. Comparison of A) Glutathione S-transferase (GST) activity and B) Malondialdehyde (MDA) quantity in male and female individuals fed with Mash bean. For each diet, significant differences are indicated by different lowercase letters (a to f) over the line graphs by Mann Whitney U test; b was statistically different from a ($p < 0.05$), c was significantly different from a ($p < 0.01$), d was different from c ($p < 0.05$), e was very significantly different from d ($p < 0.001$), f was very significantly different from e ($p < 0.001$). Control, NC-MB: Non-commercial/local Mash bean, C-MB: Commercial/local Mash bean, HFD: High-fat diet (20% palmitic acid).

males. However, when fat was not involved in the nutrition, it was determined that antioxidant activity made female individuals more resistant than males, and the GST activity of males was more effective in fat use (Figure 2).

DISCUSSION

It is stated that Mash bean is an important component of the intestinal flora due to the high rate of resistant starch in its content (37,38). Mash bean sprout is known to have antimicrobial activity against the gastroduodenal diseases in humans, the immune stimulatory effect of the seed, antioxidant, anti-inflammatory, and anti-diabetic activity, while the mungin protein isolated from the seeds has an antifungal effect (39-45). Globulin-rich, Mash bean, reduces fat accumulation and fatty liver in rodents induced for obesity by HFD (46). Against liver and kidney damage, Mash bean seeds have hepatoprotective and nephroprotective activity (47). It has a protective effect against alcohol-induced liver damage (48). Mash bean, known for its detoxification properties, has been used to reduce the sensation of swelling, superficial infections, acne, eczema, dermatitis and itching (48). It is known that Mash bean soup, cooked in the traditional way in Asian countries, has a protective effect against heat stress (26), lowers LDL cholesterol with its antioxidants, has a protective effect on DNA, and has anti-cancer and liver protective effects (32,49,50).

Mash bean shows anti-lipid peroxidation activity and superoxide anion cleansing activity (28). It is seen in the literature that Mash bean has significant changes in nutritional and anti-nutritional properties by cooking and germinating (51). Mash bean significantly increased antioxidant enzymes such as superoxide dismutase (SOD) and catalase in rats (52). *Vigna mungo* shell extract provides protection against the oxidative stress caused by hydrogen peroxide in DNA and erythrocytes (53).

Similarly, in our study, It was determined that Mash bean increased GST activity of female insects compared to control. Antioxidants in Mash bean reduce inflammation by regulating

cholesterol levels, cleaning free radicals, and reversing the damage to blood vessels (32,50). The effect seen in our experiment is thought to be due to this feature. In addition, Vitexin and Isovitexin (43,54,55), which are two types of flavonoids with high free radical cleansing activity in Mash bean, have approximately 70% inhibition of SOD radicals (56) supports our study. In a study of Liyanage et al. (32), it was observed that the cooking process increased the soluble fiber content of Mash bean and its hypocholesterolemic potential in vivo, preserved the hypoglycemic potential, and decreased total phenolic and flavonoid content and antioxidant activity. It is known that male GST activity is better than females because of the significant sex-dependent differences with low basal levels and egg production (57). When the beans were cooked, in male individuals fed with and without fat, continuing the feeding with C-MB decreased the GST activity. Although other studies have suggested that Mash bean can be used in the development of food supplements for patients with hypercholesterolemia, according to our findings, it is necessary to adjust the amount of use according to sex and the way of the feeding of the individual. In addition, the non-commercial or commercial origin of a product or even the conditions of cultivation of herbal products may lead to changes in the antioxidant activity in vivo. As in this study, C-MB seeds showed generally limited antioxidant activity compared to NC-MB seeds. Differently, Wang et al. (58), reported that the cooking process significantly increased the dietary fiber content (dry weight basis) in beans but had no effect on iron, zinc and phytic acid contents. The content of soluble dietary fiber in boiled Mash beans is higher than that of raw Mash beans (59). When these results are considered in terms of digestibility, it has been shown that Mash bean which is added to the nutrient prepared with the mashed potatoes, which provide the carbohydrate and fat intake, provide the insects with more nutritive carbohydrates. Soluble dietary fibers are known to significantly reduce bad (LDL) cholesterol (60). The fact that LPO is lower in cooked Mash beans compared to unprocessed beans in our study is similar to the results of previous studies (cooked LPO < unprocessed LPO). Increased soluble dietary fiber in cooked beans is believed to in-

crease the LPO inhibition of Mash beans. It is also seen that LPO is different depending on gender (30). In this study, Mash bean in female individuals achieved similar results compared to control (excluding NC-MB unprocessed only), whereas in females fed with fat diet, C-MB increased LPO (Table 1). Similar results were found in the study which are related to fat diet and gender (3). In our study, feeding of male individuals with a fat diet and fat-free diet change the amount of LPO. Nutrition with HFD increased MDA, protein carbonyl levels in liver, heart and kidney tissues in obese rats and decreased the activity of GST and paraoxonase enzymes (61). It has been reported in the studies that flies fed with HFD have an increase in triglyceride levels fat similar to that of mammals, and exhibit changes in insulin/glucose homeostasis (62). In our study, besides the use of C-MB and NC-MB Mash beans, the effect of fat and fat-free nutrition was also examined. In the individuals fed with HFD, C-MB generally increased the amount of MDA in comparison to NC-MB and control. This has proven that the local beans were more reliable in terms of consumption compared to the commercial ones. NC-MBs have proven to be more reliable in terms of consumption than C-MBs. As a result, nutrition with HFD increased the amount of MDA in vivo as in other studies. However, non-commercial beans generally used in the fatty diet reduced the amount of MDA produced.

CONCLUSIONS

It is determined that the cooking process applied to the mash bean and its raw (unprocessed powder) usage was effective on the fatty and non-fat diet, and the insect changes the oxidant antioxidant activity depending on the gender. Continuing feeding of the females regardless of the origin of unprocessed Mash beans increased antioxidant activity in a fat-free diet and caused a change in the activity of GST, which is one of the determining factors for resistance. Regardless of the processing, the use of the non-commercial product caused the LPO to fall in the individuals fed with the fat diet. A similar effect was observed in male subjects.

As a result, the fat intake and cooking process in males decreased oxidation, and the opposite was observed in female individuals. However, it was determined that females became more resistant to increasing GST activity. In the comparison of commercial and non-commercial products, NC-MB has been shown to be more useful than C-MB by reducing oxidation. According to these results, it is observed that NC-MB has a positive effect on both insect mechanism and oxidant-antioxidant activity. Thus, the use of the Mash bean as a beneficial nutritional supplement was determined by looking at the effect of our model resembling the vertebrate organisms. It is likely that our study will serve to guide the advancing studies based on nourishment for the correct use of unconsciously used alternative medicine products.

Peer-review: Externally peer-reviewed.

Author Contributions: Conception/Design of study: E.G.; Data Acquisition: E.G., G.R.Ş.; Data Analysis/Interpretation: G.R.Ş.; Drafting Manuscript: E.G., G.R.Ş.; Critical Revision of Manuscript:

E.G.; Final Approval and Accountability: E.G., G.R.Ş.; Technical or Material Support: E.G., G.R.Ş.; Supervision: E.G.

Conflict of Interest: The authors declare that they have no conflicts of interest to disclose.

Financial Disclosure: Necmettin Erbakan University, Graduate Education and Scientific Research as a research project supported by the Unit. Project No: 171322003.

REFERENCES

1. Yilmaz İ. Some Food Containing Antioxidants and Oxidatif Stress. *J Turgut Ozal Med Cent* 2010; 17: 143-53.
2. Smith S, Paladino A. Eating clean and green? Investigating consumer motivations towards the purchase of organic food. *AMJ* 2010; 18: 93-104.
3. Heinrichsen ET, Haddad GG. Role of high-fat diet in stress response of *Drosophila*. *PLoS one* 2012; 7: e42587.
4. Bahadorani S, Hilliker AJ. Cocoa confers life span extension in *Drosophila melanogaster*. *Nutr Res* 2008; 28: 377-82.
5. Heinrichsen ET, Zhang H, Robinson JE, Ngo J, Diop S, Bodmer R, et al. Metabolic and transcriptional response to a high-fat diet in *Drosophila melanogaster*. *Mol Metab* 2014; 3: 42-54.
6. Gunes E. *Drosophila* in food and nutrition studies. *Ksü Doğa Bil Derg* 2016; 19: 236-43.
7. Ha EM, Oh CT, Ryu JH, Bae YS, Kang SW, Jang IH, Lee WJ, et al. An antioxidant system required for host protection against gut infection in *Drosophila*. *Dev cell* 2005; 8: 125-32.
8. Casali A, Batlle E. Intestinal stem cells in mammals and *Drosophila*. *Cell Stem* 4: 124-7.
9. Zhao HW, Haddad GG. Hypoxic and oxidative stress resistance in *Drosophila melanogaster*. *Placenta* 2011; 32: 104-8.
10. Padmanabha D, Baker KD. *Drosophila* gains traction as a repurposed tool to investigate metabolism. *Trends Endocrinol Metab* 2014; 25: 518-27.
11. Demir E. The Use of *Drosophila melanogaster* (fruit fly) as an *In Vivo* Model Organism in the Toxicity and Genotoxicity Studies of Nanomaterials. *Türk Bilimsel Derlemeler Derg* 2016; 9: 1-11.
12. Ataş H, Hacınecipoğlu F, Gönül M, Öztürk Y, Kavutçu M. Clinical Value of Antioxidant Enzymes and Oxidative Biomarkers in Psoriasis. *Okmeydanı Med J* 2017; 33: 270-80.
13. Zhang Y, Shen T, Liu SW, Zhao J, Chen W, Wang H. Effect of Hawthorn on *Drosophila melanogaster* antioxidant-related gene expression. *Trop J Pharm Res* 2014; 13: 353-7.
14. Fang YZ, Yang S, Wu G. Free radicals, antioxidants, and nutrition. *Nutrition* 2002; 18: 872-9.
15. Vijayakumar RS, Surya D, Nalini N. Antioxidant efficacy of black pepper (*Piper nigrum* L.) and piperine in rats with high fat diet induced oxidative stress. *Redox Rep* 2004; 9: 105-10.
16. Çaylak E. Hayvan ve bitkilerde oksidatif stres ve antioksidanlar. *Med Res J* 2011; 9: 73-83.
17. Özcan O, Erdal H, Çakırca G, Yönden Z. Oxidative stress and its impacts on intracellular lipids, proteins and DNA. *J Clin Exp Invest* 2015; 6: 331-6.
18. Tu CPD, Akgül B. *Drosophila* glutathione S transferases. *Methods Enzymol* 2005; 401: 204-26.
19. Xu BJ, Chang SKC. A comparative study on phenolic profiles and antioxidant activities of legumes as affected by extraction solvents. *J Food Sci* 2007; 72: 159166.
20. Amarowicz R, Pegg RB. Legumes as a source of natural antioxidants. *Euro Fed Lipid* 2008; 110: 865-78.

21. Silva-Cristobal L, Osorio-Díaz P, Tovar J, Bello-Pérez LA. Chemical composition, carbohydrate digestibility, and antioxidant capacity of cooked black bean, chickpea, and lentil Mexican varieties. Composición química, digestibilidad de carbohidratos, y capacidad antioxidante de variedades mexicanas cocidas de frijol negro, garbanzo, y lenteja. *CYTA-J Food* 2010; 8: 7-14.
22. Djordjevic TM, Šiler-Marinkovic SS, Dimitrijevic-Brankovic SI. Antioxidant activity and total phenolic content in some cereals and legumes. *Int J Food Prop* 2011; 14: 175-84.
23. Sasipriya G, Siddhuraju P. Effect of different processing methods on antioxidant activity of underutilized legumes, *Entada scandens* seed kernel and *Canavalia gladiata* seeds. *Food Chem Toxicol* 2012; 50: 2864-72.
24. Li X, Gao P, Zhang C, Wu T, Xu Y, Liu D. Reduced bioavailability of cyclosporine a in rats by mung bean seed coat extract. *Braz J Pharm Sci* 2014; 50: 591-7.
25. Zhao Y, Du SK, Wang H, Cai M. In vitro antioxidant activity of extracts from common legumes. *Food Chem* 2014; 152: 462-6.
26. Cao D, Li H, Yi J, Zhang J, Che H, Cao J, Jiang W, et al. Antioxidant properties of the mung bean flavonoids on alleviating heat stress. *PLoS one* 2011; 6: e21071.
27. Kurniadi M, Poeloengasih CD, Frediansyah A, Susanto A. Folate content of mung bean flour prepared by various heat-treatments. *Procedia Food Sci* 2015; 3: 69-73.
28. Lin CC, Wu SJ, Wang JS, Yang JJ, Chang C. H. Evaluation of the antioxidant activity of legumes. *Pharma Biol* 2001; 39: 300-4.
29. Koç Y, Gülel A. Effects of photoperiod and the natural food quality on the preadult developmental time, adult longevity, fecundity and sex-ratio of *Drosophila melanogaster* meigen, 1830. *OMU J Fac Agric* 2006; 21: 204-12.
30. Sun X, Seeberger J, Alberico T, Wang C, Wheeler CT, Schauss AG, Zou S. Açai palm fruit (*Euterpe oleracea* Mart.) pulp improves survival of flies on a high fat diet. *Exp Gerontol* 2010; 45: 243-51.
31. Güneş E, Şahin GR. An *In vivo* Study On The Use Of Local Phaseolus Shoots In Food. *Acta Bio Turcica* 2018; 31: 146-51.
32. Liyanage R, Kiramage C, Visvanathan R, Jayathilake C, Weththasinghe P, Bangamuwage R, Vidanarachchi J, et al. Hypolipidemic and hypoglycemic potential of raw, boiled, and sprouted mung beans (*Vigna radiata* L. Wilczek) in rats. *J Food Biochem* 2018; 42: e12457.
33. Taşkın V, Küçükakyüz K, Arslan T, Çö B, Taşkın BG. The biochemical basis of insecticide resistance and determination of esterase enzyme patterns by using PAGE in field collected populations of *Drosophila melanogaster* from Muğla province of Turkey. *J Mol Cell Biol* 2007; 6: 31-40.
34. Jain SK, Levine SN. Elevated lipid peroxidation and vitamin E-quinone levels in heart ventricles of streptozotocin-treated diabetic rats. *Free Radical Bio Med* 1995; 18: 337-41.
35. Habig WH, Pabst MJ, Jakoby WB. Glutathione S-transferases the first enzymatic step in mercapturic acid formation. *J Biol Chem* 1974; 249: 7130-9.
36. Lowry OH, Rosebrough NJ, Farr AL, Randall RJ. Protein measurement with the Folin phenol reagent. *J Biol Chem* 1951; 193: 265-75.
37. Kotancılar HG, Gerçekaslan KE, Karaoğlu MM, Boz H. Besinsel lif kaynağı olarak enzime dirençli nişasta. *Ata Uni J Fac Agric* 2010; 40: 103-7.
38. Shi Z, Yao Y, Zhu Y, Ren G. Nutritional composition and antioxidant activity of twenty mung bean cultivars in China. *Crop J* 2016; 4: 398-406.
39. Ye XY, Ng TB. Mungin, a novel cyclophilin-like antifungal protein from the mung bean. *Biochem Biophys Res Commun* 2000; 273: 1111-5.
40. Randhir R, Lin YT, Shetty K. Stimulation of phenolics, antioxidant and antimicrobial activities in dark germinated mung bean sprouts in response to peptide and phytochemical elicitors. *Process Biochem* 2004; 39: 637-46.
41. Solanki YB, Jain SM. Immunostimulatory activities of *Vigna mungo* L. extract in male Sprague–Dawley rats. *J Immunotoxicol* 2010; 7: 213-8.
42. Zhang X, Shang P, Qin F, Zhou Q, Gao B, Huang H, Yu LL, et al. Chemical composition and antioxidative and anti-inflammatory properties of ten commercial mung bean samples. *LWT-Food Sci Technol* 2013; 54: 171-8.
43. Tang D, Dong Y, Ren H, Li L, He C. A review of phytochemistry, metabolite changes, and medicinal uses of the common food mung bean and its sprouts (*Vigna radiata*). *Chem Cent J* 2014; 8: 4.
44. Dahiya PK, Linnemann AR, Van Boekel MAJS, Khetarpaul N, Grewal RB, Nout MJR. Mung bean: Technological and nutritional potential. *Crit Rev Food Sci Nutr* 2015; 55: 670-88.
45. Luo J, Cai W, Wu T, Xu B. Phytochemical distribution in hull and cotyledon of adzuki bean (*Vigna angularis* L.) and mung bean (*Vigna radiata* L.), and their contribution to antioxidant, anti-inflammatory and anti-diabetic activities. *Food Chem* 2016; 201: 350-60.
46. Nakatani A, Li X, Miyamoto J, Igarashi M, Watanabe H, Sutou A, Inoue H, et al. Dietary mung bean protein reduces high-fat diet-induced weight gain by modulating host bile acid metabolism in a gut microbiota-dependent manner. *Biochem Biophys Res Commun* 2018; 501: 955-61.
47. Nitin M, Ifthekar SQ, Mumtaz M. Evaluation of hepatoprotective and nephroprotective activity of aqueous extract of *Vigna mungo* (Linn.) Hepper on rifampicin-induced toxicity in albino rats. *Int J Res Health Allied Sci* 2012; 1: 85.
48. Liu T, Yu XH, Gao EZ, Liu XN, Sun LJ, Li HL, Yu ZG, et al. Hepatoprotective effect of active constituents isolated from mung beans (*Phaseolus radiatus* L.) in an alcohol-induced liver injury mouse model. *J Food Biochem* 2014; 38: 453-9.
49. Tachibana N, Wanezaki S, Nagata M, Motoyama T, Kohno M, Kitagawa S. Intake of mung bean protein isolate reduces plasma triglyceride level in rats. *FFHD* 2013; 3: 365-76.
50. Bai Y, Chang J, Xu Y, Cheng D, Liu H, Zhao Y, Yu Z. Antioxidant and myocardial preservation activities of natural phytochemicals from mung bean (*Vigna radiata* L.) seeds. *J Agric Food Chem* 2016; 64: 4648-55.
51. Pekşen E, Artık C. Antibesinsel maddeler ve yemeklik tane baklagillerin besleyici değerleri. *OMU J Fac Agric* 2005; 20: 110-20.
52. Rajagopal V, Pushpan CK, Antony H. Comparative effect of horse gram and black gram on inflammatory mediators and antioxidant status. *TFDA* 2017; 25: 845-53.
53. Girish TK, Vasudevaraju P, Rao UJP. Protection of DNA and erythrocytes from free radical induced oxidative damage by black gram (*Vigna mungo* L.) husk extract. *Food Chem Toxicol* 2012; 50: 1690-6.
54. Peng X, Zheng Z, Cheng KW, Shan F, Ren GX, Chen F, Wang M. Inhibitory effect of mung bean extract and its constituents vitexin and isovitexin on the formation of advanced glycation endproducts. *Food Chem* 2008; 106: 475-81.
55. Yang YAO, Cheng XZ, Ren GX. Contents of D-chiro-Inositol, vitexin, and isovitexin in various varieties of mung bean and its products. *Agr Sci China* 2011; 10: 1710-5.
56. Kim JH, Lee BC, Kim JH, Sim GS, Lee DH, Lee KE, Pyo HB, et al. The isolation and antioxidative effects of vitexin from *Acer palmatum*. *Arch Pharmacol Res* 2005; 28: 195.
57. Le Goff G, Hilliou F, Siegfried BD, Boundy S, Wajnberg E, Sofer L, Feyereisen R. Xenobiotic response in *Drosophila melanogaster*: sex dependence of P450 and GST gene induction. *Insect Biochem Mol Biol* 2006; 36: 674-82.

58. Wang N, Hatcher DW, Tyler RT, Toews R, Gawalko EJ. Effect of cooking on the composition of beans (*Phaseolus vulgaris* L.) and chickpeas (*Cicer arietinum* L.). *Food Res Int* 2010; 43: 589-94.
59. Chandrasiri SD, Liyanage R, Vidanarachchi JK, Weththasinghe P, Jayawardana BC. Does processing have a considerable effect on the nutritional and functional properties of Mung bean (*Vigna radiata*)? *Procedia Food Sci* 2016; 6: 352-5.
60. Brown L, Rosner B, Willett WW, Sacks FM. Cholesterol-lowering effects of dietary fiber: a meta-analysis. *Am J Clin Nutr* 1999; 69: 30-42.
61. Noeman SA, Hamooda HE, Baalash AA. Biochemical study of oxidative stress markers in the liver, kidney and heart of high fat diet induced obesity in rats. *Diabetol Metab Syndr* 2011; 3: 17.
62. Birse RT, Choi J, Reardon K, Rodriguez J, Graham S, Diop S, Oldham S, et al. High-fat-diet-induced obesity and heart dysfunction are regulated by the TOR pathway in *Drosophila*. *Cell metab* 2010; 12: 533-44.

Apoptosis Signaling Pathway Regulates the Gene Expression in the Yeast Retrotransposons Ty1 and Ty2

Ceyda Colakoglu¹ , Sezai Türkel¹ 

¹Bursa Uludag University, Faculty of Arts and Sciences, Department of Molecular Biology and Genetics, Bursa, Turkey

ORCID IDs of the authors: C.C. 0000-0002-7471-5071; S.T. 0000-0001-7128-6948

Please cite this article as: Colakoglu C, Türkel S. Apoptosis Signaling Pathway Regulates the Gene Expression in the Yeast Retrotransposons Ty1 and Ty2. Eur J Biol 2020; 79(1): 36-42. DOI: 10.26650/EurJBiol.2020.0016

ABSTRACT

Objective: Ty elements are retroviral-like entities present in the yeast *Saccharomyces cerevisiae*. Apoptosis is a programmed cell death mechanism, conserved in all eukaryotes. In this study, we aimed to analyze how apoptotic signals affect the transcriptions of Ty1 and Ty2 elements in *S. cerevisiae*.

Materials and Methods: To analyze the effects of apoptotic signals on the transcription of Ty element, Ty1-LacZ, and Ty2-LacZ gene fusions were used as reporter genes. These gene fusions were transformed into the wild type and certain yeast mutants that are defective in various signaling pathways. Acetic acid was added to the growth medium of logarithmically growing yeast transformants to induce apoptosis. Transcription levels of the Ty-lacZ gene fusions were analyzed by β -Galactosidase assays.

Results: The results of this study show that transcription of Ty1 and Ty2 decreases approximately 3-fold in response to apoptosis in *S. cerevisiae*. It appears that apoptosis acts through the transcription factors Tec1p and Sgc1p that associate with the regulatory region of Ty1 and Ty2. Moreover, AMP-activated protein kinase Snf1p, and to a lesser extent Tor1p, seem to be required for the transcriptional repression of Ty1 and Ty2 in apoptosis-induced yeast cells.

Conclusion: Ty1 and Ty2 transcription is regulated in response to apoptosis signaling in a differential manner. It seems that protein kinases Tor1p and Snf1p and transcription factors Tec1p and Sgc1p are involved in the apoptosis dependent regulation of Ty transcription.

Keywords: Ty elements, Apoptosis, Transcription, Yeast, Protein kinases

INTRODUCTION

Saccharomyces cerevisiae contains 5 different classes of retrotransposons, called Ty1-Ty5, in its genome (1). Transposition of these retrotransposons takes place via an RNA intermediate (2). Due to their genome organization and their intracellular propagation pattern, Ty elements are classified within the pseudovirales class of vires order (3). Ty1, Ty2, and Ty4 have a similar genome structure and organization. Ty1 and Ty2 have 334 bp Long Terminal Repeat (LTR) sequences in their 5' and 3' ends, named as delta elements. Ty1 has 30 copies per genome while Ty2 has about 10 copies per genome in yeast (1). Apart from full length Ty elements, the yeast genome contains a large number of solo LTR

sequences. Ty3 and Ty5 have a different genome organization (1). The genome organization of Ty3 is similar to the human immunodeficiency virus. It is present as 4 copies per genome. Its LTRs are called sigma elements. The genome sizes of Ty elements vary from 4 Kbp to 6 Kbp (1). Ty elements encode two overlapping peptides, named TYA and TYB. These coding regions show structural and functional homologies to retroviral gag and pol polypeptides, respectively (4,5). TYB is translated by programmed ribosomal frameshift mechanisms as a TYA-TYB fusion protein (6).

Transcription of Ty elements starts at 5' Delta and ends at 3' Delta. Promoter elements of Ty elements are located both upstream and downstream of the transcription



Corresponding Author: Sezai Türkel E-mail: sturkel@uludag.edu.tr
Submitted: 11.04.2020 • **Revision Requested:** 17.05.2020 • **Last Revision Received:** 22.05.2020 •
Accepted: 26.05.2020 • **Published Online:** 12.06.2020

© Copyright 2020 by The Istanbul University Faculty of Science • Available online at <http://ejb.istanbul.edu.tr> • DOI: 10.26650/EurJBiol.2020.0016

initiation site (7,8). The transcriptional regulatory region of Ty2 is located within the first 750 regions of these elements (8,9). Regulatory regions of Ty1 encompass much longer regions and extend up to the first 1800 bp region of Ty1 (10,11). In upstream, TATA and UAS sequences are located within the first 150 bp region of Ty1 and Ty2. Unexpectedly, most of the transcription regulatory sites, such as enhancer elements, downstream repression sites, and cell type-specific transcription factors' binding sequences are located within the coding region of Ty1 and Ty2 (7-11). Both cis-acting regulatory sequences and transcriptional activators that associate with regulatory sites of Ty 1 and Ty2 have been identified in previous molecular and biochemical studies (7-11). Ty1 transcription is 10-times lower in diploids than in haploid yeast cells (12). The transcription of Ty1 is controlled by the heterodimeric repressor factor in diploids (13).

Ty1 is under the control of at least nine different transcription factors. These are Ste12, Tye7, Tec1, Mcm1, Rap1, Tea1/Ibf1, Gcn4, Gcr1 and Mot3 (5,13-17). Besides transcription factors, chromatin-modifying complexes such as Swi/Snf, SAGA and ISWI are also involved in the regulation of Ty transcription (5). Transcription of Ty2 is controlled by glucose signaling (17).

Apoptosis is an evolutionary conserved programmed cell death mechanism that takes place in all eukaryotes (18-20). Different external and internal signals trigger apoptotic signaling in eukaryotes (21,22). Upon activation of apoptosis by one of the signaling pathways, initiator caspases trigger a caspase cascade, which ends up with the complete destruction of targeted cells (21,22).

Apoptosis is also defined in the yeast cells. The first time, apoptosis-like cellular processes are defined in *cdc48* mutants of *S. cerevisiae* (23,24). Madeo et al, (1997) found that when starved for nutrients, *cdc48* mutants of *S. cerevisiae* go through cellular destruction, similar to apoptotic events in human cells. Later, it was shown that over-expression of the human Bax gene, a proapoptotic factor for human cells, also activated apoptosis-like cell death in *S. pombe* (25).

In search of molecular components of apoptotic signaling pathways in *S. cerevisiae*, the *YCA1* gene (also known as Metacaspase-1, *MCA1*) has been identified and its function in *S. cerevisiae* apoptosis has been confirmed by genetic analyses (26,27). Unlike human caspases, yeast caspase Mca1p has a calcium-dependent cysteine-type endopeptidase activity on the targeted proteins (28,29). Excess H₂O₂, acetic acid, osmotic stress, and certain metal ions are the external activator of apoptosis in yeast. Aging, DNA-damaging drugs, expression of heterologous genes such as human Bax, and α -synuclein are known intracellular effectors that activate apoptosis in *S. cerevisiae* (30). Acetic acid is the well-defined activator of the apoptosis in *S. cerevisiae* (31,32).

Apoptosis has global effects on the metabolism of eukaryotic cells. Once the apoptosis is triggered by internal or external signaling, different kinases are activated or repressed. It is known that protein kinases Tor1p, Snf1p, and Gcn2p have significant

and multiple functions in the nutrient signaling in yeast (33-35). These protein kinases are also conserved in human cells. Recent evidence indicates that Tor1p and Snf1p also have a function in apoptosis (33-35).

Unlike retroviruses, Ty elements cannot leave the yeast cells. Therefore Ty elements can be considered as mandatory genetic components of the yeast cells. Ty genomes do not encode any known transcription or translation regulatory factors. Hence, Ty viruses are completely dependent on the yeast encoded transcription and translation factor for their genomic propagation. In this study, we investigated how apoptotic signals affect the transcriptional regulations of Ty1 and Ty2 elements in *S. cerevisiae*. Our results indicate that activation of apoptosis in yeast cells result in significant decreases in Ty1 and Ty2 transcription. We also show that protein kinases Tor1p and Snf1p were involved in the apoptosis-dependent repression of Ty1 and Ty2 transcription, albeit at the differential level. Effects of Tec1p and Sgc1p were also analyzed to test if apoptosis operates through these factors to regulate Ty transcription.

MATERIALS AND METHODS

Yeast Strains and Ty Expression Vectors

S. cerevisiae strains used in this research were purchased from the EUROSCARF (University of Frankfurt, Germany). Their genotypes and accession numbers for EUROSCARF collection are given in Table 1. The construction of kanMX deletion mutants of these strains was explained previously (36). It is known that these yeast strains do not contain any other mutations in their genomes other than the indicated ones.

The plasmids Ty1-144-lacZ, Ty2-754-lacZ, p-ENC and Ty2-555-lacZ are 2 micron-*URA3* based, yeast episomal (YE_p) type expression vectors. The Ty2-754-lacZ plasmid contains the first 754 nucleotides of the Ty2 genome fused to *E. coli* lacZ gene. It contains all of the regulatory sequences required for the regulated transcription of Ty2. The Ty2-555-lacZ reporter plasmid has the same general features except that it does not contain downstream repression sites for Ty2. p-ENC is also a 2 μ m-*URA3* based expression vector that contains an enhancer region of Ty2, upstream of the TATA box in the UAS-less His4-lacZ gene fusion. Structure and constructions of Ty2-lacZ gene fusions have been published previously (7-9).

Ty1-144-lacZ plasmid is a 2 μ m-*URA3* based, YE_p vector and contains the first 1571 bp region of Ty1 element fused to LacZ gene. Its whole structure and construction have been explained previously (10,11). It is known that these yeast expression vectors are stably maintained in the selective growth medium, and their copy number does not vary in yeast transformants (7).

Growth Conditions and Transformation

Yeast strains were cultured in YPD (yeast extract, peptone, dextrose) media for transformations. Transformation of Ty expression vectors to competent *S. cerevisiae* strains was done using the Polyethylene glycol-lithium acetate method as described previously (37). Yeast transformants were grown in 10 ml of

Table 1. *S. cerevisiae* strains and their relevant genotypes used in this research

Yeast Strains' Lab Code, (relevant mutations) and EUROSCARF Accession numbers	Genotypes
YST124 (wild type) Y00000 (BY4741)	MAT α <i>his</i> Δ 1; <i>leu</i> 2 Δ 0; <i>met</i> 15 Δ 0; <i>ura</i> 3 Δ 0
YST155 (<i>tor</i> 1 Δ) Y06864	MAT α <i>his</i> Δ 1; <i>leu</i> 2 Δ 0; <i>met</i> 15 Δ 0; <i>ura</i> 3 Δ 0; YJR66w::kanMX4
YST159 (<i>snf</i> 1 Δ) Y14311	MAT α <i>his</i> Δ 1; <i>leu</i> 2 Δ 0; <i>met</i> 15 Δ 0; <i>ura</i> 3 Δ 0; YDR477w::kanMX4
YST230 (<i>gcn</i> 2 Δ) Y03642	MAT α <i>his</i> Δ 1; <i>leu</i> 2 Δ 0; <i>met</i> 15 Δ 0; <i>ura</i> 3 Δ 0; YDR283c::kanMX4
YST265 (<i>tec</i> 1 Δ) Y07155	MAT α <i>his</i> Δ 1; <i>leu</i> 2 Δ 0; <i>met</i> 15 Δ 0; <i>ura</i> 3 Δ 0; YBR083w::kanMX4
YST289 (<i>sgc</i> 1 Δ) Y01641	MAT α <i>his</i> Δ 1; <i>leu</i> 2 Δ 0; <i>met</i> 15 Δ 0; <i>ura</i> 3 Δ 0; YOR344c::kanMX4

synthetic complete medium without uracil that contains 2% glucose (Sc-Ura, Dext) in triplicates as described (38). At logarithmic stages, yeast cultures were divided into two aliquots (5 ml each). To induce apoptosis, acetic acid was added to yield 60 mM (pH 3) final concentration to the growth medium of the one portion (5 ml) of the yeast transformants. Yeast cultures (control group and apoptosis induced ones) further grown for five hours at 30°C in an incubator shaker at 150 revolutions per minute. At the end of growth periods, yeast transformants were harvested and processed for β -galactosidase assays.

β -Galactosidase Enzyme Assays

The yeast transformants that were grown with or without acetic acid, harvested at the end of 5 hours of incubation periods, were spun down with centrifugation at 1000 g for 5 minutes. Harvested yeast cells washed with 1 ml of sterile distilled water and transferred to microfuge tubes and harvested again by centrifugation at 15,000 g for 1 minute. Yeast pellets were resuspended in 200 μ l of break buffer and stored at -80°C till enzyme assays. β -galactosidase assays were done essentially as described by Guarantee (39). In brief, yeast cells, suspended in break buffer, were permeabilized with 20 μ l of chloroform and 20 μ l of 0.1% SDS by vortexing at top speed for 1 minute to get permeabilized yeast cell suspensions (39). β -galactosidase assays were done in triplicates using permeabilized yeast cell suspensions and ONPG as substrate as described (39). Protein concentrations in permeabilized yeast cells were determined by the Lowry assay (40). β -galactosidase units are expressed in nm ONPG cleaved per minute per mg of protein in the permeabilized yeast cell suspensions. All assays were repeated at least twice in triplicates. The number representing β -galactosidase units in figures are the averages of 9 independent β -galactosidase assays. Standard deviations were less than 10% in all of the β -galactosidase units given in figures. We have used the T-test to compare two groups of data (such as wild type versus mu-

tant, normal growth versus apoptosis conditions). Transcription units were significantly different ($p < 0.05$).

RESULTS

Effects of Apoptosis Signaling on the Transcription of Ty Elements

We analyzed the effects of apoptosis on two different Ty elements, Ty1 and Ty2, respectively. Under normal growth conditions, transcription from Ty1-144-LacZ gene fusion yields a high level of expression (3074 Units), as expected. However, induction of apoptosis by acetic acid for 5 hours resulted in more than a 3-fold decrease in Ty1 transcription (Figure 1). Similarly, transcription from the Ty2-754-LacZ reporter gene is also repressed upon the activation of apoptosis. Transcription from Ty2-754-LacZ gene fusion is determined as 185 units under normal growth conditions. Induction of apoptosis by acetic acid result-

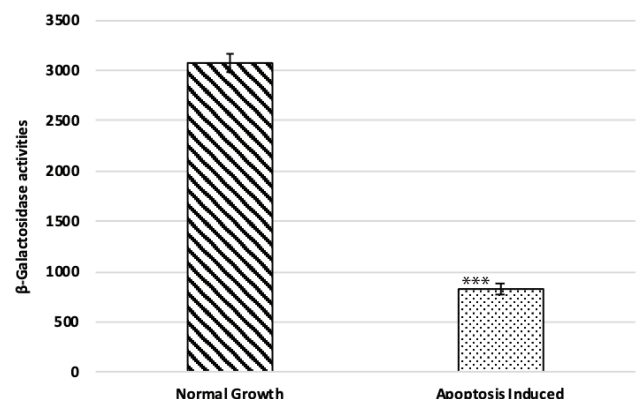


Figure 1. Effects of apoptosis induction on Ty1-144 transcription in wild type yeast. Error bars indicate the standard deviations (***) $p < 0.001$ compared with untreated control.

ed in a nearly 3-fold decrease in Ty2 transcription too (Figure 2). It is known that Ty1 is transcribed at much higher rates than Ty2 (12). It was previously reported that Ty1 mRNA constitutes about 0.8% of total cellular RNA in yeast (12). Hence, there is a clear difference between Ty1 and Ty2 transcriptions in normal growth medium, as seen in Figures 1 and 2. The transcription of both Ty elements decreases approximately 3-fold by the apoptosis signaling. A p -value which is less than 0.001 ($p \leq 0.001$) indicates that there are statistically significant differences in expression levels of Ty1 and Ty2 elements compared to untreated control.

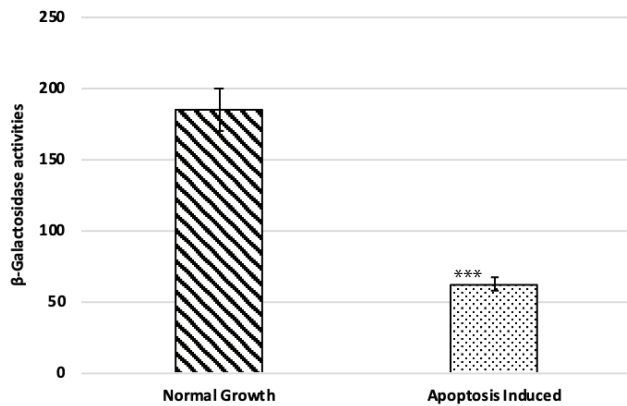


Figure 2. Effects of apoptosis induction on Ty2-754 transcription in wild type yeast. Error bars indicate the standard deviations (***) $p < 0.001$ compared with untreated control).

Effects of Different Protein Kinases on Ty Transcription in Apoptosis Induced Cells

Transcription of Ty1 decreased 20-40% in these kinase mutants in normal growth conditions (Figure 3). But the highest decrease in Ty1 transcription was seen in *snf1* deletion mutant yeast cells, indicating that functional Snf1p kinase is essential for optimal level transcription of Ty1. It has already been shown that Snf1p is required for Ty transcription (41). Activation of apoptosis by acetic acid leads to a further decrease in the transcription of Ty1-144-LacZ gene fusion in this kinase mutant. It seems that

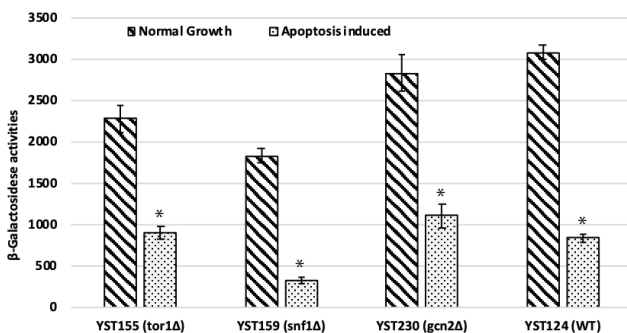


Figure 3. Effects of different protein kinases on the Ty1-144-LacZ transcription in apoptosis induced conditions. Error bars indicate the standard deviations (* $p < 0.05$ compared with untreated control).

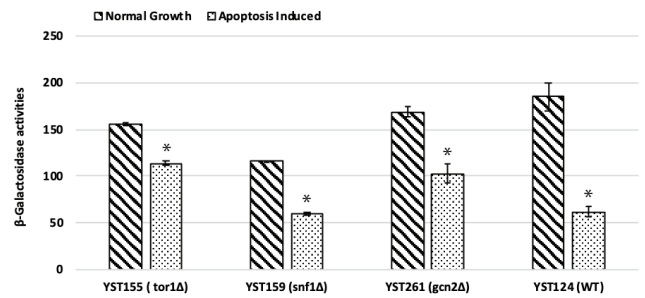


Figure 4. Effects of different protein kinases on the Ty2-754-LacZ transcription in apoptosis induced conditions. Error bars indicate the standard deviations (* $p < 0.05$ compared with untreated control).

inactivation or degradation of Snf1p in apoptosis-induced cells results in a nearly 6-fold decrease (from 1824 units to 323 units) in Ty1 transcription (Figure 4). Ty1 transcription also decreased approximately 2-fold in apoptosis induced Δ *tor1* and Δ *gcn2* mutants and was reduced down to wild type level expression. These results indicate that Tor1p and Gcn2p are not involved in the Ty1 transcription when apoptosis-induced, although they are required for transcription in normal growth conditions. A p -value which is less than 0.05 ($p \leq 0.05$) indicates that there are statistically significant differences in expression levels of Ty1 compared to untreated control (Figure 3).

We also tested the effects of the above-mentioned kinases if they were involved in the Ty2 transcription when yeast cells shifted to apoptotic growth conditions. Interestingly, lack of Tor1p, Gcn2p or Snf1p in normal growth conditions did not influence Ty2 transcription at significant levels. (Figure 4). However, once apoptosis was induced by adding acetic acid to the growth medium of these kinase mutants, transcription of Ty2-754-lacZ gene fusion differentially affected by each mutant. Transcription of Ty2-754-LacZ in Δ *snf1* decreased to wild type level expression in the apoptosis induced yeast cells. It is clear that transcription of Ty2 in apoptosis-induced Δ *tor1* and Δ *gcn2* mutants are not affected by these mutations as much as in Ty1-LacZ transcription (Figure 4). A p -value which is less than 0.05 ($p \leq 0.05$) indicates that there are statistically significant differences in expression levels of Ty2 compared to untreated control (Figure 3).

To see if the apoptosis signaling acts on the transcriptional activators that associate with the Ty2 enhancer region, we also tested the effects of apoptosis signaling on Ty2 enhancer element-dependent transcription independent of Ty2 promoter context. Enhancer element-dependent transcription of a heterologous promoter from p-ENC-LacZ expression vector was analyzed under normal and apoptosis induced growth conditions (Figure 5). In addition, we also tested the effects of apoptosis on the Ty2 transcription that contains upstream activation sequence (UAS) and enhancer elements only as the activator regions in the native Ty2 promoter context. Ty2-555-LacZ expression vector is the truncated version of Ty2-754-LacZ vec-

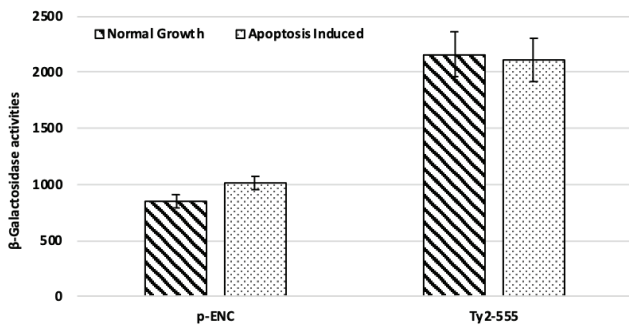


Figure 5. Analysis of the effects of apoptosis on the Ty2-555 and Ty2-Enhancer element dependent transcription in the wild type yeast. Error bars indicate the standard deviations.

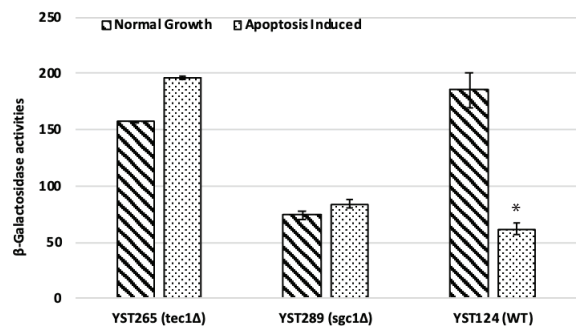


Figure 7. Effects of Tec1p and Sgc1p on Ty2-754-LacZ transcription in apoptosis induced yeast cells. Error bars indicate the standard deviations (* $p < 0.05$ compared with untreated control).

tor that does not contain a negative regulatory region of Ty2 (7-9). Hence, transcription from Ty2-555-LacZ gene fusion was much higher than the Ty2-754-LacZ gene fusion that contained negative regulatory sites for Ty2. As seen in Figure 5, apoptosis signaling did not affect transcription from Ty2-555-LacZ nor p-ENC-LacZ dependent transcription (Figure 5). These results suggest that apoptosis signaling targets regulatory factors that associate with the full-length promoter region of Ty2 in its native context (Figure 5).

Effects of Tec1p and Sgc1p on the Ty1 and Ty2 Transcription in Apoptosis Induced Cells.

To analyze if Tec1p and Sgc1p were involved in the apoptosis signaling-dependent repression of Ty1 and Ty2 transcription, we analyzed the transcription levels of Ty1-144-LacZ and Ty2-754-LacZ gene fusion in $\Delta tec1$ and $\Delta sgc1$ mutant strains of *S. cerevisiae* (Figures 6 and 7).

When compared to the expression levels of Ty1-144-LacZ gene fusions in the wild type yeast strains, Ty1 transcription was not affected by the apoptosis signaling in $\Delta tec1$ and $\Delta sgc1$ mutants. In other words, it seems that functional Tec1p and Sgc1p were the targets of apoptosis signaling for repression of Ty1 transcription. Similarly, transcription from Ty2-754-LacZ gene fusion

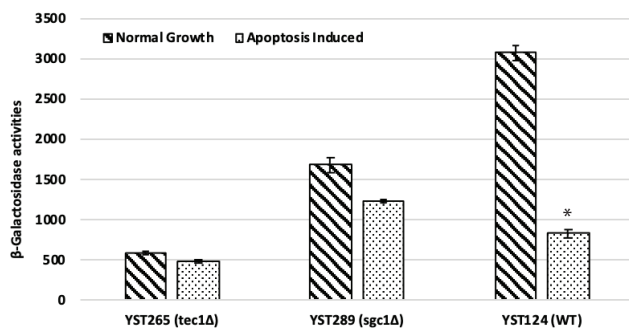


Figure 6. Effects of Tec1p and Sgc1p on Ty1-144-LacZ transcription in apoptosis induced yeast cells. Error bars indicate the standard deviations (* $p < 0.05$ compared with untreated control).

also was not affected by apoptosis signaling in $\Delta tec1$ and $\Delta sgc1$ mutants. We saw slight increases in Ty2-754-LacZ transcription in these mutants when apoptosis was induced by acetic acid (Figure 7).

DISCUSSION

Ty elements have been identified as intracellular mobile genetic elements of the yeast *S. cerevisiae* (1). Their genome structures and intracellular propagation mechanisms resemble retroviruses (2,5). Ty elements do not encode any regulatory factors for their transcription and translation from their genomes. Hence, transcription of Ty elements and translation of their mRNA completely depends on yeast encoded regulatory factors. Regulator factors that are involved in the transcription of Ty have been identified previously (5,13-17). It can be expected that the cellular metabolic events that affect gene expression in the yeast genome should also affect the gene expression in Ty. In accord with this, it has been shown that glucose signaling, amino acid starvation, and adenine starvation affects the transcription of Ty1 and Ty2 (10,17). It is known that the Ty1 transcription is regulated by a cell type-dependent manner, and repressed several-fold by repressor proteins in diploid *S. cerevisiae* cells (13). The expression of Ty2 is not affected by a cell type. Nonetheless, even though the transcription of Ty1 and Ty2 is activated or repressed by cellular signals, it is known that the genomic copy numbers of Ty elements within the yeast genome do not change drastically during consecutive cell divisions. Several mechanisms have been proposed for the copy number maintenance for the Ty element (5,42).

Programmed cell death is a global cellular response to various extracellular and intracellular signals for cell destruction without any cellular artifact (21,22). Molecular mechanisms and biological functions of apoptosis in multi-cellular organisms have been studied extensively (21,22). Apoptosis and its function have also been explained in the yeast *S. cerevisiae* (23,26,27). It occurs in response to external chemical stressors, like acetic acid and hydrogen peroxide in *S. cerevisiae* (30-33). Apoptosis is also activated in aging yeast cells (30-33).

It appears that transcription of Ty1 and Ty2 is also affected by external apoptosis signaling generated by acetic acid. Our results indicated that while the levels of transcription show large differences between Ty1 and Ty2, their transcription was repressed at about the same levels, by 3-fold, in response to apoptosis signaling in the wild type *S. cerevisiae* cells. This result implies that common regulator factors act on Ty1 and Ty2 promoter for repression of Ty transcription when apoptosis-induced. Several transcription factors are involved in the transcriptional activation of both Ty1 and Ty2. Some of these well-known transcriptional activators are Gcn4p, Gcr1p, Tec1p and Sgc1p (Tye7p). The deletion of *GCR1* gene has a severe defect on *S. cerevisiae*, and its deletion has lethal effects on some yeast strains (43). Therefore, we could not analyze the effects of Gcr1p on Ty transcription in apoptosis-induced $\Delta gcr1$ mutant strain.

Transcription factor Gcn4p is also involved in transcriptional activation of Ty1 when amino acid or adenine starvation-induced (10,11). But, Gcn4p is not actively expressed in normal growth conditions, and its activation requires amino acid or purine starvation (10,11). To test the effects of Gcn4p on the Ty1 and Ty2 transcription in apoptosis induced cells, expression of *GCN4* gene must be activated by amino acid or purine starvation. This type of experimental set up will lead to the application of two independent stress conditions, apoptosis and amino acid starvation, on the same yeast cells, which might result in misleading evaluations for the effects of Gcn4p involvement in apoptosis-induced cells. Therefore, we did not test the effects of Gcn4p on Ty1 and Ty2 transcription in apoptosis induced $\Delta gcn4$ mutants.

Instead, we analyzed the effects of Tec1p and Sgc1p on the transcription of Ty1 and Ty2 in the wild type and mutant yeast that is viable under normal growth conditions. Recent evidence indicates that Tec1p also involves the TOR and other MAPK signaling pathways (44,45). Ty1 transcription largely depends on Tec1p (14). Therefore, transcription of Ty1 decreased nearly 6-fold in $\Delta tec1$ mutants strain grown in normal conditions. The transcript of Ty2 is not affected by $\Delta tec1$. It was already shown that Tec1p has no drastic effects on Ty2 transcription (14). But, when apoptosis-induced by acetic acid, transcription Ty2 also remained at the same levels. In other words, apoptosis signaling did not affect Ty2 transcription in $\Delta tec1$ mutants (Figure 7). These results indicated functional Tec1p is one of the targeted regulatory factors for the Ty1 repression in apoptosis induced conditions. The effects of Tec1p in apoptosis-induced and uninduced cells for Ty2 seems to be more complex than Ty1. First of all, a lack of functional Tec1p in $\Delta tec1$ mutant did not have any effects on Ty2 transcription. But, the induction of apoptosis by acetic acid did not repress Ty2 transcription in this mutant. This result suggests that although functional Tec1p is not essential for Ty2 transcription in normal conditions, it is essential for the repression or downregulation of Ty2 transcription by apoptosis.

Ty promoters contain activator and repressor binding sites in both upstream and also in downstream of transcription initiation sites (7-9). We analyzed the effect of apoptosis signaling on the truncated Ty2 promoter (Ty2-555-LacZ reporter) that contains

only the enhancer region (7,8). Interestingly, our results indicated that activation of apoptosis signaling did not have any effects on Ty2 transcription when it contains only the enhancer region. We also tested the effects of apoptosis signaling on the Ty2 enhancer element-dependent transcription when present outside of the Ty2 promoter. As in the truncated Ty2 promoter, enhancer element-dependent transcription of a heterologous promoter is not affected by apoptosis signaling (Figure 5). These results may indicate that apoptosis signaling targets the regulatory factors that associate with the negative regulatory region of Ty2 element that is located within the 555-754 bp region of this element (7,8).

S. cerevisiae has many different protein kinases that share functional and structural homologies to their human counterparts. Some of these kinases are Tor1p, Snf1p, and Gcn2p. These kinases are essential for nutrient signaling in yeasts. They also have functional roles in the signaling and progression of apoptosis and autophagy in yeast (34,35,45). The functional involvement of these kinases in the Ty1 and Ty2 transcription under apoptosis induced conditions were analyzed in the mutant yeast strains that do not have one of these kinases. Our results indicated that Snf1p has a significant function in the basal level transcription of Ty1 and Ty2 in normal growth conditions since the transcription of Ty1 and Ty2 decreased significantly in $\Delta snf1$ mutants. On the other hand, in apoptosis induced conditions, only transcription Ty1 further decreased in $\Delta snf1$ mutant yeast, showing the functional involvement of Snf1p kinase in Ty1 transcription in apoptosis conditions.

Ty1 and Ty2 transcription affected at the differential manner in the yeast mutants that do not contain functional Tor1p kinase. Transcription of Ty2 is not affected by apoptosis signaling in $\Delta tor1$ mutation, indicating that Tor1p kinase is involved in the repression of Ty2 transcription in apoptosis-induced cells. Gcn2p kinase seems to have a moderate level effect on Ty2 transcription both in normal and also in apoptosis induced conditions.

CONCLUSION

In this study, we have shown that the transcription of retroviral-like elements Ty1 and Ty2 was regulated in differential manners when the apoptosis signal was induced by acetic acid. It seems that protein kinases Tor1p and Snf1p and transcriptional activators Tec1p and Sgc1p are involved in the repression of Ty1 and Ty2 transcription in apoptosis induced yeast cells.

Peer-review: Externally peer-reviewed.

Author Contributions: Conception/Design of study: S.T., C.C.; Data Acquisition: C.C., S.T.; Data Analysis/Interpretation: S.T., C.C.; Drafting Manuscript: S.T., C.C.; Critical Revision of Manuscript: S.T.; Final Approval and Accountability: S.T.; Technical or Material Support: S.T., C.C.; Supervision: S.T.

Conflict of Interest: The authors declare that they have no conflicts of interest to disclose.

Financial Disclosure: There are no funders to report for this submission.

REFERENCES

1. Kim JM, Vanguri S, Boeke JD, Gabriel A, Voytas DF. Transposable elements and genome organization: A comprehensive survey of retrotransposons revealed by the complete *Saccharomyces cerevisiae* genome sequence. *Genome Res* 1998; 8: 464-78.
2. Boeke J, Garfinkel DJ, Styles CA, Fink G. Ty elements transpose through an RNA intermediate. *Cell* 1985; 40: 491-500.
3. Capy P. Classification and nomenclature of retrotransposable elements. *Cytogenet Genome Res* 2005; 110: 457-61.
4. Farabaugh PJ. Translational frameshifting: implications for the mechanism of translational frame maintenance. *Prog Nucleic Acid Res Mol Biol* 2000; 64: 131-70.
5. Curcio MJ, Lutz S, Lesage P. The Ty1 LTR-retrotransposon of budding yeast, *Saccharomyces cerevisiae*. *Microbiol Spectr* 2015; 3: 1-35.
6. Belcourt MF, Farabaugh PJ. Ribosomal frameshifting in the yeast retrotransposon Ty: tRNAs induce slippage on a 7 nucleotide minimal site. *Cell* 1990; 62: 339-52.
7. Farabaugh PJ, XB. Liao, Belcourt M, Zhao H, Kapakos J, Clare J. Enhancer and silencer-like sites within the transcribed portion of a Ty2 transposable element of *S. cerevisiae*. *Mol Cell Biol* 1989; 9: 4824-34.
8. Farabaugh PJ, Vimaladithan A, Türkkel S, Johnson R, Zhao H. Three downstream sites repress transcription of a Ty2 retrotransposon in *Saccharomyces cerevisiae*. *Mol Cell Biol* 1993; 13: 2081-90.
9. Türkkel S, Farabaugh PJ. Interspersion of an unusual GCN4 activation site with a complex transcriptional repression site in Ty elements of *Saccharomyces cerevisiae*. *Mol Cell Biol* 1993; 13: 2091-103.
10. Morillon A, Bénard L, Springer M, Lesage P. Differential effects of chromatin and Gcn4 on the 50-fold range of expression among individual yeast Ty1 retrotransposons. *Mol Cell Biol* 2002; 22: 2078-88.
11. Todeschini AL, Morillon A, Springer M, Lesage P. Severe adenine starvation activates Ty1 transcription and retrotransposition in *Saccharomyces cerevisiae*. *Mol Cell Biol* 2005; 25: 7459-72.
12. Curcio MJ, Hedge AM, Boeke JD, Garfinkel DJ. Ty RNA levels determine the spectrum of retrotransposition events that activate gene expression in *Saccharomyces cerevisiae*. *Mol Gen Genet* 1990; 220: 213-21.
13. Company M, Errede BA. Ty1 cell-type-specific regulatory sequence is a recognition element for a constitutive binding factor. *Mol Cell Biol* 1988; 8: 5299-309.
14. Laloux I, Dubois E, Dewerchin M, Jacobs E. *TEC1*, a gene involved in the activation of Ty1 and Ty1-mediated gene expression in *Saccharomyces cerevisiae*: Cloning and molecular analysis. *Mol Cell Biol* 1990; 10: 3541-50.
15. Löhning C, Ciriacy M. The TYE7 gene of *Saccharomyces cerevisiae* encodes a putative bHLH-LZ transcription factor required for Ty1-mediated gene expression. *Yeast* 1994; 10: 1329-39.
16. Türkkel S, Yenice B. Analysis of the Effects of Chromatin Modifying Complexes on the Transcription of Retrotransposon Ty2-917 in *Saccharomyces cerevisiae*. *Turk J Biol* 2006; 30: 101-6.
17. Türkkel S, Liao XB, Farabaugh PJ. Gcr1-dependent transcriptional activation of yeast retrotransposon Ty2-917. *Yeast* 1997; 13: 917-30.
18. Kerr JFR, Wyllie AH, Currie R. Apoptosis: A basic biological phenomenon with wide-ranging implications in tissue kinetics. *Br J Cancer* 1972; 26: 239-57.
19. Ellis HM, Horvitz HR. Genetic control of programmed cell death in the nematode *C. elegans*. *Cell* 1986; 44: 817-29.
20. Nunez G, Benedict MA, Hu Y, Inohara N. Caspases: the proteases of the apoptotic pathway. *Oncogene* 1998; 17: 3237-45.
21. Elmore S. Apoptosis: A Review of Programmed Cell Death. *Toxicol Pathol* 2007; 35: 495-516.
22. D'Arcy MS. Cell death: A review of the major forms of apoptosis, necrosis and autophagy. *Cell Biol Int* 2019; 43: 582-92.
23. Madeo F, Herker E, Wissing S, Jungwirth H, Eisenberg T, Fröhlich KU. Apoptosis in yeast. *Curr Opin Microbiol* 2004; 7: 655-60.
24. Stolz A, Hilt W, Buchberger A, Wolf DH. Cdc48: a power machine in protein degradation. *Trends Biochem Sci* 2011; 36: 515-23.
25. Jürgensmeier JM, Krajewski S, Armstrong RC, Wilson GM, et al. Bax- and Bak-induced cell death in the fission yeast *Schizosaccharomyces pombe*. *Mol Biol Cell* 1997; 8: 325-39.
26. Mazzoni C, Falcone C. Caspase-dependent apoptosis in yeast. *Biochim Biophys Acta (BBA)*. 2008; 1783: 1320-7.
27. Madeo F, Herker E, Maldener C, Wissing S. et al. A caspase-related protease regulates apoptosis in yeast. *Mol Cell* 2002; 9: 911-7.
28. Wilkinson D, Ramsdale M. Proteases and caspase-like activity in the yeast *Saccharomyces cerevisiae*. *Biochem Soc Trans* 2011; 39: 1502-8.
29. Shrestha A, Brunette S, Lloyd W, Lynn S, Megeney A. The metacaspase Yca1 maintains proteostasis through multiple interactions with the ubiquitin system. *Cell Discovery* 2019; 5: Article: 6.
30. Falcone C, Mazzoni C. External and internal triggers of cell death in yeast. *Cell Mol Life Sci* 2016; 73(11-12): 2237-50.
31. Giannattasio S, Guaragnella N, Zdravlevic M, Marra E. Molecular mechanisms of *Saccharomyces cerevisiae* stress adaptation and programmed cell death in response to acetic acid. *Front Microbiol* 2013; 4, article 33.
32. Corte-Real M, Sousa MJ. Genome-wide identification of genes involved in the positive and negative regulation of acetic acid-induced programmed cell death in *Saccharomyces cerevisiae*. *BMC Genomics*, 2013; 14: 838.
33. Almeida B, Ohlmeier S, Almeida AJ, Madeo F, Leão C, Rodrigues F, Ludovico P. Yeast protein expression profile during acetic acid-induced apoptosis indicates causal involvement of the TOR pathway. *Proteomics* 2009; 9: 720-32.
34. Bonomelli B, Martegani E, Colombo S. Lack of SNF1 induces localization of active Ras in mitochondria and triggers apoptosis in the yeast *Saccharomyces cerevisiae*. *Biochem Biophys Res Commun* 2020; 523:130-4.
35. Xia X, Lei L, Qin W, Wang L, Zhang G, Hu J. GCN2 controls the cellular checkpoint: potential target for regulating inflammation. *Cell Death Discovery* 2018; 4: 20.
36. Brachmann CB, Davies A, Cost GJ, Caputo E, Li J, Hieter P, Boeke JD. Designer Deletion Strains derived from *Saccharomyces cerevisiae* S288C: a Useful set of Strains and Plasmids for PCR-mediated Gene Disruption and Other Applications. *Yeast* 1998; 14: 115-32.
37. Gietz RD, Schiestl RH, Willems AR, Woods RA. Studies on the transformation of intact yeast cells by the LiAc/SS-DNA/PEG procedure. *Yeast* 1995; 11: 355-60.
38. Rose MD, Winston F, Heiter P. *Methods in Yeast Genetics. A Laboratory Course Manual*. Cold Spring Harbor Laboratory Press, Cold Spring Harbor, NY, USA. 1990.
39. Guarente L. Yeast promoters and lacZ fusions designed to study expression of cloned genes in yeast. *Methods Enzymol* 1983; 101: 181-91.
40. Lowry OH, Rosebrough NJ, Farr AL, Randall RJ. Protein measurement with the Folin phenol reagent. *J Biol Chem* 1951; 193:265-75.
41. Risler JK, Kenny AE, Palumbo RJ, Eric R, Gamache ER, Curcio MJ. Host co-factors of the retrovirus-like transposon Ty1. 2012; *Mobile DNA* 2012; 3: 12.
42. Garfinkel DJ, Nyswaner KM, Stefanisko KM, Chang C, Moore SP. Ty1 Copy number dynamics in *Saccharomyces*. *Genetics* 2005; 169: 1845-57.
43. Lopez MC, Baker HV. Understanding the growth phenotype of the yeast gcr1 mutant in terms of global genomic expression patterns. *J Bacteriol* 2000; 182: 4970-8.
44. Brückner S, Kern S, Birke R, Saugar I, Ulrich HD, Mösch HU. The TEA transcription factor Tec1 links TOR and MAPK pathways to coordinate yeast development. *Genetics* 2011; 189: 479-94
45. Carmona-Gutierrez D, Eisenberg T, Büttner S, Meisinger C, Kroemer G, Madeo F. Apoptosis in yeast: triggers, pathways, subroutines. *Cell Death Differ* 2010; 17: 763-73.

Conserved Protein YpmR of Moderately Halophilic *Bacillus licheniformis* has Hydrolytic Activity on p-Nitrophenyl Laurate

Abdoulie O. Touray¹ , Ayse Ogan² , Kadir Turan³ 

¹Pan African University, Technology and Innovation, Institute of Basic Sciences, Department of Molecular Biology and Biotechnology, Nairobi, Kenya

²Marmara University, Faculty of Arts and Sciences, Department of Chemistry, Istanbul, Turkey

³Marmara University, Faculty of Pharmacy, Department of Basic Pharmaceutical Sciences, Istanbul, Turkey

ORCID IDs of the authors: A.O.T. 0000-0002-2983-1559; A.O. 0000-0002-8973-9762; K.T. 0000-0003-4175-3423

Please cite this article as: Touray AO, Ogan A, Turan K. Conserved Protein YpmR of Moderately Halophilic *Bacillus licheniformis* has Hydrolytic Activity on p-Nitrophenyl Laurate. Eur J Biol 2020; 79(1): 43-50. DOI: 10.26650/EurJBiol.2020.0018

ABSTRACT

Objective: Hydrolases are of great use in many industries including food, textile, paper, detergent, and pharmaceutical production. These enzymes are abundant in all eukaryotic and prokaryotic organisms. Microbial enzymes are relatively tolerant to changes in pH, temperature and salt concentration and are capable of catalyzing reactions with high substrate specificity. Therefore they are potentially important for industrial applications. In this study we aimed to clone and characterize a hypothetically defined moderately *Bacillus licheniformis* YpmR enzyme, a member of the SGNH-hydrolase superfamily.

Materials and Methods: The hypothetical YpmR gene was amplified with PCR using specific oligonucleotide primers and genomic DNA of *B. licheniformis*. The purified PCR products were cloned under the control of *Escherichia coli* lac promoter. Expression of the recombinant YpmR protein in the *E. coli* cells was assessed using SDS-PAGE/Western blotting. The enzymatic activities were spectrophotometrically determined using p-nitrophenyl laurate (pNPL) and p-nitrophenyl acetate (pNPA).

Results: The YpmR enzyme showed a 7-8 fold higher enzymatic activity against the pNPL substrate as compared to the negative controls. Hydrolysis of the pNPL substrate was found to be due to the *B. licheniformis* YpmR enzyme. In contrast, high hydrolytic activity in bacterial lysates not encoding YpmR enzyme on pNPA substrate indicated that the hydrolysis is due to the presence of other intracellular hydrolases. *B. licheniformis* YpmR enzyme was shown to be tolerant to high NaCl and Triton X-100 concentration.

Conclusion: The moderate halophilic *B. licheniformis* hypothetical YpmR enzyme heterologously synthesized in *E. coli* cells has hydrolytic activity on pNPL substrate. The enzyme was observed to be more tolerant to an increase in NaCl and Triton X-100 concentrations compared to the *Candida rugosa* lipase enzyme used in this study as a control.

Keywords: YpmR gene, Gene cloning, *Bacillus licheniformis*, Hydrolase activity, p-nitrophenyl laurate (pNPL)

INTRODUCTION

Hydrolases are a class of enzymes that catalyze covalent bond cleavage in the presence of water molecules. Some members of this class of enzymes include the carboxylesterases and proteases that act on ester bonds like lipases and esterases and amide bonds in peptides, respectively (1,2). Hydrolases have vast applications in food, detergent and leather industries as well as pharmaceutical industries (3,4). These enzymes are divided into superfamilies based on the type of 3D structural features

and this includes the broader group α/β -hydrolase superfamily with Ser, His and Asp residues as the catalytic triad and the relatively recently identified SGNH-hydrolase superfamily (a diverse family of lipases and esterases) (5,6). A large number of hydrolases in this family have a common catalytic Ser, oxyanion-hole forming Gly, Asn, and invariant His residues (2,7). Different substrates were described for the members of SGNH-hydrolases including acyl-CoA esters (8) lysophospholipids (9), and complex polysaccharides (10). Lipases (EC 3.1.1.3, triacylglycerol acyl hydrolases) are members of the hydrolase



Corresponding Author: Kadir Turan

E-mail: kadiraturan@marmara.edu.tr

Submitted: 29.04.2020 • **Revision Requested:** 18.05.2020 • **Last Revision Received:** 31.05.2020 •

Accepted: 03.06.2020 • **Published Online:** 15.06.2020

© Copyright 2020 by The Istanbul University Faculty of Science • Available online at <http://ejb.istanbul.edu.tr> • DOI: 10.26650/EurJBiol.2020.0018

family that catalyze both the hydrolysis and synthesis of long chain triacylglycerol in the presence or absence of a water medium respectively (11). Lipases are of animal, plants and microbial origins. Among the different sources of lipases, microbial lipases have displayed greater popularity due to their diverse properties and ease of genetic manipulations (11-14). One property of microbial lipases that is of particular importance in many biotechnological transformations is their ability to catalyze reactions in a wide range of temperatures (15,16). As a result, many attempts has been made to isolate new microbial lipases that have the potential to remain active in harsh industrial reaction conditions like high temperatures, presence of alkaline or acidic conditions, etc. The isolation of such robust new enzymes is largely through genetic engineering of the already existing ones or screening for new microorganisms (17). Recently, a new member of the SGNH-hydrolase superfamily called the "SGNH-hydrolase YpmR like" subfamily was identified. This enzyme was reported to have different tertiary fold as compared to the alpha/beta hydrolase family and is generally unique among all the known hydrolase enzymes with an active site similar to the Ser-His-Asp (Glu) triad, but it might lack the carboxylic acid (18,19). Based on sequence alignment analysis, *Bacillus YpmR* gene sequence is reported to be similar to the "SGNH-hydrolase YpmR like" subfamily (19). Despite this finding, the enzymatic activity of the YpmR protein is yet to be experimentally determined. Proteins whose existence has been predicted based on their gene sequences but which lack the experimental evidence of *in vivo* or *in vitro* expression are termed hypothetical proteins. Consequently, the YpmR is only a hypothetical protein with putative hydrolytic activity. Therefore, in a quest to generate novel lipolytic enzymes suitable for both basic research and varied industrial applications, the *Bacillus YpmR* enzyme may be a potential candidate. Hence, the main aim of this study was to seek to establish the hydrolytic activity and enzymatic characteristics of this putative enzyme.

MATERIALS AND METHODS

Chemicals and Reagents

p-nitrophenyl laurate (p-NPL), p-nitrophenyl acetate (pNPA), SDS gel electrophoresis markers and reagents, *Candida rugosa* lipase were purchased from Sigma Aldrich Chemical Co. (St., Louis, USA) and yeast extract and agar from Merck, (Darmstadt, Germany). Bradford reagent and ovalbumin were the commercial product of BioRad (BioRad Laboratories, Hercules CA, USA). All other chemicals were of analytical grade and used without further purification. *Bacillus licheniformis* isolated from nature was kindly provided by Dr. M. Birbir (Biology Department, Marmara University).

Genomic DNA (gDNA) Isolation from Bacteria

Genomic DNA (gDNA) was isolated from the moderately halophilic *B. licheniformis* using a commercial gDNA isolation kit (Invitrogen Cat No. K1820-01). The bacterial cells were cultured in a 5 ml Complex Media at 37°C for 24 hours. The cells were precipitated by centrifuging the culture at 7,500 rpm for 10 minutes. The precipitated cells were used to isolate gDNA based on the manufacturer's protocol.

Construction of Expression Vectors

Hypothetically defined YpmR gene of *B. licheniformis* was amplified using the forward primer 5'-ATGAACATACGTTTTAT-TACAGTC-3' (or using 5'-ACATACGTTTTATTACAGTCATG-3' for gene without the ATG start code) and reverse primer 5'-TTAT-TCTGCTGGGAGGTCTTCG-3'. The primers were phosphorylated using T4 polynucleotide Kinase (New England Biolabs) enzyme prior to their use. All the primers used in this study were originally designed using the NCBI primer design tool. The KOD-plus (Toyobo, Japan) thermostable DNA polymerase enzyme was used for amplification of YpmR gene fragment. The cycling conditions for PCR were: initial denaturation for 3 min at 95°C, 32 cycles of 20 seconds at 95°C, 20 seconds at 55°C and 1 min at 68°C, and in the final extension for 5 min at 68°C. The PCR products were extracted with phenol: chloroform: isoamyl alcohol (25:24:1) followed by ethyl alcohol precipitation. The samples were dissolved in 15 µl of deionized distilled water and purified using agarose gel extraction kit (QIAEX II Gel Extraction Kit). The plasmid vectors pGFP (Clontech) and pET-14b (Novagen) were used for cloning of the YpmR gene. We cloned the amplified *B. licheniformis* YpmR gene with and without histidine (x6 his) tag under the control of *E. coli* lac promoter. The pGFP plasmid vector was linearized using the inverse PCR technique. The vector was amplified using a primer pair targeting the regions bounding the GFP ORF (forward primer: 5'- CATTTCG-TAGAATTCCAACACTG-3' and reverse primer: 5'-AGCTGTTTCCT-GTGTGAAATTG-3'). The cycling conditions for this PCR reaction were: initial denaturation for 3 min at 95°C, 32 cycles of 20 seconds at 95°C, 15 seconds at 52°C and 3 min at 68°C, and in the final extension for 10 min at 68°C. The PCR products were purified using gel extraction kit. The PCR products carrying the ATG start codon were ligated with the linearized plasmid vector using T4 DNA ligase enzyme (TaKaRa, Japan). The obtained plasmid vector was named pLac-YpmR. The YpmR gene having a histidine tag coding sequence at 5'-end was cloned in two stages. In the first stage, the gene without ATG start code was cloned into the *NdeI* restriction site of the pET-14b plasmid. For this, the pET-14b plasmid was linearized by cutting it with *NdeI* restriction enzyme (New England Biolabs) and the sticky ends of the plasmid were blunted using the Klenow enzyme (New England Biolabs). For these processes, 5 µg plasmid DNA in 45 µl of deionized distilled water was mixed with 5 µl of x10 concentrated reaction buffer and 1 µl (10U) *NdeI* restriction endonuclease enzyme. The restriction digestion process was carried out at 37°C for 1 hour. Agarose gel electrophoresis was used to check whether the plasmid DNAs were cut. The samples were kept at 65°C for 20 minutes in order to inactivate the restriction enzyme. After the inactivation step, 2.5 µl of 2 mM dNTP mix and 1 µl (1U) Klenow enzyme (New England Biolabs) were added to the reaction mix and incubated at 37°C for 30 minutes. The DNA samples were extracted using phenol: chloroform: isoamyl alcohol and precipitated with ethyl alcohol. The precipitated samples were then dissolved in 22.5 µl deionized distilled water. For the dephosphorylation of plasmid DNA, 2.5 µl of x10 concentrated buffer and 1 µl (1U) of shrimp alkaline phosphatase (SAP; Fermentas) were added to the sample and kept for 1

hour at 37°C and this was followed by incubation of the reaction medium at 65°C for 20 minutes for the inactivation of the SAP enzyme. The plasmid DNA, which was linearized by digestion with *Nde*I restriction enzyme, was ligated with the YpmR gene without the start code (ATG). The plasmid vector obtained was named pET-14b-hYpmR. The hYpmR gene in pET-14b-hYpmR plasmid vectors was sub-cloned under the control of the lac promoter. The pET-14b-hYpmR plasmid was digested with *Nco*I (New England Biolabs) and *Xho*I (New England Biolabs) restriction endonuclease enzymes and the sticky ends were blunted using the Klenow enzyme. The hYpmR DNA fragment was purified with agarose gel extraction kit then ligated with the plasmid DNA obtained from pGFP by inverse PCR as mentioned above. The generated plasmid vector was named pLac-hYpmR.

SDS-PAGE and Western Blotting

The pLac-YpmR and pLac-hYpmR plasmid vectors were transformed in competent *Escherichia coli* Mach1 cells. Small-scale saturated cultures (3 ml) of the transformed bacterial cells were prepared on LB (+amp) medium. The cells in a 0.5 ml samples were precipitated by centrifuging at 7,500 rpm for 5 minutes. The cell precipitates were suspended in 100 µl of deionized distilled water and mixed with an equal volume of 2x concentrated SDS sample loading buffer. The samples were passed through a 27G needle for 10-15 times and centrifuged at 15,000 rpm for 5 minutes. The proteins in the supernatant were denatured at 95°C for 5 minutes and then loaded onto a 10% denatured polyacrylamide gel. Proteins separated by SDS-PAGE were either stained using silver staining technique or transferred to PVDF membranes to detect the hYpmR protein by Western blotting. For blotting, mouse anti-his monoclonal antibody (Santa Cruz # sc-57598) and goat anti-mouse IgG-HRP (Invitrogen # 31420) were used as the primary and secondary antibodies, respectively. The proteins were detected using the ECL Western Blotting Detection Reagent (GE Healthcare # RPN2235).

Preparation of Cell Lysates and Hydrolytic Activity Assays

E. coli cells transformed with the plasmids coding *B. licheniformis* YpmR protein were cultured in 100 ml LB media (+amp) until saturation. Non-transformed *E. coli* cells were cultured in a LB (-). The cells were precipitated by centrifuging at 7,500 rpm for 10 minutes. The cell precipitates were washed with sterile deionized distilled water and then suspended in 5 ml cold Tris-CaCl₂ buffer (100 mM Tris-CL, pH: 7; 5 mM CaCl₂). Cell suspensions were sonicated on ice with a sonicator (Bandalin) using 80% power 10 seconds on and 10 seconds off for 10 min. The samples were centrifuged at 4°C at a speed of 15,000 rpm for 15 minutes. The Bradford method was used to determine the amounts of protein in the supernatants and these samples were used in the subsequent enzyme activity tests (20). Hydrolysis activities of the cell lysates were determined at different reaction conditions using *p*-nitrophenyl laurate (pNPL) and *p*-nitrophenyl acetate (pNPA). For the enzyme activity assays, 20 µl of substrate (10 mM pNPL or 10 mM pNPA) and 30 µl cell lysate (1-2 µg protein / µl) were added to 950 µl Tris-CaCl₂ buffer (pH: 7); followed by incubation of the reaction mixtures at 30°C, 37°C or 55°C for 15-30 minutes.

In order to determine the effects of salt (NaCl) concentration on the hypothetical YpmR enzyme, Tris-CaCl₂ buffer containing different concentrations of NaCl (0.1 M, 0.5 M, and 2.5 M final concentrations) were used. In addition, the effect of pH on the hypothetical enzyme was also determined using Tris-CaCl₂ buffers adjusted to pH 6 and pH 9.5. To determine the effects of Triton X-100, a non-ionic detergent, different concentrations of the detergent ranging from 0.01% to 1% were added to the reaction mixture. *C. rugosa* lipase enzyme (Sigma-Aldrich # L1754; ≥700 unit/mg solid) solution (15 ng protein/30 µl equivalent to ~ 10 mU) was used as the positive control for the reactions. After incubation, the reaction mixtures were kept at 90°C for 5 minutes in order to inactivate the enzyme followed by centrifugation at 14,000 rpm for 5 minutes. The absorbance (OD₄₀₅) of samples was determined with a spectrophotometer. The relative enzymatic activities were given as a ratio to the negative control or to the sample showing the lowest enzyme activity.

Statistical Analysis

Statistical methods used in this work include descriptive statistics (arithmetic mean and standard deviation) and the nonparametric Mann-Whitney test. P < 0.05 defined statistical significance.

RESULTS

Electrophoretic analysis of recombinant YpmR enzyme produced in *E. coli* cells

The plasmids pLac-YpmR, pLac-hYpmR and pET14b-hYpmR were transformed in *E. coli* Mach1, BL21 and/or JM107 strains, and the YpmR and his-tagged YpmR enzymes produced in these cells were analyzed using SDS-PAGE. The plasmid vectors were found to effectively express in the *E. coli* strains used. Fig-

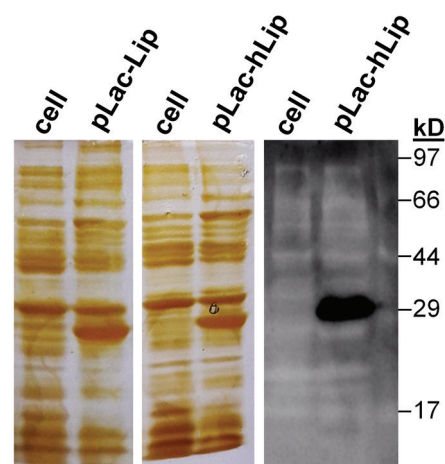


Figure 1. SDS-PAGE/silver staining (left two panels) and Western blotting (right panel) analysis of *B. licheniformis* hypothetical YpmR enzymes synthesized in *E. coli* Mach1 cells transformed with pLac-YpmR and pLac-hYpmR plasmids. The proteins were separated on a 10% denatured polyacrylamide gel. The mouse monoclonal anti-his antibody and HRP-conjugated goat anti-mouse IgG were used as the primary and secondary antibodies, respectively.

Figure 1 shows the SDS-PAGE/silver staining and Western blotting results of the heterologously expressed recombinant *B. licheniformis* YpmR enzymes in *E. coli* Mach1 cells.

Enzymatic Activity of *B. licheniformis* YpmR on pNPL and pNPA

Enzyme activities of the lysates prepared from the transformed *E. coli* cells (*E. coli* BL21 and/or *E. coli* JM107) encoding the *B. licheniformis* hypothetical YpmR enzyme were determined through spectrophotometry using pNPL and pNPA as substrates. The activity of the recombinant YpmR enzyme produced in two different bacterial strains was 7-8 fold higher ($P \leq 0.01$) than that of the non-transformed control cells using pNPL substrate at 37°C, in Tris-CaCl₂ buffer (pH 7). The purified *C. rugosa* lipase enzyme used as the reference in our experiment (Sigma # L1754; 15 ng protein equivalent to ~ 10 mU), produced high level of hydrolysis activity on pNPL substrate (Figure 2A). In contrast, using pNPA substrate, a similar level of enzyme activities (0.9-1.2-fold changes) ($P \geq 0.05$) was detected in both the transformed and non-transformed cells lysates. The purified *C. rugosa* lipase enzyme did not show hydrolytic activity on pNPA substrate (Figure 2B). These results showed that, pNPA, a substrate used for different esterase enzymes (21), is hydrolyzed by intracellular esterases other than YpmR and lipase enzymes.

Effect of NaCl on Enzymatic Activity of *B. licheniformis* YpmR

In this study, the enzyme activity of a hypothetical YpmR enzyme belonging to the moderately halophilic *B. licheniformis* was investigated. Therefore, the recombinant YpmR enzyme synthesized in *E. coli* cells, is believed to be active in relatively high salt concentrations. Based on this assumption, the hydrolysis activity of the enzyme expressed in *E. coli* JM107 cells was tested at salt concentrations of 0.1 M, 0.5 M and 2.5 M. The maximum enzyme activity was obtained at 0.5 M NaCl concentration. It was observed that the enzyme lost approximately 50% activity at 2.5 M NaCl concentration. The YpmR enzyme was found to be more tolerant against increasing salt concentration as compared to the *C. rugosa* lipase enzyme used as reference (Figure 3).

Effect of pH on Enzymatic Activity of *B. licheniformis* YpmR

The activity of *B. licheniformis* YpmR enzyme synthesized in *E. coli* JM107 strain on pNPL substrate in Tris-CaCl₂ buffer at different pH was determined through spectrophotometry (Figure 4). The enzyme was found to have a low level of activity at pH 6 but to show a higher activity between pH 7-9.5. The maximum activity of the enzyme was obtained at pH 8. In comparison to the *C. rugosa* lipase enzyme, the *B. licheniformis* YpmR enzyme was found to be much more active at pH 9.5.

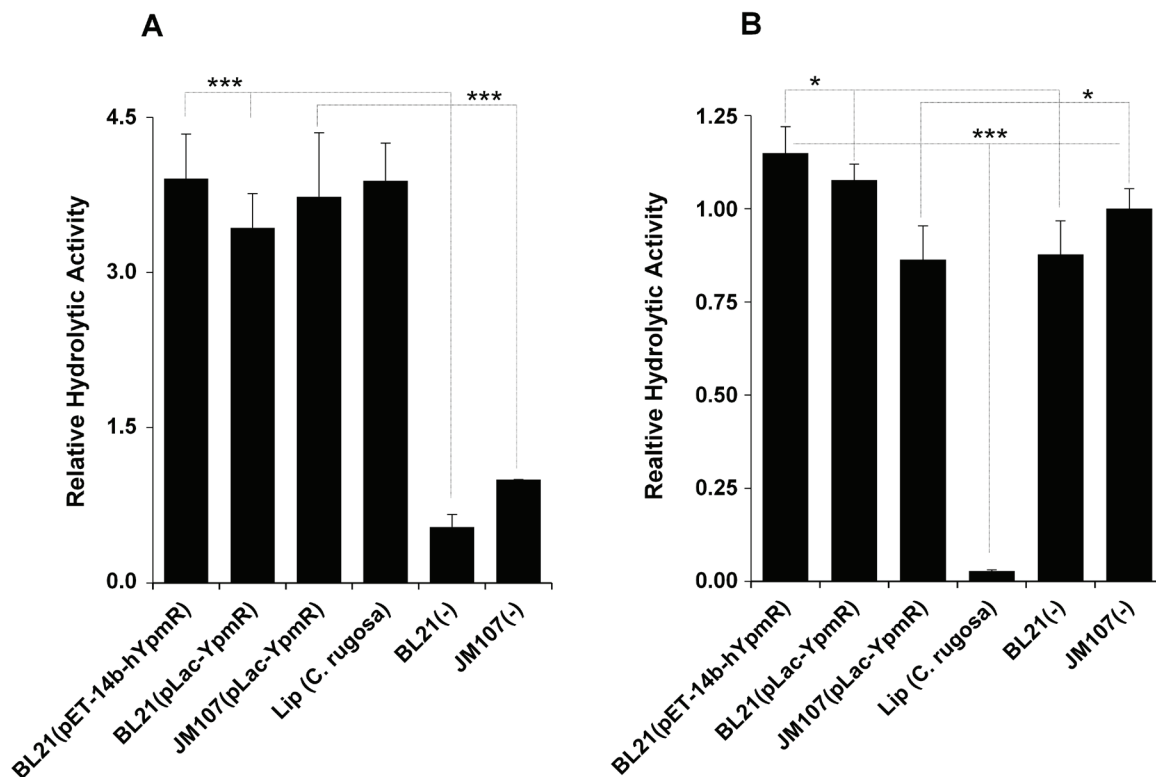


Figure 2. Hydrolytic activities shown by *B. licheniformis* hypothetical YpmR enzyme heterologously expressed in *E. coli* BL21 and JM107 bacterial strains in Tris-CaCl₂ buffer (pH 7), at 37°C, using pNPL and pNPA substrates. In the experiments, 15 ng (30 µl) of *C. rugosa* lipase enzyme (~700 U/mg) was used as a reference. Results are presented in terms of mean±SD (n = 5); (*) - $P \geq 0.05$; (***) - $P \leq 0.01$.

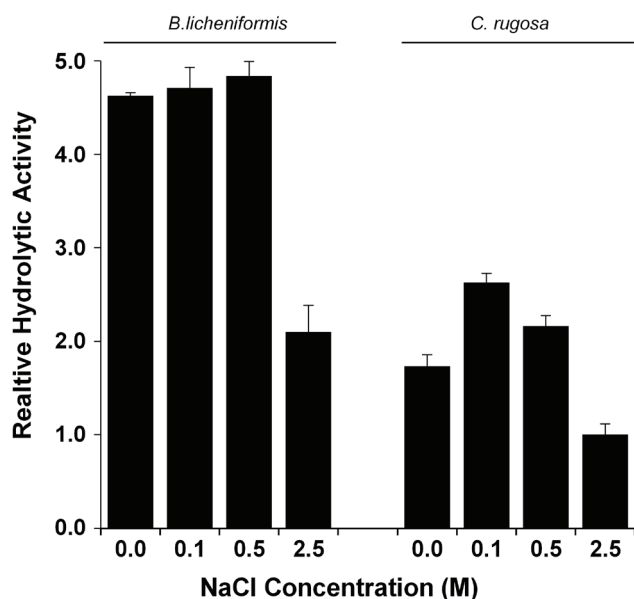


Figure 3. Hydrolytic activities of the hypothetical YpmR enzyme of *B. licheniformis* synthesized in *E. coli* JM107 strain and *C. rugosa* lipase enzyme on pNPL substrate at different salt (NaCl) concentrations. The experiments were performed at 37°C in Tris-CaCl₂ (pH.7) buffer containing different concentrations of NaCl. Results are presented in terms of mean±SD (n = 3).

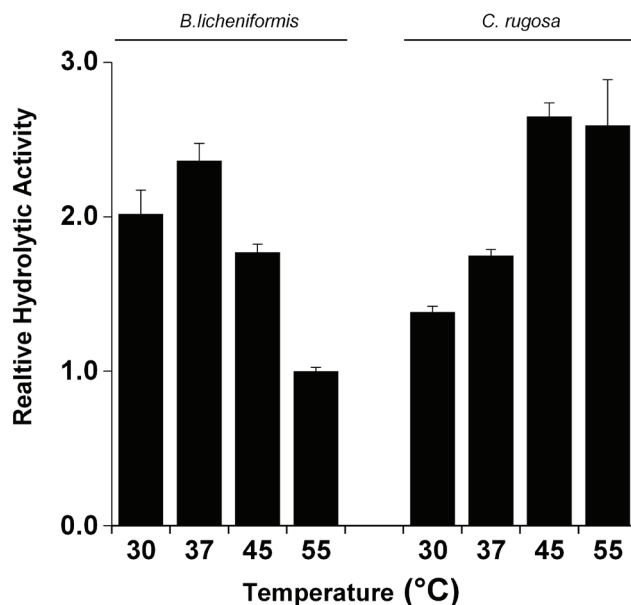


Figure 5. Hydrolytic activities of YpmR enzyme synthesized in *E. coli* JM107 strain and *C. rugosa* lipase at different temperature on pNPL substrate. The experiments were carried out using the cell lysate and 15 ng (30 µl) of *C. rugosa* lipase enzyme at different temperatures as per the values on the figure in Tris-CaCl₂ buffer at pH 7. Results are presented in terms of mean±SD (n = 3).

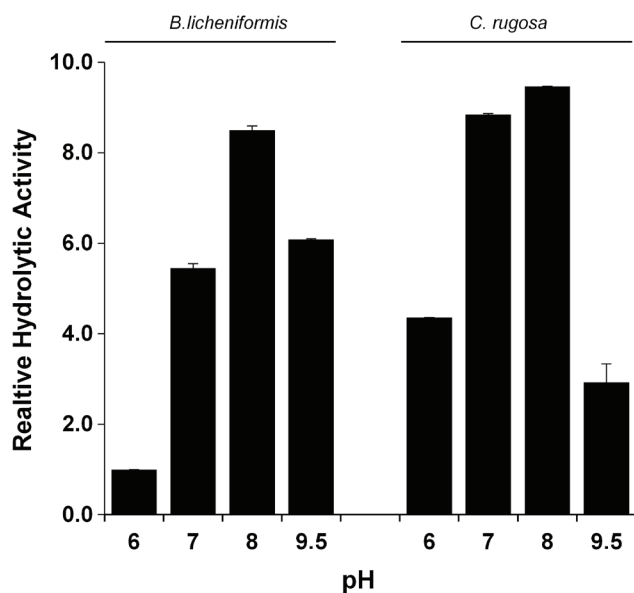


Figure 4. Hydrolytic activities of *B. licheniformis* YpmR enzyme synthesized in *E. coli* JM107 strain and *C. rugosa* lipase enzyme on pNPL substrate at different pH values. The experiments were performed at 37°C in Tris-CaCl₂ buffer at different pH. Results are presented in terms of mean±SD (n = 3).

Enzymatic Activity of *B. licheniformis* YpmR at Different Temperatures

The activity of the YpmR enzyme was tested at 30°C, 37°C, 45°C and 55°C temperatures. The catalytic activity of the enzyme produced in *E. coli* JM107 cells on pNPL substrate at specified temperatures was determined using spectrophotometry (Figure 5). The enzyme showed high enzymatic activities at 30°C, 37°C and 45°C but the activity decreased by approximately 50% at 55°C. However, it was observed that the *C. rugosa* lipase enzyme used as reference showed maximum hydrolytic activity at 45-50°C.

Enzymatic Activity of *B. licheniformis* YpmR in the Presence of Triton X-100

One of the industrial applications of hydrolytic enzymes is the detergent industry. In this regard, it is of particular importance that lipase enzymes are active in the presence of detergent. Therefore, the activity of the *B. licheniformis* YpmR enzyme produced in *E. coli* JM107 was tested in the presence of Triton X-100, a non-ionic detergent, at varied concentrations. The pNPL hydrolysis activity of the hypothetical YpmR enzyme in 0.01-1% concentrations of Triton X-100 was determined using spectrophotometry. The enzyme maintains its activity up to 0.25% Triton X-100 concentration. At a concentration of 0.5% Triton X-100, the enzyme still shows approximately 50% enzymatic activity and the activity decreases to 25% in 1% Triton X-100 concentration (Figure 6). *B. licheniformis* YpmR enzyme was found to have higher tolerance against Triton-X-100 as compared to *C. rugosa* lipase enzyme.

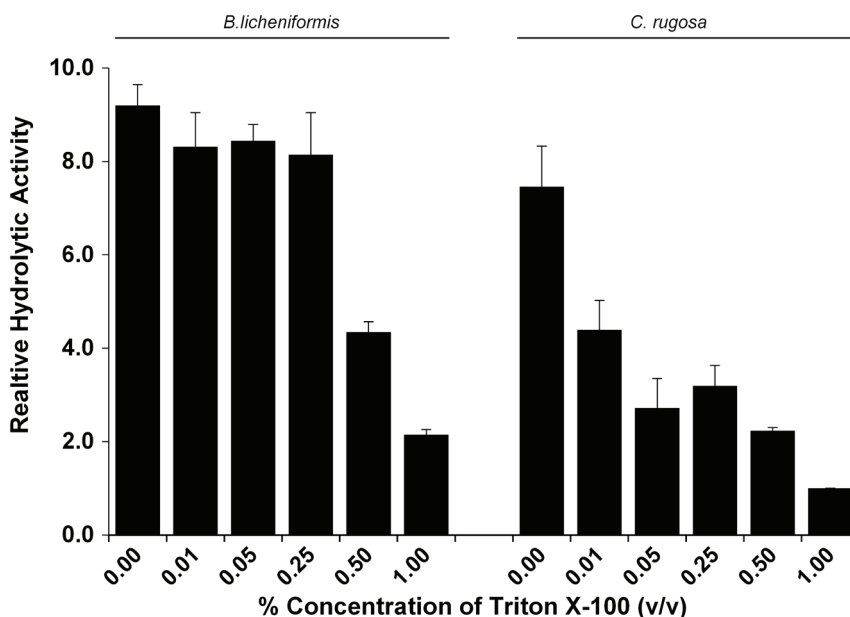


Figure 6. Hydrolytic activities of YpmR enzyme synthesized in *E. coli* JM107 strain and *C. rugosa* lipase at different temperature on pNPL substrate. The experiments were carried out using the cell lysate and 15 ng (30 μ l) of *C. rugosa* lipase enzyme at different temperatures as per the values on the figure in Tris-CaCl₂ buffer at pH 7. Results are presented in terms of mean \pm SD (n = 3).

DISCUSSION

Hydrolytic enzymes such as esterases (E.C. 3.1.1.1) and lipases (E.C. 3.1.1.3) are very important enzymes for biotechnological applications. Lipases preferentially hydrolyse insoluble triglycerides while esterases hydrolyse water-soluble esters (22). These enzymes are frequently used as biocatalysts in industrial fields such as the food industry, the detergent industry, and alternative energy production. As a result, hydrolytic enzymes that are active in extreme conditions are of great importance. In this study, the hydrolytic activity of YpmR enzyme of a moderately halophilic bacteria *B. licheniformis* was investigated. Based on *B. licheniformis* ATCC 14580 genome analysis, the hypothetically defined YpmR protein was identified as member of the SGNH hydrolase superfamily (<https://www.ncbi.nlm.nih.gov/protein/52003893>). However, there is no concrete data regarding its hydrolytic activity. Therefore, in order to determine the hydrolytic activity of *B. licheniformis* YpmR hypothetical enzyme, the gene was cloned in bacterial expression vectors and subsequently synthesized as a recombinant protein into *E. coli* cells. The synthesis of YpmR protein in the transformed cells was demonstrated by SDS-PAGE analyses (Figure 1). The hydrolytic activities of cell lysates containing the YpmR protein were tested using pNPL and pNPA substrates. Interestingly, from the experiments to determine the esterase group enzymatic activities using the pNPA substrate (23-26), high levels of hydrolytic activities were detected in both the plasmid transformed bacterial cell lysates and the untransformed cell lysate used as a negative control. As a standard control used in this study, *Candida rugosa* lipase enzyme showed no enzymatic activity against pNPA substrate. Therefore, the high activity detected in the transformed

cell lysates is most likely due to endogenous esterases. The detection of extracellular esterase activity in *B. licheniformis* has also been reported in other studies (27-29). In contrast, the enzymatic activity experiments using pNPL as the substrate have detected hydrolytic activity in the YpmR expressing cell lysates, while very low levels of activity were measured in non-transformed cell lysates (Figure 2). While the *C. rugosa* lipase has no effect on pNPA substrate, it has shown to have hydrolytic effect on pNPL substrate. Therefore, like other true lipase enzymes, the experimental results obtained in this study show that the hypothetical *B. licheniformis* YpmR enzyme has hydrolytic activity on pNPL substrate indicating high preference for medium and long chain triglycerols substrates. This result corroborates with other studies (30-33).

The ability of enzymes to preserve their structural properties and enzymatic activities in different environmental conditions particularly increases their industrial importance (34). The stability of the YpmR enzyme synthesized in *E. coli* cells was tested at different pH values, salt (NaCl) concentrations, temperatures and in the presence of a non-ionic detergent Triton X-100. Based on the test results, the pH range in which YpmR enzyme showed the highest activity was at 7.0 - 9.5, while a 70-80% reduction in the enzyme activity was recorded at pH 6. In comparison to the *C. rugosa* lipase enzyme, it was concluded that the maximum activity of the synthesized YpmR enzyme was slightly more basic (Figure 4). In this respect, the *B. licheniformis* YpmR enzyme can be seen as a little more advantageous for industrial applications. The pH range in which the hypothetical *B. licheniformis* YpmR enzyme remains stable as reported in this study is similar to the pH values reported elsewhere (30,35-37).

One of the most important factors that affects the activities of enzymes is environmental temperatures. In this regard, proteins and enzymes from thermophilic bacteria living in hot springs have much more stable structures and, as a result, have high economic values (38-41). However, enzymes from halophilic bacteria are not expected to withstand very high temperatures. By evaluating the enzymatic activities of the YpmR enzyme containing cell lysates on pNPL substrate at a temperature ranging from 30°C to 55°C, it was revealed that the maximum activity of this enzyme was obtained at a temperature range of 30-45°C with an average of 50% activity reduction at 55°C. The maximum activity was observed for *C. rugosa* lipase used as a control at a temperature range of 45-55°C (Figure 5). This result showed that moderate halophilic *B. licheniformis* YpmR enzyme has a potential application in the detergent industry where the maximum temperature for most reactions is below 60°C. The impact of temperature on the enzyme activity of the recombinant *B. licheniformis* YpmR reported in our study corroborates with that of Selvin *et al.* 2012 and Annamalai *et al.* 2011 (30,36).

The maintenance of enzymatic activity at high salt concentrations by enzymes is of great importance in industrial applications. For this reason, many studies have been conducted on lipase enzymes from diverse halophilic organisms (42,43). Lipase enzymes isolated from many halophilic bacteria have exhibited the ability to withstand high salt concentrations (44). The *B. licheniformis* YpmR enzyme synthesized in *E. coli* cells have shown maximum activity using pNPL substrate at 0.5 M NaCl concentration. When compared to *C. rugosa* lipase enzyme, the YpmR enzyme was found to be more tolerant to high salt concentrations (Figure 3). Similar results of salt tolerant lipase enzymes have been recorded elsewhere (30,31,35).

The enzymatic activity of the YpmR enzyme on pNPL substrate was also tested in the presence of a non-ionic detergent, Triton X-100. The test results showed that the *B. licheniformis* YpmR enzyme retains its enzymatic activity in media containing about 0.01 to 0.25% Triton X-100. However, even in very low concentrations such as 0.05% Triton X-100 medium, the enzymatic activity of *C. rugosa* lipase enzyme, on average decreased by 60-70% (Figure 6). These data have highlighted the potential applicability of *B. licheniformis* YpmR enzyme as an additive in detergents. Reports about the stability of other *Bacillus* lipases in the presence of nonionic surfactants like Triton X-100 have been documented by other studies (31,33,35,45).

CONCLUSION

The moderate halophilic *B. licheniformis* hypothetical YpmR enzyme heterologously synthesized in *E. coli* cells has hydrolytic activity on pNPL substrate. The enzyme was observed to be more tolerant to an increase in NaCl and Triton X-100 concentrations compared to the *C. rugosa* lipase enzyme used as a control and showed potential for application in the detergent industry. Therefore, further purification and characterization of this promising hypothetical enzyme are important for future research goals.

Peer-review: Externally peer-reviewed.

Author Contributions: Conception/Design of study: A.O.T., A.O., K.T.; Data Acquisition: A.O.T., A.O., K.T.; Data Analysis/Interpretation: A.O.T., A.O., K.T.; Drafting Manuscript: A.O.T., A.O., K.T.; Critical Revision of Manuscript: A.O.T., A.O., K.T.; Final Approval and Accountability: A.O.T., A.O., K.T.; Technical or Material Support: A.O.T., A.O., K.T.; Supervision: A.O.T., A.O., K.T.

Conflict of Interest: The authors declare that they have no conflicts of interest to disclose.

Financial Disclosure: This work was supported by a grant from the Marmara University Research Foundation. Grant no: FEN-C-YLP-131216-0550

Acknowledgements: The authors would like to thank Dr. Meral Birbir for providing us with the *B. licheniformis* strain.

REFERENCES

1. Bornscheuer UT. Microbial carboxyl esterases: classification, properties and application in biocatalysis. *FEMS Microbiol Rev* 2002; 26: 73-81.
2. Bae SY, Ryu BH, Jang E, Kim S, Kim TD. Characterization and immobilization of a novel SGNH hydrolase (Est24) from *Sinorhizobium meliloti*. *Appl Microbiol Biotechnol* 2013; 97: 1637-47.
3. Casas-Godoy L, Duquesne S, Bordes F, Sandoval G, Marty A. Lipases: an overview. *Methods Mol Biol* 2012; 861: 3-30.
4. Sharma S, Kanwar SS: Organic solvent tolerant lipases and applications. *Scientific World Journal* 2014; 2014: 625258.
5. Akoh CC, Lee GC, Liaw YC, Huang TH, Shaw JF. GDSL family of serine esterases/lipases. *Prog Lipid Res* 2004; 43: 534-52.
6. Holmquist M. Alpha Beta-Hydrolase Fold Enzymes Structures, Functions and Mechanisms. *Curr Protein Pept Sc* 2005; 1: 209-35.
7. Knizewski L, Steczkiewicz K, Kuchta K, et al. Uncharacterized DUF1574 leptospira proteins are SGNH hydrolases. *Cell Cycle* 2008; 7: 542-44.
8. Wang J, Zhang H, Wang F, et al. Enzyme-responsive polymers for drug delivery and molecular imaging. Makhlof ASH, Abu-Thabit NY, editors. *In Stimuli Responsive Polymeric Nanocarriers for Drug Delivery Applications*, Woodhead Publishing 2018; V-1.p101-19.
9. Lo YC, Lin SC, Shaw JF, Liaw YC. Crystal structure of *Escherichia coli* thioesterase I/protease I/lysophospholipase L1: consensus sequence blocks constitute the catalytic center of SGNH-hydrolases through a conserved hydrogen bond network. *J Mol Biol* 2003; 330: 539-51.
10. Molgaard A, Kauppinen S, Larsen S. Rhamnolacturonan acetylase elucidates the structure and function of a new family of hydrolases. *Structure* 2000; 8: 373-83.
11. Jaeger KE, Reetz MT. Microbial lipases form versatile tools for biotechnology. *Trends Biotechnol* 1998; 16: 396-403.
12. Borrelli GM, Trono D. Recombinant Lipases and Phospholipases and Their Use as Biocatalysts for Industrial Applications. *Int J Mol Sci* 2015; 16: 20774-20840.
13. Sharma R, Chisti Y, Banerjee UC. Production, purification, characterization, and applications of lipases. *Biotechnol Adv* 2001; 19: 627-62.
14. Hasan F, Shah AA, Hameed A. Industrial applications of microbial lipases. *Enzyme Microb Tech* 2006b; 39: 235-51.

15. Choo DW, Kurihara T, Suzuki T, Soda K, Esaki N. A cold-adapted lipase of an Alaskan psychrotroph, *Pseudomonas* sp. strain B11-1: gene cloning and enzyme purification and characterization. *Appl Environ Microbiol* 1998; 64: 486-91.
16. Herbert RA. A perspective on the biotechnological potential of extremophiles. *Trends Biotechnol* 1992; 10: 395-402.
17. Adamczak M, Krishna SH. Strategies for Improving Enzymes for Efficient Biocatalysis. *Food Technol Biotechnol* 2004; 42: 251-64.
18. Reina JJ, Guerrero C, Heredia A. Isolation, characterization, and localization of AgaSGNH cDNA: a new SGNH-motif plant hydrolase specific to *Agave americana* L. leaf epidermis. *J Exp Bot* 2007; 58: 2717-31.
19. Lu S, Wang J, Chitsaz F, et al. CDD/SPARCLE: the conserved domain database in 2020. *Nucleic Acids Res* 2020; 48: D265-D268.
20. Bradford MM. A rapid and sensitive method for the quantitation of microgram quantities of protein utilizing the principle of protein-dye binding. *Anal Biochem* 1976; 72: 248-54.
21. Wang B, Wang A, Cao Z, Zhu G. Characterization of a novel highly thermostable esterase from the Gram-positive soil bacterium *Streptomyces lividans* TK64. *Biotechnol Appl Biochem* 2016; 63: 334-43.
22. Chahinian H, Sarda L. Distinction between esterases and lipases: comparative biochemical properties of sequence-related carboxylesterases. *Protein Pept Lett* 2009; 16: 1149-61.
23. De Yan H, Zhang YJ, Liu HC, Zheng JY, Wang Z. Influence of ammonium salts on the lipase/esterase activity assay using p-nitrophenyl esters as substrates. *Biotechnol Appl Biochem* 2013; 60: 343-47.
24. Fu C, Hu Y, Xie F, et al. Molecular cloning and characterization of a new cold-active esterase from a deep-sea metagenomic library. *Appl Microbiol Biotechnol* 2011; 90 961-70.
25. Jiang X, Xu X, Huo Y, et al. Identification and characterization of novel esterases from a deep-sea sediment metagenome. *Arch Microbiol* 2012; 194: 207-14.
26. Riedel K, Talker-Huiber D, Givskov M, Schwab H, Eberl L. Identification and characterization of a GDSL esterase gene located proximal to the swr quorum-sensing system of *Serratia liquefaciens* MG1. *Appl Environ Microbiol* 2003; 69: 3901-10.
27. Alvarez-Macarie E, Augier-Magro V, Baratti J. Characterization of a Thermostable Esterase Activity from the Moderate Thermophile *Bacillus licheniformis*. *Biosci Biotechnol Biochem* 1999; 63(11): 1865-70.
28. Torres S, Martínez MA, Pandey A, Castro GR. An organic-solvent-tolerant esterase from thermophilic *Bacillus licheniformis*S-86. *Biore-sour Technol* 2009; 100(2): 896-902.
29. Torres S, Baigori MD, Pandey A, Castro GR. Production and purification of a solvent-resistant esterase from *Bacillus licheniformis* S-86. *Appl Biochem Biotechnol* 2008; 151(2-3): 221-32.
30. Selvin J, Kennedy J, Lejon DPH, Kiran GS, Dobson ADW. Isolation identification and biochemical characterization of a novel halo-tolerant lipase from the metagenome of the marine sponge *Haliclona simulans*. *Microb Cell Fact* 2012; 11(1): 1.
31. Bora L, Bora M. Optimization of extracellular thermophilic highly alkaline lipase from thermophilic bacillus sp isolated from hot spring of Arunachal Pradesh, India. *Brazilian J Microbiol* 2012; 43(1): 30-42.
32. Brabcová J, Zarevucká M, Macková M. Differences in hydrolytic abilities of two crude lipases from *Geotrichum candidum* 4013. *Yeast* 2010; 27: 1029-38.
33. Niyonzima FN, More S. Biochemical properties of the alkaline lipase of *Bacillus flexus* XJU-1 and its detergent compatibility. *Biol* 2014; 69(9): 1108-17.
34. Dumorné K, Córdova DC, Astorga-eló M, Renganathan P. Extremozymes: A Potential Source for Industrial Applications. *J Microbiol Biotechnol* 2017; 27: 649-59.
35. Bora L. Purification and characterization of highly alkaline lipase from *Bacillus licheniformis* MTCC 2465: And study of its detergent compatibility and applicability. *J Surfactants Deterg* 2014; 17(5): 889-98.
36. Gupta S, Sharma P, Dev K, Sourirajan A. Halophilic Bacteria of Lunsu Produce an Array of Industrially Important Enzymes with Salt Tolerant Activity. *Biochem Res Int*. 2016; 2016(1): 1-10.
37. Annamalai N, Elayaraja S, Vijayalakshmi S, Balasubramanian T. Thermostable, alkaline tolerant lipase from *Bacillus licheniformis* using peanut oil cake as a substrate. *African J Biochem Res* 2011; 5(6): 176-81.
38. Fitter J, Haber-Pohlmeier S. Structural stability and unfolding properties of thermostable bacterial alpha-amylases: a comparative study of homologous enzymes. *Biochemistry* 2004; 43: 9589-99.
39. Parvareh F, Vic G, Thomas D, Legoy MD. Uses and potentialities of thermostable enzymes. *Ann NY Acad Sci* 1990; 613: 303-12.
40. Ward OP, Moo-Young M. Thermostable enzymes. *Biotechnol Adv* 1988; 6: 39-69.
41. Chien A, Edgar DB, Trela JM. Deoxyribonucleic acid polymerase from the extreme thermophile *Thermus aquaticus*. *J Bacteriol* 1976; 127: 1550-57.
42. Li X, Yu H-Y. Characterization of a novel extracellular lipase from a halophilic isolate, *Chromohalobacter* sp. LY7-8. *Afr J Microbiol Res* 2012; 6: 3516-22.
43. Esteban-Torres M, Mancheño JM, Rivasa B, Muñoz R. Characterization of a halotolerant lipase from the lactic acid bacteria *Lactobacillus plantarum* useful in food fermentations. *LWT-Food Sci Technol* 2015; 60: 246-52.
44. Ozgen M, Attar A, Elalmis Y, Birbir M, Yucel S. Enzymatic activity of a novel halotolerant lipase from *Haloarcula hispanica* 2TK2. *Polish J Chem Technol* 2016; 18: 20-25.
45. Saraswat R, Verma V, Sistla S, Bhushan I. Evaluation of alkali and thermotolerant lipase from an indigenous isolated *Bacillus* strain for detergent formulation. *Electron J Biotechnol* 2017; 30: 33-8.

Caspase-1: Past and Future of this Major Player in Cell Death and Inflammation

Elif Eren^{1,2} , Nesrin Ozoren^{1,2} 

¹Boğaziçi University, Department of Molecular Biology and Genetics, Apoptosis and Cancer Immunology Laboratory (AKIL), Istanbul, Turkey
²Boğaziçi University, Center for Life Sciences and Technologies Istanbul, Turkey

ORCID IDs of the authors: E.E. 0000-0002-0328-5609; N.O. 0000-0002-8580-618X

Please cite this article as: Eren E, Ozoren N. Caspase-1: Past and Future of this Major Player in Cell Death and Inflammation. Eur J Biol 2020; 79(1): 51-61. DOI: 10.26650/EurJBiol.2020.0038

ABSTRACT

Inflammation is a major physiological process required for the detection of pathogens and their elimination from an organism. It is triggered by the innate immune system that gets activated through the recognition of danger- or pathogen-associated molecular patterns by protein complexes called inflammasomes. The activation of inflammasomes does not only eliminate the replicative niche of pathogens by inducing infected cells' death (called pyroptosis) but also leads to the secretion of pro-inflammatory cytokines such as Interleukin-1 β (IL-1 β) and IL-18, which in turn triggers the recruitment of other immune cells to the infection site and mediates communication with neighboring resident cells. The cysteine aspartate protease Caspase-1 is the common effector enzyme of different inflammasomes and is responsible for the maturation of Gasdermin D and IL-1 β required for the induction of pyroptosis and the secretion of IL-1 β through the Gasdermin D pores. Several gain of function mutations in inflammasome forming receptor proteins including Caspase-1 were associated with severe auto-immune and auto-inflammatory diseases pointing out the necessity of the tight regulation of these complexes. In this review, we focused on Caspase-1 that is at the crossroad of inflammatory cell death and IL-1 β secretion. We describe its discovery, Caspase-1 activator signals, its substrates and the inhibitors that have been designed. We also discuss ongoing research that reveals novel unexpected roles for this protease. This review is a good reference not only for the beginners in innate immunity and inflammation but also provides an update on Caspase-1's biology for more advanced researchers.

Keywords: Caspase-1, inflammasomes, pyroptosis, interleukin-1, Gasdermin D

INTRODUCTION

Inflammation is an important physiological process triggered by tissue injury of endogenous or exogenous origin and is characterized by redness, heat, swelling and pain (1). It involves the cooperation of endothelial cells forming the blood vessels and different immune cell types that secrete several critical cytokines [Interleukin-1 (IL-1) family members IL-1 β , IL-18; Tumor necrosis factor alpha (TNF α); IL-6], chemokines (IL-8) and lipids (prostaglandin) (2). Among these different signaling molecules released in the extracellular milieu, IL-1 β is involved in the induction of fever and its over-secretion is associated with many pro-inflammatory disorders

(3). Interestingly, unlike other mediators, IL-1 family members IL-1 β and IL-18 are synthesized as precursors that lack a signal sequence triggering their secretion through the conventional endoplasmic reticulum/ Golgi pathway (4). Instead, the maturation of pro-IL-1 β and pro-IL-18 in the cytosol through their proteolytic cleavage by Caspase-1 is required for their secretion (4). Although the secretion pathways are not fully understood, the mechanisms that activate Caspase-1 have been characterized in the last fifteen years (5).

Synthesized as an inactive precursor itself, Caspase-1 is recruited to multiprotein complexes called inflammasomes formed by a receptor protein and the adaptor



Corresponding Author: Nesrin Özören

E-mail: nesrin.ozoren@boun.edu.tr

Submitted: 06.11.2019 • **Revision Requested:** 06.12.2019 • **Last Revision Received:** 11.02.2020 • **Accepted:** 16.03.2020

© Copyright 2020 by The Istanbul University Faculty of Science • Available online at <http://ejb.istanbul.edu.tr> • DOI: 10.26650/EurJBiol.2020.0038

ASC (6). Different types of inflammasomes able to sense diverse danger and pathogen-associated molecules assemble and trigger pro-Caspase-1 cleavage into mature and active Caspase-1. Activation of Caspase-1 results in two major outcomes: the induction of an inflammatory cell death called pyroptosis by the cleavage of the Gasdermin D protein and the processing of pro-IL-1 β into mature IL-1 β that will be secreted from the cell through Gasdermin D pores and will mediate inflammation (7-9). Because over-activation of these complexes results in IL-1-dependent auto-inflammatory diseases, the development of inhibitors for inflammasome components and their usage in the cure of these diseases are hot topics in the field (10). This review focuses on Caspase-1 as a central player in the initiation of the immune response and mounting of the first line of immune defenses.

Caspases are proteases synthesized as zymogens with an N-terminal pro-domain that is removed by proteolytic cleavage when they get activated (11). The human Caspase family contains 12 fully characterized members (Caspase-1 to 10, Caspase-12 and Caspase-14) that can be classified into three groups according to their principal functions: inflammation, apoptosis and differentiation (Figure 1). Inflammatory Caspases family consists of Caspase-1, -4, -5 (Caspase-11 in mouse) and -12 (11-13). Apoptotic Caspases are involved in either intrinsic (mitochondria-dependent) or extrinsic (through the induction of death receptors such as Fas or Trail) pathways of apoptosis (14). While some of them initiate the apoptotic signaling cascade (Caspase-2, -9, 8, -10), others are responsible for the cleavage of substrates that mediate apop-

totic cell death (Caspase-3, -6 and -7) (Figure 1). Caspase-14, on the other hand, gets activated during the terminal differentiation of keratinocytes and protects the skin against UVB radiations (15).

Caspase-1, the founder protein of the Caspase family involved in the maturation of the main inflammation mediator IL-1 β , is conserved between various species from human to *Drosophila* (Figure 2) and is ubiquitously expressed in various cell types and tissues including immune cells such as macrophages, neutrophils and dendritic cells; cells of the nervous system, epithelial cells and intestinal cells (16). Among the other pro-inflammatory Caspases, Caspase-4, Caspase-5 and their murine homolog Caspase-11 are both receptors and effectors of the non-canonical inflammatory pathway (7). Caspase-4 and Caspase-11 directly bind a bacterial wall component - the lipopolysaccharide (LPS) - and induce cell death that in turn triggers the induction of the canonical NLRP3 pathway and leads to Caspase-1 and IL-1 β activation (7). Although the non-canonical pathway is well characterized in mice, the mechanism is less understood in humans. Caspase-5 that is a gene duplication of Caspase-4, is only expressed in humans and is not implicated in the maturation of Caspase-1 and IL-1 β (17). The exact role of Caspase-5 is still under investigation.

Caspase-12, the last member of the inflammatory Caspases (Figure 2), has acquired a polymorphism resulting in the expression of a short protein only containing the pro-domain. A catalytically inactive long form resulting from T125C polymorphism is found in African populations giving them susceptibility to

				Accession (human)	Total aa number	
Inflammatory Caspases	Caspase-1	CARD	p20 p10	NP_150634	404 aa	
	Caspase-4	CARD	Large Small	NP_001216	377 aa	
	Caspase-5	CARD	Large Small	NP_001129584	447 aa	
	Caspase-12- S	CARD	—		125 aa	
	Caspase-12- L		p20 p10	NP_001177945	341 aa	
Apoptotic Caspases	Initiators	Caspase-2	CARD	p18 p13	NP_116764	452 aa
		Caspase-9	CARD	p20 p10	NP_001220	416 aa
		Caspase-8	DED DED	p18 p10	NP_001073594	538 aa
		Caspase-10	DED DED	Large Small	NP_116759	522 aa
	Effectors	Caspase-3		p17 p12	NP_004337	277 aa
		Caspase-6		p18 p11	NP_001217	293 aa
		Caspase-7		p20 p11	NP_001218	303 aa
Differentiation	Caspase-14		p17 p11	NP_036246	242 aa	

Figure 1. Functional classification and structure of Caspases.

certain infection (Figure 1) (13,18). Whereas murine Caspase-12 induces ER-dependent apoptosis in response to amyloid β stimulation, human Caspase-12 displays an anti-inflammatory role through the inhibition of NF κ B pathway (13,19).

Taking into consideration the importance of inflammation in the immune response and the fact that all substrates and activator pathways are not yet fully understood, we will, in this review, focus on the founder of the Caspase family, the Caspase-1 protein by surveying its discovery, the available mouse models, the established and emerging cellular functions, the molecular mechanisms of its activation, the associated diseases and designed inhibitors.

DISCOVERY of CASPASE-1 and GENERATION of CASPASE-1 KNOCKOUT MICE

Caspase-1 was discovered following extensive research conducted to identify the enzyme responsible for the maturation of IL-1 β , an important cytokine mediator of inflammation and implicated in many pathologies. The 31 kDa precursor pro-IL-1 β protein was found to be cleaved into its 17 kDa active form after the Asp116 when incubated with the cytosolic extract of human monocytes. This enzyme was called ICE for interleukin converting enzyme (20,21). ICE was synthesized as a 45 kDa inactive protein and two subunits: p20 (19,866 kDa) and p10 (10,248 kDa) were mediating its catalytic activity (22,23). Because of the presence of a catalytically essential cysteine residue in the p20 subunit of ICE and the requirement of an Aspartate in the substrate for the cleavage, ICE was nominated as “Caspase-1” for Cysteine Aspartate Protease (20,22,24).

Caspase-1 knockout mice were generated through the insertion of a neomycin selection cassette into the sixth exon of *Caspase-1* gene encoding for the active site of the enzyme resulting in the synthesis of truncated and non-functional Caspase-1 protein lacking residues important for substrate recognition and catalysis. Caspase-1 knockout (KO) mice developed normally, were fertile and contrary to expectations at that time, Caspase-1 absence had no effect on apoptosis but presented reduced IL-1 β and IL-1 α secretions in response to ATP or Nigericin stimulations (25,26). While two independently generated Caspase-1 KO mice were used to elucidate Caspase-1’s functions for years, an important publication showed that the 129S mouse strain used to generate Caspase-1 KO mice also contains a splicing mutation in the *Caspase-11* gene that leads to the synthesis of a truncated and inactive Caspase-11 protein (Caspase-11 Δ 110; 12). Thus, the previously generated Caspase-1 KO mice by using 129S mouse strain were Caspase-1/11 double KO (dKO) mice (12). These findings led to a series of experiments that elucidated the exact role of Caspase-1 that will be presented below.

CASPASE-1 ACTIVATORY PATHWAYS

Caspase-1 is synthesized as an inactive pro-Caspase-1 enzyme and is cleaved into biologically active Caspase-1 in response to different inflammatory stimuli. Caspase-1 can be activated directly by canonical inflammasomes or indirectly following the induction of the non-canonical Caspase-11 inflammasome.

Among the canonical inflammasomes, the NLRP1 inflammasome assembles in response to anthrax lethal toxin that directly activates NLRP1b through cleavage and triggers Caspase-1

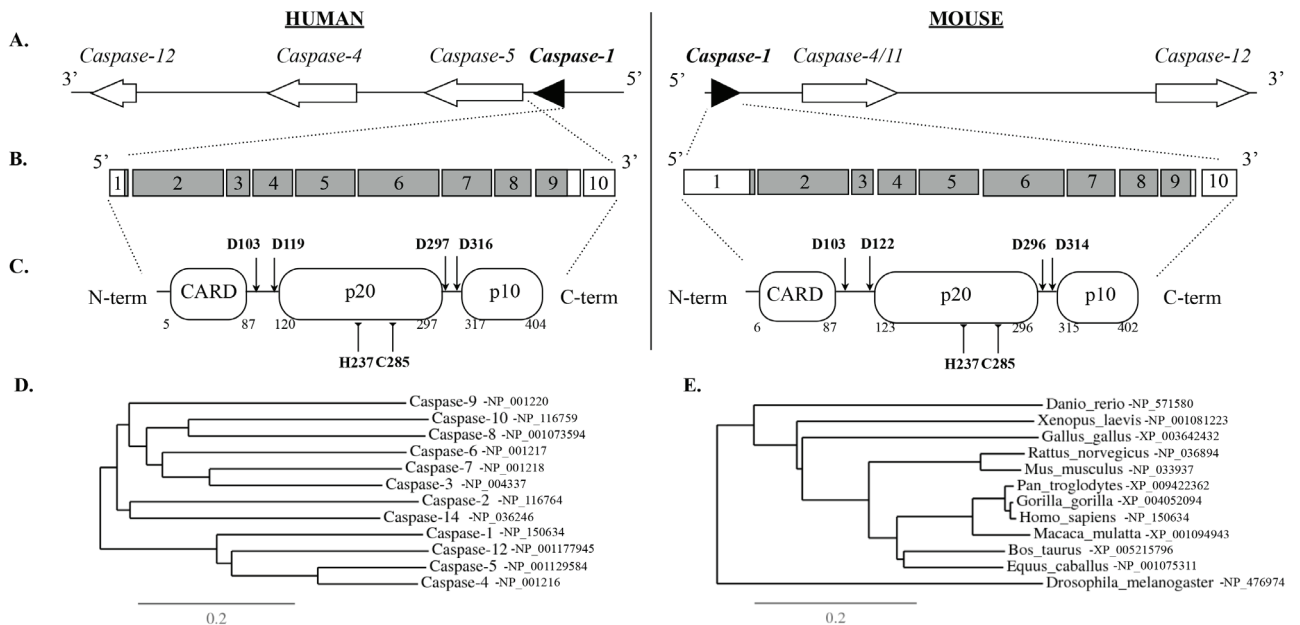


Figure 2. Genomic structure and phylogenetic analysis of Caspase-1. A. Organization of the locus encoding different inflammatory Caspases. B. Exons of Caspase-1. C. Structure and critical amino acids of Caspase-1. D,E. Phylogenetic analysis of different caspases in human (D) and mouse (E).

maturation (27). The widely studied NLRP3 inflammasome is activated in response to MSU crystals, synthetic bacterial RNA and small components, bacterial toxins and ATP and *Listeria monocytogenes* infections (28-31). Caspase-1 is also directly interacting with NLRC4/IPAF protein. NLRC4/IPAF has CARD, NACHT and LRR domains and interacts with pro-Caspase-1 through its CARD domain (32). *Pseudomonas aeruginosa* stimulation assembles the NLRC4/IPAF inflammasome and activates pro-Caspase-1 (33). Finally the pyrin and HIN domain-containing protein AIM2 also formed an inflammasome and activated Caspase-1 after cytoplasmic DNA sensing (34,35). Moreover, Caspase-1 is also the effector Caspase of the NLRP7 inflammasome activated in response to microbial lipopeptides stimulations and the NLRP2 in the central nervous system through ATP induction (36,37).

The non-canonical Caspase-11 inflammasome also activates Caspase-1 but through an indirect mechanism. Cytosolic Caspase-11 recognizes lipopolysaccharide (or LPS) that is a structural component of Gram-negative bacteria such as *Salmonella typhimurium* or *Pseudomonas aeruginosa* (38,39). Active Caspase-11 cleaves Gasdermin D that forms pores into the plasma membrane and induces pyroptosis (7). Changes in ionic fluxes in the pyroptosis-undergoing cells are sensed by the NLRP3 inflammasome that gets activated and induce the processing of Caspase-1 (40). Direct processing of Caspase-1 by Caspase-11 was also proposed but needs further confirmation (41).

Caspase-1 was also described to be activated in response to apoptosis inducing stimuli. Apoptosis was first described in *C. elegans* and is mediated by the Ced-3 protein (42). Because Caspase-1's sequence was highly similar to Ced-3 and overexpression of Caspase-1 in cells induced death, Caspase-1 was considered as an inducer of apoptosis (43). The role of Caspase-1 in apoptosis was further confirmed by the finding that the stimulation of thymocytes isolated from Caspase-1 KO mice with Fas ligand did not undergo apoptosis (26). Similarly, overexpression of Caspase-1 induced apoptosis in response to Fas stimulation in colon cancer cell lines (44). Indeed, overexpression of Caspase-1 triggers apoptosis in prostate cancer cell lines in response to ionizing radiation (45). Caspase-1 also induces cell death in human neurons by proteolytic cleavage of its target Caspase-6, an effector apoptotic Caspase (46). Moreover, Caspase-1 is implicated in *Yersinia pseudotuberculosis* induced apoptosis and is directly processed by Caspase-8 after the infection (47). Besides its intracellular apoptotic function, Caspase-1 is also present in microvesicles secreted outside the cell and the treatment of lymphocytes with these Caspase-1 charged vesicles induces apoptosis (48). However, since pyroptosis was only defined in late 2000s and the only programmed cell death was considered to be apoptosis, this data has to be taken with caution and need verifications. Nonetheless, recent evidences suggest that in the absence of Gasdermin D, Caspase-1-dependent cell death followed by Caspase-3 and Caspase-9 activation can be induced in response to classical inflammasome-activator stimuli (49). These findings need to be further characterized.

MOLECULAR MECHANISM of CASPASE-1 ACTIVATION

Caspase-1 is synthesized as a 45 kDa precursor pro-Caspase-1 formed by a CARD domain, p20 and p10 subunits that is activated by auto-processing in response to stimulations. Pro-Caspase-1 is cleaved at Asp103, Asp119, Asp297 and Asp316 sites and the N-terminal CARD domain is released to generate p20 and p10 subunits (22) (Figure 2). *In vitro* studies demonstrate that oligomerization of pro-Caspase-1 is required prior to the self-cleavage (50). Overexpression of the p45 precursor or CARD domain lacking p30 peptide formed by p20 and p10 subunits is sufficient to induce the processing of Caspase-1 into p20 and p10 active subunits suggesting that Caspase-1 is activated by auto-processing (50) and that bringing pro-Caspases in close proximity is enough to activate the enzyme (induced proximity model). Solving the Caspase-1 crystal structure revealed that active Caspase-1 forms a tetramer constituted by a central dimer of p10 subunits and two surrounding p20 subunits (51).

The ASC protein that is formed by PYRIN and CARD domains acts as an adaptor between Caspase-1 and receptors lacking a CARD domain (52). Upon inflammasome activation, ASC and pro-Caspase-1 directly interact with each other through homotypic CARD/CARD interactions forming multimeric scaffolds, called foci or specks (52). ASC speck brings pro-Caspases-1 into close proximity and promotes their cleavage by induced proximity (52). While transfection of ASC CARD domains alone or PYRIN domains alone cannot form specks, foci formation is triggered by full length ASC or by co-transfection of ASC CARD and Caspase-1 CARD (53).

The Death Domain family is known to form filamentous structures. While overexpression of full-length ASC forms specks, overexpression of PYRIN or CARD domains alone results in filamentous structures. In our laboratory, we proposed by mutational analyses that ASC protein aggregation occurs at two levels: first of all, filament formation is induced, and these filaments compact further to form specks (54).

In conclusion, ASC and Caspase-1 oligomerize with themselves through respectively PYRIN/PYRIN and CARD/CARD domains and are maintained in an inactive state (55,56). Upon stimulation, ASC gets activated by transient PYRIN/PYRIN interactions with NLRP proteins and forms specks by recruiting Caspase-1 proteins through the interaction of its CARD domain with Caspase-1's CARD and activates Caspase-1 cleavage by induced proximity (55). We also showed in a recently published paper that ASC speck formation could be disrupted by CARD containing NLR proteins such as NLRC3 (57).

Caspase-1 activates its substrates by cleavage at a specific aspartate residue. Alignment of known Caspase-1's target proteins and *in vitro* studies with inhibitory peptides revealed that the preferential cleavage site of Caspase-1 is the "WEHD" amino acid sequence (58). Arg179 and Gln283 residues of p20 subunits and Arg341 of p10 subunit of Caspase-1 recognize WEHD sequence and cleaves after the aspartate on the target sequence

(59). Crystallography of Caspase-1 with Ac-YVAD-CHO inhibitor and mutant analyses showed that Caspase-1's catalytic site is formed by both p20 and p10 subunits (51,59). The Cysteine in the active site is the Cys285 and has an adjacent His237 and these two residues are responsible for catalysis (59).

SUBSTRATES of CASPASE-1

Once it gets activated, Caspase-1 is responsible for the cleavage of pro-inflammatory cytokines IL-1 β , IL-18 and IL-33; the pyroptosis mediating pore forming protein Gasdermin D; MyD88 adaptor-like protein Mal and the inflammasome forming Pyrin protein.

Pro-IL-1 β is the first substrate that led to the discovery of Caspase-1 (21,60). TLR receptor stimulation activates the NF κ B pathway and induces the synthesis of pro-IL-1 β . Pro-IL-1 β is a 31 kDa precursor and is processed at Asp116 into its mature 17 kDa form by Caspase-1 and gets secreted from the cell to initiate inflammation. The second pro-inflammatory cytokine pro-IL-18 is identified as an 18 kDa IFN- γ inducing factor (or IGIF) and is cleaved by Caspase-1 at Asp35 residue in response to inflammasome activation (61). Mature IL-18 is secreted from activated cells and together with IL-12 induces the production and secretion of IFN- γ from neighboring cells (62).

Identification of Gasdermin D as a substrate of Caspase-1 was an important milestone in the inflammasome research field. Although it was clear that a programmed cell death distinct from apoptosis and depending on Caspase-1 was triggered, it is only in 2014 that pro-Gasdermin D protein was characterized as the substrate of Caspase-1. N-terminal domain of Gasdermin D was released from the inhibitory C-terminal domain and formed pores at the plasma membrane of the cells. These Gasdermin D pores not only formed conduits for IL-1 β secretion but also induced pyroptosis (9,63).

Another Caspase-1 target is IL-33. While full-length IL-33 is biologically active and promotes pro-inflammatory cytokines secretion to alert the immune system, processing of IL-33 at Asp178 by Caspase-1 produces an inactive product and inhibits inflammation (64). Besides the regulation of cytokines, Caspase-1 also modulates the NF κ B pathway. Caspase-1 processes Pyrin protein between residues Asp330 and Ser331 and the cleaved 30 kDa Pyrin translocates into the nucleus and activates the NF κ B pathway. Mutations of the *MEFV* gene encoding Pyrin is associated with Familial Mediterranean Fever (FMF). Mutant Pyrin proteins are more susceptible to Caspase-1 cleavage and cause the aberrant inflammatory cytokine secretion observed in patients (65). MyD88-adaptor like Mal protein is another target of Caspase-1. Mal is involved in the activation of NF κ B upon TLR4 and TLR2 stimulations. Whereas full-length Mal is inactive, Caspase-1 cleaved Mal induces the NF κ B pathway. Caspase-1 cleaves Mal at Asp198 and generates an active 21 kDa peptide (66).

Proteomic screen of Caspase-1's substrate revealed that the apoptotic effector Caspase-7 is a Caspase-1 target. Upon

Salmonella infection or LPS and ATP treatment of macrophages, Caspase-1 cleaves Caspase-7 at two sites: Asp23 and Asp198. Caspase-1 is required for Caspase-7 activation in response to *Salmonella* infection since Caspase-7 is not activated in Caspase-1 KO macrophages (67). Caspase-6 is another protein regulated by Caspase-1. Caspase-6 is expressed in neuronal cells and induces apoptosis in response to serum starvation. Caspase-1 was shown to be the upstream regulator of Caspase-6. Caspase-1 activated Caspase-6 by proteolytic cleavage and triggers cell death. Caspase-1 inhibition or depletion prevents Caspase-6 activation (46).

CASPASE-1 IN HUMAN DISEASES

A number of physiologically occurring *Caspase-1* variations were identified in patients with auto-inflammatory diseases and suffering from different types of cancer, but no association was established between these variations and the disease phenotype (Table 1). Indeed, the screen of tumors for *Caspase-1* mutations did not reveal any variations (Table 1).

Only neurological and cardiovascular diseases were associated with some *Caspase-1* polymorphisms. In a screen of elderly persons, rs554344 (10643C allele) and rs580253 (5352A allele) were shown to correlate with low IL-1 β levels in the LPS-stimulated blood of carriers and with improvement of their memory performance (68). Thus, polymorphisms decreasing Caspase-1's activity and resulting in lower IL-1 β levels had a protective effect on neurological functions.

The G+7/in6A polymorphism (also called Aⁱⁿ⁶) was significantly more represented in controls compared to patients with myocardial infarctus or with a history of cardiovascular disease. Carriers of Aⁱⁿ⁶ variation had a lower level of IL-18 in the circulating blood compared to the non-carriers. Moreover, Aⁱⁿ⁶ polymorphism resulted in a decrease of Caspase-1's mRNA levels *in vitro* (69). Thus, Aⁱⁿ⁶ has a protective effect on cardiovascular diseases by decreasing Caspase-1 levels and lowering IL-18 secretions. Taken together, these data suggest a deleterious role of Caspase-1 induced excessive IL-1 β and IL-18 secretion in neurological and cardiovascular diseases.

Caspase-1 p.N263S (rs 139695105), p.K319R (rs1751523) and p.R240Q (rs45617533) polymorphisms were identified in patients with auto-inflammatory diseases and decreased both the enzyme's activity and IL-1 β secretion *in vitro*. Crystal structure analysis showed that these variants affect the formation of H-bonds between the subunits of Caspase-1 dimers and destabilized the stability of the enzyme in high temperatures. Moreover, patients with homozygote R240Q polymorphism had a decrease in IL-1 β secretions compared to wild-type controls (70).

Deregulation of Caspase-1's functions had also an impact on different human pathologies (Table 2). Caspase-1's inflammatory activity negatively correlates with neurological disorders such as Huntington's disease, Amyotrophic Lateral Sclerosis and with cerebral ischemic injury. Knock-in of the dominant

Table 1. Caspase-1's variations and association with diseases.

Disease	Identified variations	Phenotype	References
Auto-inflammatory	p.N263S, p.K319R and p.R240Q	Decrease in Caspase-1 activation and IL-1 β cleavage <i>in vitro</i> ; R240Q has an effect on IL-1 β secretion <i>in vivo</i> .	70
Gastric cancer	p.M345K and IV2-3C>A	Unknown.	71
	No mutation identified	Screen for <i>Caspase-1</i> mutations.	72
Prostate cancer	No mutation identified	Decrease in Caspase-1 levels in tissues. Screen for <i>Caspase-1</i> mutations.	73,74
All types of cancer	rs501192	No difference between patient and healthy groups.	75
Age-related cognitive functions	rs554344 and rs580253 (A allele)	Decrease in IL-1 β secretion, better cognitive function.	68
	rs488992 and rs1977989	No effect on IL-1 β secretion, no correlation with cognitive function.	
Alzheimer's disease	rs501192, rs556205 and rs530537	No difference between patient and healthy groups.	76
Cardiovascular disease	A ⁱⁿ⁶	Decrease in Caspase-1 mRNA <i>in vitro</i> . Less IL-18 secretion in the patient sera.	69

negative C285G Caspase-1 protein caused the regression of Huntington's disease whereas inhibition of Caspase-1 by zVAD-fmk had a protective effect on the SOD mutant mice model of ALS (77,78). Indeed, expression of dominant negative Caspase-1 or injection of Caspase-1 inhibitors resulted in a decrease in IL-1 β levels in the injured brain, inhibited cell death and rescued the normal phenotype in a mouse model of transient ischemia (79-81).

Caspase-1 is also implicated in different types of cancer and acts as a pro- or anti- tumorigenic protein depending on which pathway it activates (inflammation or cell death respectively). Caspase-1 exerted an anti-tumorigenic effect through the induction of apoptosis in LNCaP prostate cancer lines upon TGF- β stimulation or in DU-145 prostate cancer cell lines upon irradiation (82). Caspase-1 had a tumor suppressor effect in a model of azoxymethane dextran sodium sulfate colitis-associated colorectal cancer in cooperation with NLR4, which is known to induce a p53-dependent apoptosis (83). Finally, Caspase-1's expression is regulated by the tumor suppressor p63 and low Caspase-1 levels correlate with a mild cancer phenotype (84).

In contrast, Caspase-1 has a pro-tumorigenic impact by inducing inflammation. Caspase-1 was activated in hepatocellular carcinoma cell lines under hypoxic conditions through the HMGB1/TLR4/RAGE pathways and promoted metastasis and invasion of these cells (85). Caspase-1 was also implicated in leukemia by promoting acute myeloid leukemia cell lines' prolifera-

tion through IL-1 β secretion (86). The proteins forming different inflammasomes NLRP3, AIM2 and NLRP1 were associated with colorectal, and skin cancers respectively (87-89).

As an essential protein of inflammasomes and a regulator of the inflammation mediator IL-1 β , Caspase-1 deregulation was associated with different inflammatory diseases. Cryopyrin-associated periodic syndromes or CAPS are characterized by the presence of mutations in the *NLRP3* gene leading to the over-activation of NLRP3 inflammasome, thus Caspase-1 is activated and induces IL-1 β secretion constitutively (90). *NLRP3* mutations were also found to cause increased IL-1 β secretion in FMF and Behcet's disease (91,92). Similarly, Caspase-1 also has an impact on arthritis since its depletion declined IL-1 β levels in joint and ameliorate the disease phenotype in a mouse model of chronic arthritis (93). Caspase-1 also plays a role in endometriosis. Examination of the peritoneal fluid of infertile women showed that IL-1 β and Caspase-1 levels are higher compared to unaffected controls and correlate with the severity of the diseases (94).

Caspase-1 is also implicated in metabolic pathologies such as diabetes or obesity. In retinal diabetes, in the presence of high glucose concentrations, Caspase-1 gets activated and an increase in IL-1 β levels was observed together with degeneration of retinal capillaries (95). An absence of Caspase-1 also caused diabetes and obesity in male mice with a high fat diet because IL-18 could not be activated and active IL-18 deficiency led to insulin resistance (96).

Table 2. Diseases influenced by deregulation of Caspase-1's functions.

Disease	Induced Genetic Alterations	Phenotype	References
Huntington's disease	Dominant negative Caspase-1 (C285G) Knock-In.	Delay of disease progression and mortality in mice.	77
Amyotrophic Lateral Sclerosis	Caspase-1 inhibition by zVAD-fmk.	Protective effect.	78
Cerebral ischemic injury	Dominant negative Caspase-1 (C285G) Knock-In.	Decline of IL-1 β levels. Resistance to trophic factors.	79,80
	Caspase-1 inhibition by zVAD-fmk and others.	Increase in tumor size through induced cell proliferation.	81
Colon cancer	Caspase-1 KO mice	Increase in tumor size through induced cell proliferation.	83
Leukemia	Caspase-1 inhibition.	Suppression of leukemia cell lines' growth.	71
Hepatocellular carcinoma	Caspase-1 activation during hypoxia through HMGB1-TLR4 signaling.	Promotes metastasis and invasion of hypoxic HCC or Hepa cell lines.	70
Prostate cancer	Overexpression of TGF- β in prostate cancer lines.	Caspase-1 activation and apoptosis induction.	82
CAPS, FMF and Behcet's disease	NLRP3 mutations.	Overactive Caspase-1 and enhanced IL-1 β secretion.	72-74
Arthritis	Caspase-1 KO mice	Caspase-1 KO inhibits chronic arthritis.	75
Diabetes	Caspase-1 inhibition by minocycline.	Prevents capillarity degeneration induced by diabetes.	77
Obesity	Caspase-1 KO.	Lack of IL-18 cause obesity in male.	78

CASPASE-1 INHIBITORS

As Caspase-1 is an important player in the crossroad of inflammation and cell death and is implicated in various diseases, Caspase-1 inhibitors were identified and designed early after its discovery. The cowpox virus expresses Cytokine Response Modifier A (CrmA) protein that inhibits Caspase-1-induced inflammation to escape the clearance of the infected cell by the host immune system (97). CrmA directly binds Caspase-1's active site through its "LVAD" sequence, forms a stable complex with the p20 subunit and prevents the IL-1 β maturation. Caspases -8 and -6 are also inhibited by CrmA (98). Similarly, p35 forms an irreversible inhibitory complex with Caspase-1 and prevents IL-1 β maturation *in vitro* (99). p35 also inhibits Caspases -1, -3, -6, -8 and -10 but has a higher affinity for Caspase-3 (100).

Synthetic inhibitory peptides compete with the substrate for binding to the catalytic site of the Caspases' catalytic site. The first minimal substrate found to bind Caspase-1 was Ac-Tyr-Val-Ala-Asp-CHO (Ac-YVAD-CHO) and it acted as a reversible com-

petitive inhibitor.¹⁴ Analyses of the target substrates sequences revealed that the 'W-E-H-D' consensus motif is recognized by Caspases -1, -4 and -5. These tetrameric peptides were engineered in order to increase cell permeability and minimize cell toxicity. They contain a benzyloxycarboxyl group (-Z) or butyloxycarboxyl group (-BOC) in N-terminal and a fluoro-methyl ketone (-FMK) or chloro-methyl ketones (-CMK) or an aldehyde (-CHO) in C-terminal (101).

Ac-WEHD-CHO was used to characterize the biochemical propriety of the Caspase-1 enzyme and is a reversible competitive inhibitor (22). Ac-WEHD-CHO has the highest affinity for Caspase-1 (Ki=0,056) but also inhibits Caspase-8 (Ki=21,1), -4 (Ki=97) and -5 (Ki=43) (90). Ac-YVAD-CHO is also a reversible inhibitor highly specific to Caspase-1 (Ki=0,76 compared to Ki= 362, 163 and 352 for Caspases -4, -5, and -8 respectively (101). Z-YVAD-FMK is a competitive and irreversible pan-Caspase inhibitor and was used in many diseases both *in vitro* and *in vivo*.

Antisense Caspase-1 oligonucleotide (5'-CCT-TGT-CGG-CCA-TGG-C-3') inhibited Caspase-1 in cells from Acute Myeloid Leukemia patients and impaired the cell proliferation and reduced the levels of secreted IL-1 β (102).

VX-765 (or Belnacasan) binds Caspase-1 reversibly and inhibits LPS-induced IL-1 β and IL-18 secretions in FCAS patients' cells (103). Similarly, VX-765 inhibits IL-1 β secretion in mice after intravenous injection of LPS (104). VX-765 was also used in the treatment of depression in a mouse model and caused the regression of epilepsies (105-107). Pralnacasan (or VX-740) is also a reversible inhibitor specific to Caspase-1 (108). VX-740 was used in osteoarthritis, DSS-induced colitis and its active metabolite in cerebral brain ischemia and showed improvement of the symptoms of these pathologies (109-112).

CONCLUSIONS

Caspase-1 is an important player in immunity and constitutes an essential component of the inflammasome complexes that detect and eliminate pathogens. It was first identified by its homology with the ced-3 protein that is implicated in apoptosis (20,21). Further characterization revealed that Caspase-1 cleaves to maturation an important cytokine, IL-1 β , and thus was named IL-1 β converting. However, further characterization of the cell death induced by Caspase-1 revealed that this cell death was physiologically and morphologically different from apoptosis and was called pyroptosis (7,8).

Besides its role in the cleavage of IL-1 β and IL-18, which are two important cytokines playing an essential role in immunity and associated pathologies, Caspase-1 also induces the death of cell by the proteolysis of the Gasdermin D proteins that form pores at the plasma membrane disrupting cellular integrity and inducing pyroptosis. Gasdermin pores also constitute conduits for IL-1 β release. The absence of IL-1 β , IL-18 maturation and secretion and Gasdermin D cleavage and pyroptosis in Caspase-1 knockout macrophages shows that Caspase-1 is required for these events to occur.

In the induction of pyroptosis, Caspase-1 shares the common substrate Gasdermin D with Caspase-11. For long years, the use of Caspase-1 KO mice generated from cells containing a *Caspase-11* gene encoding a naturally mutated non-functional Caspase-11 protein, masked the crucial role of Caspase-11 in host defense against microorganisms. Caspase-11 and its human homologs Caspase-4 and Caspase-5 were found to directly sense lipopolysaccharide - a structural component of Gram-negative bacteria - through their CARD domain. This recognition triggered a cascade of signaling resulting in the cleavage of Gasdermin D by Caspase-11 and in the induction of pyroptosis.

Inflammasome overactivation by gain of function mutations or constitutive stimulation cause inflammatory diseases. Different types of Caspase-1 inhibitors have been designed: synthetic peptides binding to Caspase-1's substrate binding site, antisense oligonucleotides or non-peptidic molecules. Both peptidomimetics Pralnacasan and Belnacasan entered clinical trials

but were withdrawn due to cellular toxicity. Targeting strategies turned to the inhibition of the final product IL-1 β instead of Caspase-1. For instance, the IL-1 receptor antagonist Anakinra is used to treat inflammatory diseases. Recently, a potent NLRP3 inhibitor MCC950 was identified and entered clinical trials (113). Later studies suggested that inflammasomes are not only implicated in auto-inflammatory diseases but may also have a role in neurological disorders and different types of cancer. For instance, knockouts of inflammasome forming NLRP1 and AIM2 proteins were shown to enhance tumor growth (87-89). It is not clear yet if the phenotypes are dependent of their inflammasome forming properties (thus involving Caspase-1) or whether are they are the result of other unknown cellular functions of these proteins.

In summary, Caspase-1 is located at the crossroad of cell death and inflammation and may be the factor deciding whether the cell death should be immunologically silent (apoptosis) or active (pyroptosis). If the cell is able to clear the bacterial infection via Caspase-1-dependent inflammasome activation, then the immunological response will be silent. However, if the cell could not stop and clear the infection or the danger, the cell may activate Caspase-1 dependent pyroptosis and recruit other immune cells to the immune site. The presence of Caspase-1 into phagosomes may have a role in antigen processing and presentation to immune cells. Caspase-1 is not a simple protease but has many substrates with important cellular functions such as inflammation or cell death.

Peer-review: Externally peer-reviewed.

Author Contributions: Conception/Design of study: E.E., N.Ö.; Data Acquisition: E.E., N.Ö.; Data Analysis/Interpretation: E.E., N.Ö.; Drafting Manuscript: E.E., N.Ö.; Critical Revision of Manuscript: E.E., N.Ö.; Final Approval and Accountability: E.E., N.Ö.; Supervision: E.E., N.Ö.

Conflict of Interest: The authors declare that they have no conflicts of interest to disclose.

Financial Disclosure: There are no funders to report for this submission.

Acknowledgement: We would like to acknowledge all scientists who have put a piece into the Caspase-1 puzzle. Without their contributions this review could not have been written. This work was supported by Bogazici University Research Fund Projects BAP TUG 8400 and BAP TUG 14323.

REFERENCES

1. Murphy K, Travers P, Walport M, Janeway C. Janeway's immunobiology (8th ed.) 2012 New York: Garland Science.
2. Sadik CD, Luster AD. Lipid-cytokine chemokine cascades orchestrate leukocyte recruitment in inflammation. *J Leukoc Biol* 2012; 91: 207-15.
3. Mantovani A, Dinarello CA, Molgora M, Garlanda C. Interleukin-1 and related cytokines in the regulation of inflammation and immunity. *Immunity* 2019; 50: 778-95.

4. Monteleone M, Stow JL, Schroder K. Mechanisms of unconventional secretion of IL-1 family cytokines. *Cytokine* 2015; 74: 213-8.
5. Agostini L, Martinon F, Burns K, McDermott MF, Hawkins PN, Tschopp J. NALP3 forms an IL-1 β -processing inflammasome with increased activity in Muckle-Wells autoinflammatory disorder. *Immunity* 2004; 20: 319-25.
6. Martinon F, Burns K, Tschopp J. The inflammasome: a molecular platform triggering activation of inflammatory Caspases and processing of proIL- β . *Mol Cell* 2002;10(2):417-26.
7. Kayagaki N, Stowe IB, Lee BL, O'Rourke K, Anderson K, Warming S, et al. Caspase-11 cleaves gasdermin D for non-canonical inflammasome signalling. *Nature* 2015; 526: 666-71.
8. Shi J, Zhao Y, Wang K, Shi X, Wang Y, Huang H, et al. Cleavage of GSDMD by inflammatory Caspases determines pyroptotic cell death. *Nature* 2015; 526: 660-5.
9. Evavold CL, Ruan J, Tan Y, Xia S, Wu H, Kagan JC. The pore-forming protein Gasdermin D regulates interleukin-1 secretion from living macrophages. *Immunity* 2018; 48: 35-44.
10. Park H, Bourla AB, Kastner DL, Colbert RA, Siegel RM. Lighting the fires within: the cell biology of autoinflammatory diseases. *Nat Rev Immunol* 2012; 12: 570-80.
11. Cerretti DP, Kozlosky CJ, Mosley B, Nelson N, Van Ness K, Greenstreet TA, et al. Molecular cloning of the interleukin-1 β converting enzyme. *Science* 1992; 256: 97-100.
12. Kayagaki N, Warming S, Lamkanfi M, Vande Walle L, Louie S, Dong J, et al. Non-canonical inflammasome activation targets Caspase-11. *Nature* 2011; 479: 117-21.
13. Saleh M, Vaillancourt JP, Graham RK, Huyck M, Srinivasula SM, Alnemri ES, et al. Differential modulation of endotoxin responsiveness by human Caspase-12 polymorphisms. *Nature* 2004; 429: 75-9.
14. McArthur K, Kile BT. Apoptotic Caspases: Multiple or mistaken identities? *Trends Cell Biol* 2018; 28: 475-93.
15. Eckhart L, Declercq W, Ban J, Rendl M, Lengauer B, Mayer C, et al. Terminal differentiation of human keratinocytes and stratum corneum formation is associated with Caspase-14 activation. *J Invest Dermatol* 2000; 115: 1148-51.
16. Thul PJ, Åkesson L, Wiking M, Mahdessian D, Geladaki A, Ait Blal H, et al. A subcellular map of the human proteome. *Science* 2017; 356 pii: eaal3321.
17. Viganò E, Diamond CE, Spreafico R, Balachander A, Sobota RM, Mortellaro A. Human Caspase-4 and Caspase-5 regulate the one-step non-canonical inflammasome activation in monocytes. *Nat Commun* 2015; 6:8761.
18. Fischer H, Koenig U, Eckhart L, Tschachler E. Human Caspase 12 has acquired deleterious mutations. *Biochem Biophys Res Commun* 2002; 293, 722-6.
19. Nakagawa T, Zhu H, Morishima N, Li E, Xu J, Yankner BA, et al. Caspase-12 mediates endoplasmic-reticulum-specific apoptosis and cytotoxicity by amyloid- β . *Nature* 2000; 403: 98-103.
20. Black RA, Kronheim SR, Cantrell M, Deeley MC, March CJ, Prickett KS, et al. Generation of biologically active interleukin-1 β by proteolytic cleavage of the inactive precursor. *J Biol Chem* 1988; 263: 9437-42.
21. Kostura MJ, Tocci MJ, Limjuco G, Chin J, Cameron P, Hillman AG, et al. Identification of a monocyte specific pre-interleukin 1 β convertase activity. *Proc Natl Acad Sci U S A* 1989; 86: 5227-31.
22. Thornberry NA, Bull HG, Calaycay JR, Chapman KT, Howard AD, Kostura MJ, et al. A novel heterodimeric cysteine protease is required for interleukin-1 β processing in monocytes. *Nature* 1992; 356: 768-74.
23. Ayala JM, Yamin TT, Egger LA, Chin J, Kostura MJ, Miller DK. IL-1 β -converting enzyme is present in monocytic cells as an inactive 45-kDa precursor. *J Immunol* 1994; 153: 2592-9.
24. Alnemri ES, Livingston DJ, Nicholson DW, Salvesen G, Thornberry NA, Wong WW, et al. Human ICE/CED-3 protease nomenclature. *Cell* 1996; 87: 171.
25. Li P, Allen H, Banerjee S, Franklin S, Herzog L, Johnston C, et al. Mice deficient in IL-1 β -converting enzyme are defective in production of mature IL-1 β and resistant to endotoxic shock. *Cell* 1995; 80: 401-11.
26. Kuida K, Lippke JA, Ku G, Harding MW, Livingston DJ, Su MS, et al. Altered cytokine export and apoptosis in mice deficient in interleukin-1 β converting enzyme. *Science* 1995; 267: 2000-3.
27. Sandstrom A, Mitchell PS, Goers L, Mu EW, Lesser CF, Vance RE. Functional degradation: A mechanism of NLRP1 inflammasome activation by diverse pathogen enzymes. *Science* 2019; 364 pii: eaau1330.
28. Martinon F, Pétrilli V, Mayor A, Tardivel A, Tschopp J. Gout-associated uric acid crystals activate the NALP3 inflammasome. *Nature* 2006; 440: 237-41.
29. Kanneganti TD, Ozören N, Body-Malapel M, Amer A, Park JH, Franchi L, et al. Bacterial RNA and small antiviral compounds activate Caspase-1 through cryopyrin/Nalp3. *Nature* 2006; 440: 233-6.
30. Mariathasan S, Weiss DS, Newton K, McBride J, O'Rourke K, Roose-Girma M, et al. Cryopyrin activates the inflammasome in response to toxins and ATP. *Nature* 2006; 440: 228-32.
31. Özören N, Masumoto J, Franchi L, Kanneganti TD, Body-Malapel M, Ertürk I, et al. Distinct roles of TLR2 and the adaptor ASC in IL-1 β /IL-18 secretion in response to *Listeria monocytogenes*. *J Immunol* 2006; 176: 4337-42.
32. Poyet JL, Srinivasula SM, Tnani M, Razmara M, Fernandes-Alnemri T, Alnemri ES. Identification of Ipaf, a human Caspase-1-activating protein related to Apaf-1. *J Biol Chem* 2001; 276: 28309-13.
33. Sutterwala FS, Mijares LA, Li L, Ogura Y, Kazmierczak BI, Flavell RA. Immune recognition of *Pseudomonas aeruginosa* mediated by the IPAF/NLRC4 inflammasome. *J Exp Med* 2007; 204: 3235-45.
34. Hornung V, Ablasser A, Charrel-Dennis M, Bauernfeind F, Horvath G, Caffrey DR, et al. AIM2 recognizes cytosolic dsDNA and forms a Caspase-1-activating inflammasome with ASC. *Nature* 2009; 458: 514-518.
35. Fernandes-Alnemri T, Yu JW, Datta P, Wu J, Alnemri ES. AIM2 activates the inflammasome and cell death in response to cytoplasmic DNA. *Nature* 2009; 458: 509-13.
36. Khare S, Dorfleutner A, Bryan NB, Yun C, Radian AD, de Almeida L, et al. An NLRP7-containing inflammasome mediates recognition of microbial lipopeptides in human macrophages. *Immunity* 2012; 36: 464-76.
37. Minkiewicz J, de Rivero Vaccari JP, Keane RW. Human astrocytes express a novel NLRP2 inflammasome. *Glia* 2013; 61: 1113-21.
38. Shi J, Zhao Y, Wang Y, Gao W, Ding J, Li P, et al. Inflammatory Caspases are innate immune receptors for intracellular LPS. *Nature* 2014; 514: 187-92.
39. Hagar JA, Powell DA, Aachoui Y, Ernst RK, Miao EA. Cytoplasmic LPS activates Caspase-11: implications in TLR4-independent endotoxic shock. *Science* 2013; 341: 1250-3.
40. Yang D, He Y, Muñoz-Planillo R, Liu Q, Núñez G. Caspase-11 requires the pannexin-1 channel and the purinergic P2X7 pore to mediate pyroptosis and endotoxic shock. *Immunity* 2015; 43:923-32.
41. Sollberger G, Strittmatter GE, Kistowska M, French LE, Beer HD. Caspase-4 is required for activation of inflammasomes. *J Immunol* 2012; 188: 1992-2000.
42. Yuan J, Shaham S, Ledoux S, Ellis HM, Horvitz HR. The *C. elegans* cell death gene *ced-3* encodes a protein similar to mammalian interleukin-1 β -converting enzyme. *Cell* 1993; 75: 641-52.

43. Miura M, Zhu H, Rotello R, Hartweg EA, Yuan J. Induction of apoptosis in fibroblasts by IL-1 beta-converting enzyme, a mammalian homolog of the C. elegans cell death gene *ced-3*. *Cell* 1993; 75: 653-60.
44. Pei H, Li C, Adereth Y, Hsu T, Watson DK, Li R. Caspase-1 is a direct target gene of ETS1 and plays a role in ETS1-induced apoptosis. *Cancer Res* 2005; 65: 7205-13.
45. Winter RN, Rhee JG, Kyprianou N. Caspase-1 enhances the apoptotic response of prostate cancer cells to ionizing radiation. *Anticancer Res* 2004; 24: 1377-86.
46. Guo H, Pétrin D, Zhang Y, Bergeron C, Goodyer CG, LeBlanc AC. Caspase-1 activation of Caspase-6 in human apoptotic neurons. *Cell Death Differ* 2006; 13: 285-92.
47. Philip NH, Dillon CP, Snyder AG, Fitzgerald P, Wynosky-Dolfi MA, Zwack EE, et al. Caspase-8 mediates Caspase-1 processing and innate immune defense in response to bacterial blockade of NF- κ B and MAPK signaling. *Proc Natl Acad Sci U S A* 2014; 111: 7385-90.
48. Exline MC, Justiniano S, Hollyfield JL, Berhe F, Besecker BY, Das S, et al. Microvesicular Caspase-1 mediates lymphocyte apoptosis in sepsis. *PLoS One* 2014; 9: in press.
49. Tsuchiya K, Nakajima S, Hosojima S, Thi Nguyen D, Hattori T, et al., Caspase-1 initiates apoptosis in the absence of gasdermin D. *Nat Commun* 2019; 10:2091.
50. Gu Y, Wu J, Faucheu C, Lalanne JL, Diu A, Livingston DJ, et al. Interleukin-1 beta converting enzyme requires oligomerization for activity of processed forms in vivo. *EMBO J* 1995; 14: 1923-31.
51. Walker NP, Talanian RV, Brady KD, Dang LC, Bump NJ, Ferenz CR, et al. Crystal structure of the cysteine protease interleukin-1 beta-converting enzyme: a (p20/p10)₂ homodimer. *Cell* 1994; 78: 343-52.
52. Srinivasula SM, Poyet JL, Razmara M, Datta P, Zhang Z, Alnemri ES. The PYRIN-CARD protein ASC is an activating adaptor for Caspase-1. *J Biol Chem* 2002; 277: 21119-22.
53. Proell M, Gerlic M, Mace PD, Reed JC, Riedl SJ. The CARD plays a critical role in ASC foci formation and inflammasome signalling. *Biochem J* 2013; 449: 613-21.
54. Sahillioglu AC, Sumbul F, Ozoren N, Haliloglu T. Structural and dynamics aspects of ASC speck assembly. *Structure* 2014; 22: 1722-34.
55. Narayanan KB, Jang TH, Park HH. Self-oligomerization of ASC PYD domain prevents the assembly of inflammasome in vitro. *Appl Biochem Biotechnol* 2014; 172: 3902-12.
56. Narayanan KB, Park HH. Purification and analysis of the interactions of Caspase-1 and ASC for assembly of the inflammasome. *Appl Biochem Biotechnol* 2015; 175: 2883-94.
57. Gültekin Y, Eren E, Özören N. Overexpressed NLRC3 acts as an anti-inflammatory cytosolic protein. *J Innate Immun* 2015; 7: 25-36.
58. Thornberry NA, Rano TA, Peterson EP, Rasper DM, Timkey T, Garcia-Calvo M, et al. A combinatorial approach defines specificities of members of the Caspase family and granzyme B. Functional relationships established for key mediators of apoptosis. *J Biol Chem* 1997; 272: 17907-11.
59. Wilson KP, Black JA, Thomson JA, Kim EE, Griffith JP, Navia MA, et al. Structure and mechanism of interleukin-1 beta converting enzyme. *Nature* 1994; 370: 270-5.
60. Fantuzzi G, Dinarello CA. Interleukin-18 and interleukin-1 beta: two cytokine substrates for ICE (Caspase-1). *J Clin Immunol* 1999; 19: 1-11.
61. Ghayur T, Banerjee S, Hugunin M, Butler D, Herzog L, Carter A, et al. Caspase-1 processes IFN-gamma-inducing factor and regulates LPS-induced IFN-gamma production. *Nature* 1997; 386: 619-23.
62. Gu Y, Kuida K, Tsutsui H, Ku G, Hsiao K, Fleming MA, et al. Activation of interferon-gamma inducing factor mediated by interleukin-1beta converting enzyme. *Science* 1997; 275: 206-9.
63. Heilig R, Dick MS, Sborgi L, Meunier E, Hiller S, Broz P. The Gasdermin-D pore acts as a conduit for IL-1 β secretion in mice. *Eur J Immunol* 2018; 48: 584-92.
64. Cayrol C, Girard JP. The IL-1-like cytokine IL-33 is inactivated after maturation by Caspase-1. *Proc Natl Acad Sci U S A* 2009; 106: 9021-6.
65. Chae JJ, Wood G, Richard K, Jaffe H, Colburn NT, Masters SL, et al. The familial Mediterranean fever protein, pyrin, is cleaved by Caspase-1 and activates NF-kappaB through its N-terminal fragment. *Blood* 2008; 112: 1794-1803.
66. Migglin SM, Pålsson-McDermott E, Dunne A, Jefferies C, Pinteaux E, Banahan K, et al. NF-kappaB activation by the Toll-IL-1 receptor domain protein MyD88 adapter-like is regulated by Caspase-1. *Proc Natl Acad Sci U S A* 2007; 104: 3372-7.
67. Lamkanfi M, Kanneganti TD, Van Damme P, Vanden Berghe T, Vannoverbergh I et al. Targeted peptidomic proteomics reveals Caspase-7 as a substrate of the Caspase-1 inflammasomes. *Mol Cell Proteomics* 2008; 7: 2350-63.
68. Trompet S, de Craen J, Slagboom P, Shepherd J, Blauw GJ, Murphy MB, et al. Genetic variation in the interleukin-1 beta-converting enzyme associates with cognitive function. The PROSPER study. *Brain* 2008; 131: 1069-77.
69. Blankenberg S, Godefroy T, Poirier O, Rupprecht HJ, Barboux S, Bickel C, et al. Haplotypes of the Caspase-1 gene, plasma Caspase-1 levels, and cardiovascular risk. *Circ Res* 2006; 99: 102-8.
70. Luksch H, Romanowski MJ, Chara O, Tüngler V, Caffarena ER, Heymann MC, et al. Naturally occurring genetic variants of human Caspase-1 differ considerably in structure and the ability to activate interleukin-1 β . *Hum Mutat* 2013; 34: 122-31.
71. Soung YH, Jeong EG, Ahn CH, Kim SS, Song SY, Yoo NJ, et al. Mutational analysis of Caspase 1, 4, and 5 genes in common human cancers. *Hum Pathol* 2008; 39: 895-900.
72. Kim YR, Kim KM, Yoo NJ, Lee SH. Mutational analysis of CASP1, 2, 3, 4, 5, 6, 7, 8, 9, 10, and 14 genes in gastrointestinal stromal tumors. *Hum Pathol* 2009; 40: 868-71.
73. Kim MS, Park SW, Kim YR, Lee JY, Lim HW, Song SY, et al. Mutational analysis of Caspase genes in prostate carcinomas. *APMIS* 2010; 118: 308-12.
74. Winter RN, Kramer A, Borkowski A, Kyprianou N. Loss of Caspase-1 and Caspase-3 protein expression in human prostate cancer. *Cancer Res* 2001; 61: 1227-32.
75. Pan YL, Liu W, Gao CX, Shang Z, Ning LJ, Liu X. CASP-1, -2 and -5 gene polymorphisms and cancer risk: A review and meta-analysis. *Biomed Rep* 2013; 1: 511-6.
76. Vázquez-Higuera JL, Rodríguez-Rodríguez E, Sánchez-Juan P, Mateo I, Pozueta A, Martínez-García A, et al. Caspase-1 genetic variation is not associated with Alzheimer's disease risk. *BMC Med Genet* 2010; 11: in press.
77. Ona VO, Li M, Vonsattel JP, Andrews LJ, Khan SQ, Chung WM, et al. Inhibition of Caspase-1 slows disease progression in a mouse model of Huntington's disease. *Nature* 1999; 399: 263-7.
78. Li M, Ona VO, Guégan C, Chen M, Jackson-Lewis V, Andrews LJ, et al. Functional role of Caspase-1 and Caspase-3 in an ALS transgenic mouse model. *Science* 2000; 288: 335-9.
79. Friedlander RM, Gagliardini V, Hara H, Fink KB, Li W, MacDonald G, et al. Expression of a dominant negative mutant of interleukin-1 β converting enzyme in transgenic mice prevents neuronal cell death induced by trophic factor withdrawal and ischemic brain injury. *J Exp Med* 1997; 185: 933-40.
80. Hara H, Friedlander RM, Gagliardini V, Ayata C, Fink K, Huang Z, et al. Inhibition of interleukin 1beta converting enzyme family proteases reduces ischemic and excitotoxic neuronal damage. *Proc Natl Acad Sci U S A* 1997; 94: 2007-12.
81. Hara H, Fink K, Endres M, Friedlander RM, Gagliardini V, Yuan J, et al. Attenuation of transient focal cerebral ischemic injury in transgenic mice expressing a mutant ICE inhibitory protein. *J Cereb Blood Flow Metab* 1997; 17: 370-5.

82. Guo Y, Kyprianou N. Restoration of transforming growth factor beta signaling pathway in human prostate cancer cells suppresses tumorigenicity via induction of Caspase-1-mediated apoptosis. *Cancer Res* 1999; 59: 1366-71.
83. Hu B, Elinav E, Huber S, Booth CJ, Strowig T, Jin C, et al. Inflammation-induced tumorigenesis in the colon is regulated by Caspase-1 and NLR4. *Proc Natl Acad Sci U S A* 2010; 107: 21635-40.
84. Celardo I, Grespi F, Antonov A, Bernassola F, Garabadgiu AV, Melino G, Amelio I. Caspase-1 is a novel target of p63 in tumor suppression. *Cell Death Dis.* 2013; 4:e645.
85. Yan W, Chang Y, Liang X, Cardinal JS, Huang H, Thorne SH, et al. High-mobility group box 1 activates Caspase-1 and promotes hepatocellular carcinoma invasiveness and metastases. *Hepatology* 2012; 55: 1863-75.
86. Estrov Z, Talpaz M. Role of interleukin-1 beta converting enzyme (ICE) in acute myelogenous leukemia cell proliferation and programmed cell death. *Leuk Lymphoma* 1997; 24: 379-91.
87. Zaki MH, Boyd KL, Vogel P, Kastan MB, Lamkanfi M, Kanneganti TD. The NLRP3 inflammasome protects against loss of epithelial integrity and mortality during experimental colitis. *Immunity* 2010; 32:379-91.
88. Man SM, Zhu Q, Zhu L, Liu Z, Karki R, Malik A, et al. Critical Role for the DNA Sensor AIM2 in Stem Cell Proliferation and Cancer. *Cell* 2015; 162:45-58.
89. Zhong FL, Mamaï O, Sborgi L, Boussofara L, Hopkins R, Robinson K, et al. Germline NLRP1 mutations cause skin inflammatory and cancer susceptibility syndromes via inflammasome activation. *Cell* 2016; 167:187-202.e17.
90. Dowds TA, Masumoto J, Zhu L, Inohara N, Núñez G. Cryopyrin-induced interleukin 1beta secretion in monocytic cells: enhanced activity of disease-associated mutants and requirement for ASC. *J Biol Chem* 2004; 279: 21924-8.
91. Omenetti A, Carta S, Delfino L, Martini A, Gattorno M, Rubartelli A. Increased NLRP3-dependent interleukin 1 β secretion in patients with familial Mediterranean fever: correlation with MEFV genotype. *Ann Rheum Dis* 2014; 73: 462-9.
92. Yüksel Ş, Eren E, Hatemi G, Sahillioğlu AC, Gültekin Y, Demiröz D, et al. Novel NLRP3/cryopyrin mutations and pro-inflammatory cytokine profiles in Behçet's syndrome patients. *Int Immunol* 2014; 26: 71-81.
93. Joosten LA, Netea MG, Fantuzzi G, Koenders MI, Helsen MM, Sparner H, et al. Inflammatory arthritis in Caspase 1 gene-deficient mice: contribution of proteinase 3 to Caspase 1-independent production of bioactive interleukin-1beta. *Arthritis Rheum* 2009; 60: 3651-62.
94. Sikora J, Mielczarek-Palacz A, Kondera-Anasz Z. Imbalance in cytokines from interleukin-1 family - role in pathogenesis of endometriosis. *Am J Reprod Immunol* 2012; 68: 138-45.
95. Vincent JA, Mohr S. Inhibition of Caspase-1/interleukin-1beta signaling prevents degeneration of retinal capillaries in diabetes and galactosemia. *Diabetes* 2007; 56: 224-30.
96. Wang H, Capell W, Yoon JH, Faubel S, Eckel RH. Obesity development in Caspase-1-deficient mice. *Int J Obes (Lond)* 2014; 38: 152-5.
97. Ray CA, Black RA, Kronheim SR, Greenstreet TA, Sleath PR, Salvesen GS, et al. Viral inhibition of inflammation: cowpox virus encodes an inhibitor of the interleukin-1 beta converting enzyme. *Cell* 1992; 69: 597-604.
98. Dobó J, Swanson R, Salvesen GS, Olson ST, Gettins PG. Cytokine response modifier a inhibition of initiator Caspases results in covalent complex formation and dissociation of the Caspase tetramer. *J Biol Chem* 2006; 281: 38781-90.
99. Bump NJ, Hackett M, Hugunin M, Seshagiri S, Brady K, Chen P, et al. Inhibition of ICE family proteases by baculovirus antiapoptotic protein p35. *Science* 1995; 269: 1885-8.
100. Zhou Q, Krebs JF, Snipas SJ, Price A, Alnemri ES, Tomaselli KJ, et al. Interaction of the baculovirus anti-apoptotic protein p35 with Caspases. Specificity, kinetics, and characterization of the Caspase/p35 complex. *Biochemistry* 1998; 37: 10757-65.
101. Garcia-Calvo M, Peterson EP, Leiting B, Ruel R, Nicholson DW, Thornberry NA. Inhibition of human Caspases by peptide-based and macromolecular inhibitors. *J Biol Chem* 1998; 273: 32608-13.
102. Stosić-Grujčić S, Basara N, Dinarello CA. Modulatory in vitro effects of interleukin-1 receptor antagonist (IL-1Ra) or antisense oligonucleotide to interleukin-1 beta converting enzyme (ICE) on acute myeloid leukaemia (AML) cell growth. *Clin Lab Haematol* 1999; 21: 173-85.
103. Stack JH, Beaumont K, Larsen PD, Straley KS, Henkel GW, Randle JC, et al. IL-converting enzyme/Caspase-1 inhibitor VX-765 blocks the hypersensitive response to an inflammatory stimulus in monocytes from familial cold autoinflammatory syndrome patients. *J Immunol* 2005; 175: 2630-4.
104. Wannamaker W, Davies R, Namchuk M, Pollard J, Ford P, Ku G, et al. (S)-1-((S)-2-[[1-(4-amino-3-chloro-phenyl)-methanoyl]-amino]-3,3-dimethyl-butanoyl)-pyrrolidine-2-carboxylic acid ((2R,3S)-2-ethoxy-5-oxo-tetrahydro-furan-3-yl)-amide (VX-765), an orally available selective interleukin (IL)-converting enzyme/Caspase-1 inhibitor, exhibits potent anti-inflammatory activities by inhibiting the release of IL-1beta and IL-18. *J Pharmacol Exp Ther* 2007; 321: 509-16.
105. Zhang Y, Liu L, Liu YZ, Shen XL, Wu TY, Zhang T, et al. NLRP3 inflammasome mediates chronic mild stress-induced depression in mice via neuroinflammation. *Int J Neuropsychopharmacol* 2015; 18:pii: pyv006.
106. Ravizza T, Noé F, Zardoni D, Vaghi V, Sifringer M, Vezzani A. Interleukin converting enzyme inhibition impairs kindling epileptogenesis in rats by blocking astrocytic IL-1beta production. *Neurobiol Dis* 2008; 31: 327-33.
107. Maroso M, Balosso S, Ravizza T, Iori V, Wright CI, French J, et al. Interleukin-1 β biosynthesis inhibition reduces acute seizures and drug resistant chronic epileptic activity in mice. *Neurotherapeutics* 2011; 8: 304-15.
108. Siegmund B, Zeitz M. Pralnacasan (vertex pharmaceuticals). *IDrugs* 2003; 6: 154-8.
109. Rudolphi K, Gerwin N, Verzijl N, van der Kraan P, van den Berg W. Pralnacasan, an inhibitor of interleukin-1beta converting enzyme, reduces joint damage in two murine models of osteoarthritis. *Osteoarthritis Cartilage* 2003; 11: 738-46.
110. Loher F, Bauer C, Landauer N, Schmall K, Siegmund B, Lehr HA, et al. The interleukin-1 beta-converting enzyme inhibitor pralnacasan reduces dextran sulfate sodium-induced murine colitis and T helper 1 T-cell activation. *J Pharmacol Exp Ther* 2004; 308: 583-90.
111. Bauer C, Loher F, Dauer M, Mayer C, Lehr HA, Schönharting M et al. The ICE inhibitor pralnacasan prevents DSS-induced colitis in C57BL/6 mice and suppresses IP-10 mRNA but not TNF-alpha mRNA expression. *Dig Dis Sci* 2007; 52: 1642-52.
112. Ross J, Brough D, Gibson RM, Loddick SA, Rothwell NJ. A selective, non-peptide Caspase-1 inhibitor, VRT-018858, markedly reduces brain damage induced by transient ischemia in the rat. *Neuropharmacology* 2007; 53: 638-42.
113. Coll RC, Robertson AA, Chae JJ, Higgins SC, Muñoz-Planillo R, Inserra MC, et al. A small-molecule inhibitor of the NLRP3 inflammasome for the treatment of inflammatory diseases. *Nat Med* 2015; 21: 248-55.

Comparison of the Anti-Legionella Fill Material against Standard Polypropylene Fill Material in Model Cooling Tower Water System

Irfan Turetgen¹ , Cansu Vatansever² 

¹Istanbul University, Faculty of Science, Department of Biology, Istanbul, Turkey

²Altinbas University, Faculty of Pharmacy, Department of Pharmaceutical Microbiology, Istanbul, Turkey

ORCID IDs of the authors: I.T. 0000-0002-7866-1007; C.V. 0000-0002-2751-1033

Please cite this article as: Turetgen I, Vatansever C. Comparison of the Anti-Legionella Fill Material against Standard Polypropylene Fill Material in Model Cooling Tower Water System. Eur J Biol 2020; 79(1):62-66. DOI: 10.26650/EurJBiol.2020.0004

ABSTRACT

Objective: Cooling towers are heat exchangers which are utilized in specific industrial devices. They possess the potential to support Legionella bacteria. The objective was to evaluate the efficacy of biocide impregnated polymer against regular polypropylene polymer in terms of anti-Legionella features during a 120-day period.

Materials and Methods: To reduce the bacterial colonization in towers, anti-Legionella splash fill and regular polypropylene splash fill material were tested to compare anti-Legionella activity and biofilm formation potential within a 120-day period using a lab-scale recirculating cooling tower model system. The system was experimentally infected with Legionella suspension and operated continuously for 120 days.

Results: Legionella colonization occurred on both test material surfaces beginning at the first month. Legionella counts on surfaces were increased over time on standard polypropylene surfaces. The product with anti-Legionella activity showed significantly lower Legionella colonization in comparison to standard polypropylene fill.

Conclusion: The product with anti-Legionella activity has a significant biocidal effect against surface-associated Legionella under the above-mentioned conditions which mimics cooling tower water systems. Product seems to facilitate effective control program criteria against Legionella colonization in cooling towers.

Keywords: Legionella, cooling tower, fill material, biofilms, *Legionella pneumophila*

INTRODUCTION

Wet type cooling towers are heat exchangers that allow water and air to come in contact to decrease the temperature of the circulating water and they provide an ideal niche for bacteria to grow and colonize (1,2). One of the best known water pathogen in cooling systems is Legionella bacterium, which causes Legionnaires' disease. The ever first Legionella outbreak in 1976 led to the recognition of a new genus, responsible for both Pontiac fever and Legionnaires' disease. Legionella can flourish in cooling tower water and spread to humans when expelled aerosols containing the bacteria is inhaled (3,4). Mostly, Legionnaires' disease outbreaks

were sourced from wet cooling towers. The recent deadly Legionnaires' disease outbreak occurred in Brescia, Italy in 2018, where 42 people contracted the bacteria, two of whom died (5-7). Infections caused by Legionella are the leading cause of waterborne disease outbreaks.

The formation of a robust biofilm on a man-made distribution system can be detrimental (8). It is generally accepted that biofilms have a crucial role in the survival of Legionella bacteria within man-made water systems (9). Biofilm layers are suitable environments for pathogens microorganisms and harbors bacteria that could damage the material (10-12). Recently, microbiological



Corresponding Author: Irfan Turetgen

E-mail: turetgen@istanbul.edu.tr

Submitted: 10.01.2020 • **Revision Requested:** 11.03.2020 • **Last Revision Received:** 06.05.2020 • **Accepted:** 11.05.2020

© Copyright 2020 by The Istanbul University Faculty of Science • Available online at <http://ejb.istanbul.edu.tr> • DOI: 10.26650/EurJBiol.2020.0004

contamination in industrial and domestic water systems has been a growing problem for many years. From the water source to the industrial water systems, the bulk water passes through kilometers of pipes (13). At any point in this distribution system, the microorganisms involved in the water are transported together with the water flow and multiply by adhering to the surfaces of the man-made water systems (14,15). Biofilm layers in industrial cooling systems develop mostly on fill material, as temperatures there support the fast multiplication of the genus *Legionella* (16). The polymer surface is always at risk of becoming colonized with harmful bacteria and, therefore, it is a hazard to humans because of the potential for it to indirectly pass on these disease-causing microorganisms.

Ideally, preventing biofilm formation and *Legionella* colonization would be a more logical option than cleaning or treating it. The appearance of biofilm associated problems plainly shows that new anti-biofilm and *Legionella* control procedures are required. However, there is currently no better technique or procedure that is able to completely eradicate the unwanted biofilms (17,18). Several procedures to reduce the colonization of microbial biofilms have been studied over the years, with diverse degrees of success (19). In various industrial set-ups, toxic metals or a spectrum of biocides have been used for sanitizing purposes and biofilm reduction. However, a single strategy may not be enough for comprehensive prevention. Evidence has shown that environmental surfaces play an important role in the transmission of nosocomial pathogens like *Legionella*. Extensive research has focused on mitigating the development of biofilms at the water-solid interface (2,19-21).

The general technical performances of the cooling towers are mainly influenced by the functional characteristics of the cooling tower fill used in the cooling systems. The objective of the recent study was to evaluate the efficacy of biocide impregnated polymer against regular polypropylene polymer in terms of anti-*Legionella* features during a 120-day period. Targets have achieved enhanced cooling performance, lengthened the material life, reduced clogging and limited the growth of biofilm associated bacteria. The study was implemented using a recirculating water system under persistent hydraulic shear stress, which corresponds with the conditions in real life man-made water systems.

MATERIALS AND METHODS

The experiment was completed using a laboratory scale recirculating water system (150 l water capacity). Distributed municipality water was added to complete the water lost by evaporation and blowdown. Control and test surfaces were not immersed; they were only in contact with spray water. All test surfaces were secured with suspenders over the water surface without any touch to each other (Figure 1). During the study, the temperature of the water was set stable at 37°C, an average of general cooling tower bulk water temperature. Constant temperature also eliminates the probable effects on biofilm formation.

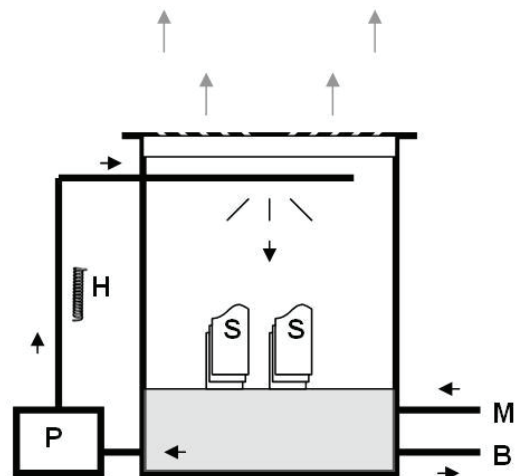


Figure 1. Schematic view of the lab-scale water system, black arrows indicate water flow, gray arrows indicate evaporation. S: surfaces, P: pump, B: blowdown outlet, M: make-up water inlet, H: heater.

At the beginning of the setup, bulk water was seeded with standard strain suspension containing *Legionella pneumophila* ATCC 33152 (1 ml of *L. pneumophila* inoculum at 10^5 cells/ml) and operated for 120-days. No chemicals were supplemented to the water, to exclude their adverse effects on natural biofilm formation and bacteria.

The test objects were a hybrid (mix) type splash fill, adapted to the technological requirements of any wet cooling tower (Figure 2). Anti-*Legionella* fills were factory produced and the anti-*Legionella* feature of the chlorine based agents was immobilized during production. Unlike classic sheet fill, the splash fill is very efficient, practically invulnerable at impurity clogging, resistant to the influence of physical and chemical factors. The splash fill consists of individual elements with network appearance from injected polypropylene with optimized apertures and plies which generate both drops and films in its volume.

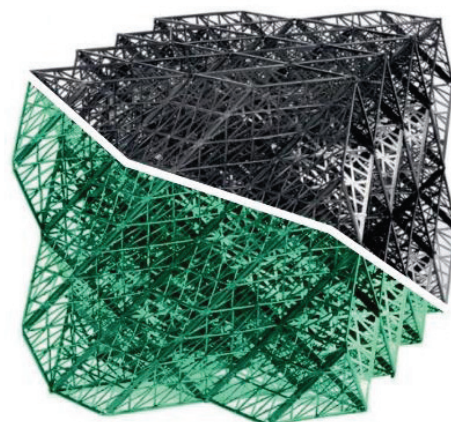


Figure 2. Cooling tower splash fill. Green one is the product with anti-*Legionella* features.

Surface sections of the two test materials were removed monthly from the model system, gently washed by sterile tap water to remove planktonic cells. Samples on preset locations were removed by sterile lancet, suspended in phosphate buffer saline and vortexed slowly for 1 min. For heterotrophic bacterial plate count (HPC) determination, 10-fold diluted biofilm and bulk water samples were spreaded (0.1 ml) onto R2A agar (OXOID, UK) containing Petri dishes and kept at 28°C for 10 days. As an ideal tool to cultivate heterotrophic bacterial numbers in oligotrophic waters, R2A plates incubated at 28°C for 10 days were recommended by Reasoner and Geldreich (22). All platings were done by triplicate analyses. To culture Legionella bacteria, biofilm samples were pre-treated with acid solution for 15 minutes (KCl-HCl solution, pH 2.2) to decrease the growth of accompanying co-flora. Pre-treated and untreated samples (0.1 ml) were inoculated onto BCYE agar (OXOID, UK) containing selective supplement and incubated at 37°C for 10 days. Colonies similar to Legionella morphology were subcultured to blood agar and BCYE agar plates. Final identification was completed using Legionella Latex Agglutination Kit (OXOID, UK) (Dennis, 1988).

Bacterial numbers were \log_{10} converted and standard errors of the means were calculated by software. Differences between numbers were tested for significance using a t-test; differences were accepted significantly different at $P < 0.05$. Statistical analyses were performed using SPSS 21.0 software.

RESULTS AND DISCUSSION

Following successful seeding of Legionella bacteria, they were rapidly adhered to surfaces, colonized and increased up to 400 CFU/cm² (CFU: Colony Forming Unit) on surfaces at the end of the first 30-days. Legionella bacteria have maintained their cultivation and viability throughout the test period on all surfaces and also in bulk water. The heterotrophic bacterial numbers showed a similar growing trend during the test period. The heterotrophic bacteria in bulk water were also adhered to the test surfaces and colonized rapidly until day 120.

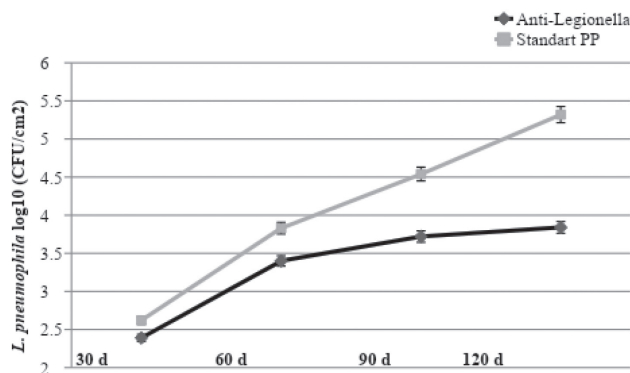


Figure 3. *L. pneumophila* numbers on surfaces during 120 days. Error bars represent standard error. * $P < 0.05$ compared with Anti-Legionella group.

Depending on the *L. pneumophila* culture results, Legionella colonization was monitored on both test material surfaces beginning at the first month of the experimental period (Figure 3). Legionella counts on surfaces were increased gradually over time. Statistically, a significant difference was found between two test materials in terms of Legionella growth on surfaces. The green colored product with anti-Legionella activity showed significantly lower Legionella colonization in comparison to standard polypropylene splash fill after completion of the 120-day test period ($P < 0.05$). Legionella counts on standard polypropylene surfaces increased gradually from 416 CFU/cm² to 208.929 CFU/cm² within the 120-day period. The highest Legionella count on anti-Legionella surfaces was recorded as 7.244 CFU/cm². The 2 log reduction on anti-Legionella test surfaces was statistically significant.

Furthermore, the fill material with anti-Legionella activity showed also significantly lower heterotrophic bacterial colonization in comparison to standard control group polypropylene fill after 120-day test period ($P < 0.05$) (Figure 4). Heterotrophic bacterial counts on standard PP surfaces increased gradually from 107.151 CFU/cm² to 2.754.228 CFU/cm² within the 4-month period. The highest heterotrophic bacterial count on anti-Legionella surfaces was recorded as 218.776 CFU/cm², where the value was one log smaller than on standard polypropylene fill surfaces.

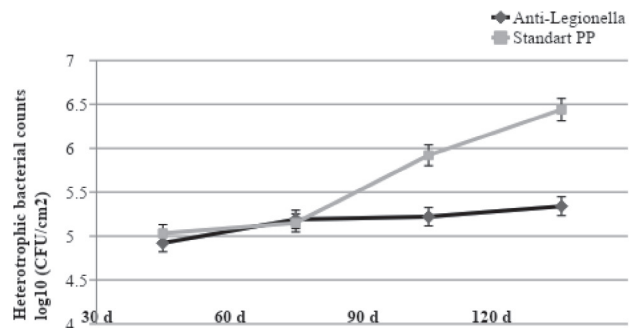


Figure 4. Heterotrophic bacterial numbers on surfaces during 120 days. Error bars represent standard error. * $P < 0.05$ compared with Anti-Legionella group.

The dissolved oxygen amount of the water circulation system was measured monthly with the oximeter (WTW-Oxi 330, Germany). The device has been calibrated before each use. Also the bulk water pH value was measured (KCP Handheld Digital pHmeter, China) and recorded every month before samples were taken (16). Despite the water blowdown regime (added daily ~3 liters of fresh network water), the dissolved oxygen amount and the pH values in the water phase were slightly increased throughout the experiment. Blowdown (make-up) was regularly done to avoid concentration of total dissolved solids in the system water. The dissolved oxygen amount and pH value raised gradually from 6.55 mg/l to 7.98 mg/l and from 6.52 to 6.96, respectively. Some selected make-up water parameters at the local water company are given in Table 1.

Table 1. Average water quality parameters at the municipal water company (units in mg/l except of turbidity and pH values).

Parameter	Value
pH	6.67
Turbidity (NTU)	0.66
Hardness - CaCO ₃	73
Na	18.1
Ca	27
Mg	4.44
K	2.77
Fe	0.044
Mn	0.010
SO ₄	41
F	0.06
NO ₂	2.92
Zn	0.011
NH ₄	0.05

Antimicrobial polymers are designed to inhibit the growth of bacterial biofilms on a variety of surfaces and the industry shows the greatest growth and growing demand (23). Our objective was to observe and evaluate the anti-Legionella property of the fill material in biofilm within mixed flora in the presence of Legionella bacteria. Data suggest that the anti-Legionella splash fill has an effective surface agent that limits Legionella colonization on its surface. A similar study also revealed significantly low counts of microorganisms colonized on the SANIPACKING® cooling tower sheet fill (24), which contains impregnated chlorine based antimicrobial agents. Damian and Paçachia (25) tested polypropylene polymers containing antimicrobial agents. They emphasize the advantages of using antimicrobial pipes in comparison to standard pipe material. On the other hand, results clearly depict that *L. pneumophila* proliferated in a very short time during the study within the bulk water system, which proves that cooling towers are ideal incubators for that bacteria and therefore regular control programs are crucial. The efficacy of the fill material against these organisms provides promise for future applications in reducing the transmission of Legionnaires' disease outbreaks sourced from cooling towers and reducing the numbers of pathogens in public spaces.

Due to increasing constraints on environmental discharge of disinfecting agents, as well as a demand to reduce costs, the water treatment industry has been looking for alternative ways to reduce biofilm formation and microbial counts in industrial

systems. There is still scope for further work in terms of controlling biofilm formation in man-made water systems (26). The results also demonstrate that one way approaches could not control the bacterial colonization efficiently. It could be concluded that polymers impregnated with antimicrobial agents might decrease biofouling on water associated surfaces. A combination of protective measurements should be routinely applied and monitored in man-made water systems for individual and environmental protection.

Peer-review: Externally peer-reviewed.

Author Contributions: Conception/Design of study: I.T., C.V.; Data Acquisition: I.T., C.V.; Data Analysis/Interpretation: I.T.; Drafting Manuscript: I.T., C.V.; Critical Revision of Manuscript: I.T.; Final Approval and Accountability: I.T., C.V.

Conflict of Interest: The authors declare that they have no conflicts of interest to disclose.

Financial Disclosure: This work was supported by Research Fund of the Istanbul University. Project number: 26088.

REFERENCES

1. Kadaifciler DG, Demirel R. Fungal biodiversity and mycotoxigenic fungi in cooling-tower water systems in Istanbul, Turkey. *J Water Health* 2017; 15: 308-20.
2. Turetgen I, Vatansever C. Survival of biofilm-associated *Legionella pneumophila* exposed to various stressors. *Wat Environ Res* 2015; 87: 227-32.
3. Dennis PJL. *A Laboratory Manual for Legionella*. USA, Chichester: Wiley and Sons; 1988.
4. Yu VL. Could aspiration be the major mode of transmission for legionella? *Am J Med* 1993; 95: 13-5.
5. Fitzhenry R, Weiss D, Cimini, D, Balter S, Boyd C, et al. Legionnaires' disease outbreaks and cooling towers in New York City, New York. *Emerg Infect Dis* 2017; 23: 1769-76.
6. Italy [online] <https://www.thelocal.it/20180918/italy-legionella-outbreak-identified-cooling-towers> (Accessed 11 January 2020)
7. Miyashita N, Higa F, Aoki Y, Kikuchi T, Watanabe A. Distribution of Legionella species and serogroups in patients with culture-confirmed Legionella pneumonia. *J Infect Chemo* 2020; 26(5): 411-7.
8. Vatansever C, Turetgen I. Investigating the effects of different physical and chemical stress factors on microbial biofilm. *Water SA* 2018; 44: 308-17.
9. Costerton JW. Introduction to biofilm. *Int J Antimicrob Agents* 1999; 11 (1): 217-21.
10. Donlan RM, Costerton JW. Biofilms: Survival mechanisms of clinically relevant microorganisms. *Clin Microbiol Rev* 2002; 15(2): 167-93.
11. Kadaifciler DG, Demirel R. Fungal contaminants in man-made water systems connected to municipal water. *J Wat Health* 2018; 16(2): 244-52.
12. Kim J, Park HD, Chung S. Microfluidic approaches to bacterial biofilm formation. *Molecules* 2012; 17: 9818-34.
13. Simões M, Pereira MO, Vieira MJ. A review of current and emergent biofilm control strategies. *Food Sci Technol* 2010; 43 (4) 573-83.
14. Momba MNB, Kfir R, Venter N, Cloete TE. An overview of biofilm formation in distribution systems and its impact on the deterioration of water quality. *Water SA* 2000; 26: 59-66.

15. Taylor M, Ross K, Bentham R. Legionella, protozoa, and biofilms: interactions within complex microbial systems. *Microb Ecol* 2009; 58: 538-47.
16. Turetgen I. Reduction of microbial biofilm formation using hydrophobic nano-silica coating on cooling tower fill material. *Water SA* 2015; 41: 295-9.
17. Elbourne A, Crawford RJ, Ivanova EP. Nano-structured antimicrobial surfaces: From nature to synthetic analogues. *J Colloid Interface Sci* 2017; 50 (8): 603-16.
18. Onan M, Hoca S, Sungur E. The effect of short-term drying on biofilm formed in a model water distribution system. *Microbiol* 2018; 87: 857-64.
19. Bruellhoff K, Fiedler J, Möller M, Groll J, Brenner RE. Surface coating strategies to prevent biofilm formation on implant surfaces. *Int J Artif Organs* 2010; 33(9): 646-53.
20. Paranjape K, Bédard É, Whyte LG, Ronholm J, Prévost M, Faucher SP. Presence of Legionella spp. in cooling towers: the role of microbial diversity, Pseudomonas, and continuous chlorine application. *Wat Res* 2020; 169: 115252
21. Walker T, Canales, M, Noimark, S, Page K, Parkin. I, et al. A light-activated antimicrobial surface is active against bacterial, viral and fungal organisms. *Scientific Reports* 2017; doi:10.1038/s41598-017-15565-5.
22. Reasoner DJ, Geldreich EE. A new medium for the enumeration and subculture of bacteria from potable water. *Appl Environ Microbiol* 1985; 49: 1-7.
23. Ahonen M, Kahru A, Ivask A, Kasemets K, Kõljalg S, et al. Proactive Approach for Safe Use of Antimicrobial Coatings in Healthcare Settings: Opinion of the COST Action Network AMiCI. *Int J Environ Res Public Health* 2017; 14(4): 36-44.
24. Turetgen I, Sanli Yürüdü NO, Norden I. Biofilm formation comparison of the Sanipacking cooling tower fill material against standard polypropylene fill material in a recirculating model water system. *Turk J Biol* 2012; 36(3): 313-8.
25. Damian L, Pațachia S. Antimicrobial polypropylene as material for safe water supply. *Bull Transilvania Uni of Braşov* 2016; 9(1): 41-8.
26. De Carvalho CCR. Biofilms: recent developments on an old battle. *Recent Patents Biotechnol* 2007; 1(1): 49-57.